The Impact of Nonideality on the Biophysical Properties of Therapeutic Antibodies in Physiological Environments

Hayli Alissa Larsen

A dissertation

submitted in partial fulfillment of the

requirements for the degree of

Doctor of Philosophy

University of Washington

2022

Reading Committee:

William M. Atkins, Chair

Abhinav Nath

Miklos Guttman

Program Authorized to Offer Degree:

Pharmacy – Medicinal Chemistry

University of Washington

Abstract

The Impact of Nonideality on the Biophysical Properties of Therapeutic Antibodies in Physiological Environments

Hayli Alissa Larsen

Chair of the Supervisory Committee:
William M. Atkins
Department of Medicinal Chemistry

Antibody-based therapeutics are some of the best-selling drugs on the market with indications in several aggressive cancers, chronic autoimmune conditions, and other disease states. They provide several advantages over traditional small molecule drugs but factors controlling the pharmacokinetics (PK) and pharmacodynamics (PD) are less understood. A key contributing factor is a lack of understanding of how proteins are affected by complex, crowded biological environments such as serum and plasma. This is largely because techniques used in the biopharmaceutical industry are poorly suited for neat ex vivo samples. For this reason, the complex effects of crowding in the therapeutic context of efficacy and clearance have not been documented. The second virial coefficient (B_2) parameter quantifies such weak interactions and can be determined by a variety of techniques; however, probing nonideality in complex biological fluids remains challenging.

Fluorescence correlation spectroscopy (FCS) is a technique capable of measuring the diffusive properties of proteins directly in biological fluids. Therefore, the focus of this dissertation is to utilize FCS to explore nonideality and antibody-target interactions directly in undilute serum. Chapter 1 introduces important topics related to antibody structure and function, therapeutic antibody optimization, and macromolecular crowding. Chapter 2 presents the development and validation of a novel in-serum FCS approach for probing nonideality via determination of apparent second virial coefficients ($B_{2,app}$). The findings revealed that nonideality effects in serum are antibody dependent. In Chapter 3, the in-serum FCS approach is utilized to further characterize the origins of nonideality. Here, $B_{2,app}$ measurements were used to identify the components of human serum responsible for non-ideal interactions with mAbs and Fab fragments. Most notably, attractive interactions were observed with serum IgGs in Fab domains. Therefore, Chapter 4 utilizes FCS to investigate the impact of nonideality on antigen binding. As a preliminary assessment, a model system was used to determine antibody-antigen affinity in buffer and serum via FCS. In addition, correlations between $B_{2,app}$ and serum-induced changes in binding affinity were explored. This provided initial insight into the significance of the magnitude of $B_{2,app}$ values, where slight attraction in the model system did not result in functional consequences to antigen binding. Together, this work demonstrates the potential utility of FCS in the biopharmaceutical industry and provides the foundation for investigating the impact of nonideality on the biophysical properties of therapeutic antibodies in physiological environments.

TABLE OF CONTENTS

LIST OF FIGURES

LIST OF TABLES

ACKNOWLEDGEMENTS

My graduate school journey has led to extensive professional and personal growth which would not have been possible without the support of many. First, I want to thank my advisors William Atkins and Abhi Nath. They provided different yet complementary mentorship styles. Abhi played a huge role in my success with FCS. I appreciate his expertise and continued help, especially with instrument issues. He was also incredibly helpful with writing. Bill often challenged me with intellectual questions that would drive me to think deeper into my research. I believe this to be one major contributor to the evolution of my project. Together, they supported opportunities that promoted growth such as internships, conferences, and presentations. They showed confidence in me by allowing a lot of independence in my research which in turn helped my self-confidence. Aside from my advisors, I also want to thank my committee members, Mike Guttman, Kelly Lee, and William Zagotta for providing support and helpful feedback on my thesis project. I also want to thank Anthony Lee, David Ortiz, and Michelle Redhair for the summer internship opportunity that taught me a lot and reignited my love for industry.

I want to thank present and past lab members of the Atkins and Nath labs: Mike Dabrowski, Dennis Goulet, Michelle Redhair, Amanda Clouser, Lorela Paco, Eleanor Vane, Ellie James, Elena Holland, Mia Cervantes for teaching and supporting me along the way. I also want to thank John Correia, John Sumida, Eddie Hodge, and Dr. Kelly lee for contributing to my project either through knowledge, training, or materials. I also want to thank my peers and the remaining staff in the medicinal chemistry department. It has been an absolute pleasure working with you over the past several years.

Finally, I want to thank my family and friends who have supported me on my science journey long before graduate school. Without you I would not be who I am today.

DEDICATION

To my loving family for always believing in me

CHAPTER 1

Introduction to Therapeutic Antibodies and Nonideality

1.1 Therapeutic antibodies are promising but challenging to develop

Therapeutic antibodies lie at the forefront of a new era of precision medicine that has emerged in recent decades. With over 100 FDA approvals since the first (muromonab-CD3) in 1986, therapeutic antibodies are now the some of the best-selling drugs on the market (Kaplon et al., 2022; Lu et al., 2020). The majority treat cancers (45%) or autoimmune disorders (27%), while others are used for infectious diseases (8%), cardiovascular disorders (7%), and other therapeutic areas (13%) (**Figure 1.1**) (Kaplon et al., 2022). Monoclonal antibodies (mAbs), exclusively IgG in format, make up the pool of approved antibody-based therapeutics (Tang et al., 2021). Major advancements in technology and protein engineering have driven novel protein engineering strategies, including development of alternative platforms, albeit with lower success rates (Hay et al., 2014). The versatility, specificity, and high affinity of therapeutic antibodies provides a major advantage over many traditional small molecule agents. However, despite higher approval rates compared to small molecule drugs (Dunlap & Cao, 2022), development remains time-consuming and expensive (Farid et al., 2020; Reichert, 2020). Furthermore, many therapeutic candidates never reach the clinic or fail during clinical trials.

Despite following similar development pathways, antibody-based therapeutics present many unique challenges compared to small molecule drugs. This arises from the complexity of proteins in general. Extensive optimization is necessary to improve therapeutic efficacy, safety, and developability (B. Wang et al., 2021). However, even the best developed therapeutics often present translational gaps between predicted efficacy and actual therapeutic effects (Dunlap & Cao, 2022).

Despite significant improvements in development since first generation mAbs, there are still many shortcomings in our ability to adequately model and predict physiological environments that govern antibody function. It is well-established that physiological environments are complex and crowded with high concentrations of macromolecules (including proteins) that complicate characterization with many traditional analytical techniques. As a result, most *in vitro* characterization is carried out in ideal buffer systems. The focus of this dissertation is to address this issue directly by investigating the behavior of therapeutic antibodies in undilute serum. More specifically, we focus on characterizing functional consequences of weak, nonspecific interactions (nonideality) between therapeutic antibodies and serum proteins. This chapter focuses on important topics related to antibody structure and function, therapeutic antibody development, and macromolecular crowding in preparation for addressing serum-induced nonideality effects in subsequent chapters.

1.2 Overview of antibody structure and function

1.2.1 Structural and functional domains of antibodies

Immunoglobulins (antibodies) are made up of either one or multiple Ig monomers (**Figure 1.2**). Each monomer is comprised of four polypeptide chains – two identical heavy chains (~50-70 kDa) and two identical light chains (~25 kDa) (Lefranc & Lefranc, 2020). The chains fold into regions called domains, where each chain contains a single n-terminal variable domain and c-terminal constant domains (one for light chains and 3-4 for heavy chains depending on antibody class) (Schroeder & Cavacini, 2010). Each Ig domain contains a single intrachain disulfide bond. Interchain disulfide bonds are also between the heavy chains (in the hinge region) and between constant domains of the heavy (CH1) and light (CL) chains (Goulet & Atkins, 2020). The Ig monomer can be further divided into two functional domains corresponding to variable and

constant regions. The adjacent n-terminal domains of the heavy (VH) and light (VL) chains contain six hypervariable loops that make up the antigen binding site (often referred to as the complementarity determining region, CDR). Thus, the two arms of and Ig monomer are termed the antigen binding fragments (Fabs). The constant region of antibody heavy chains below the hinge makes up the crystallizable fragment (Fc) which mediates specific interactions with proteins and Fc receptors necessary to elicit an immune response. Furthermore, antibodies are considered glycoproteins due to glycan modifications. Although the position and number differ across antibody isotypes and subclasses, Fc glycans modulate conformation and Fc-mediated functions (Goulet & Atkins, 2020; Schroeder & Cavacini, 2010).

1.2.2 Antibody classes

Antibodies can be divided into five classes (isotypes) – IgA, IgD, IgE, IgG, and IgM, defined by α, δ, ε, γ, μ, heavy chains, respectively. Heavy chains differ in size and amino acid composition, which result in distinct biological functions (Lefranc & Lefranc, 2020). This will be further discussed in section 1.2.6. Despite differences in heavy chains, antibody classes share the same light chains (either κ or λ). Antibody classes can also differ in hinge structure, glycosylation profile, oligomeric state, and valency. Some antibody classes can also be divided into subclasses, such as IgG (IgG1, IgG2, IgG3, and IgG4) and IgA (IgA1, IgA2) (Goulet & Atkins, 2020). Of the five classes, IgG antibodies are the most abundant in serum and have long circulating half-lives (~7-21 days depending on subclass) (Vidarsson et al., 2014). Furthermore, commercial antibodies are predominantly of the IgG class, which will be further discussed in section 1.3.2. Properties of antibody classes are compared in **Table 1.1** (Goulet & Atkins, 2020).

1.2.3 Antibody function

Antibody function begins with binding and neutralizing a target antigen which can effectively block interactions with binding partners, thereby interfering with downstream biological processes. For example, binding harmful toxins and viral envelope proteins can block entry into host cells to modulate pathogenesis or infection (Goulet & Atkins, 2020). In cancer, neutralizing growth factors and growth factor receptors can block cellular signaling associated with disease progression. However, to eliminate infected or malignant cells, more complex immunological functions are required (van der Horst et al., 2020; Van Erp et al., 2019). Such processes involve bivalent association with antigens to form immune complexes that, through Fc-mediated interactions with complement proteins and effector cells, can effectively eliminate the target cell though phagocytosis, cytolysis, or osmosis.

1.2.4 Antigen recognition

The CDR of an antibody contains the antigen binding site (paratope) responsible for high target specificity observed in therapeutic antibodies. Antigen recognition depends on many weak, noncovalent forces (hydrophobic interactions, hydrogen bonding, Van der Waals forces, and electrostatic interactions) between the antibody paratope and epitope (binding site on the antigen) (Janeway et al., 2001). The paratope is typically enriched in aromatic amino acids that participate in both hydrophobic interactions and short-range Van der Waals forces. The paratope and epitope are initially attracted via hydrophobic and long-range electrostatic interactions. As the hydrophobic surfaces approach, water is repelled from the binding interface allowing the epitope and paratope to gain closer proximity. Short-range Van der Waals forces further assist in bringing the complementary surfaces together, while electrostatic interactions, between charged residues, and hydrogen bonds strengthen the overall interaction (Frutiger et al., 2021; Janeway et al., 2001).

Although the CDR is often considered responsible for antigen binding, there is evidence that framework regions and constant regions outside of the CDR can also participate in antigen recognition. Framework regions can either interact with the antigen directly (residues within close proximity to the CDR) or indirectly by providing structural support to the CDR (Sedrak et al., 2003; Xiang et al., 1995). Constant domains may also indirectly participate in antigen recognition, likely through allosteric effects. For example, two different isotypes containing the same variable domains have been shown to have different affinity and specificity to the same antigen (Dam et al., 2008; Pritsch et al., 1996; Sela-Culang et al., 2013; Torres et al., 2007).

1.2.5 Antigen affinity vs. avidity

Affinity and avidity are both important parameters describing molecular recognition. Binding affinity is the strength of a single bimolecular interaction. For antibodies and antigens, this specifically refers to the binding strength between an individual paratope and epitope (Frutiger et al., 2021). For single site binding represented by:

$$[Ab] + [Ag] \rightleftharpoons [AbAg] \quad \text{.....(1)}$$

the concentration of bound complex (AbAg) compared to the concentration of unbound antibody (Ab) and antigen (Ag) is represented by a dynamic equilibrium governed by association and dissociation rate constants k_{on} and k_{off}, respectively. Binding affinity is often estimated by measuring the equilibrium dissociation constant (K_D), represented by the following relationship:

$$K_D = k_{off}/k_{on} \quad \text{.....(2)}$$

While some techniques such as surface plasmon resonance (SPR) and biolayer interferometry (BLI) directly measure rate constants to determine K_D, some techniques do not require measurements of individual rate constants, such as the FCS approach executed in this research, which will be further explained in Chapter 4.

In contrast, avidity refers to the increased binding strength afforded by multivalent interactions (Frutiger et al., 2021). A single antibody can bind more strongly to multiple antigens within proximity on a cell surface, for example, than it would to a single antigen. In this case, binding at one Fab arm brings the other arm closer to a neighboring antigen on the cell surface. However, this enhancement strongly depends on the density of antigen on the cell surface. In addition, avidity depends on the affinity between individual paratopes and epitopes and the valency of the antibody. For example, IgG antibodies have two binding sites (bivalent) whereas IgM has 10-12 binding sites. IgM often displays lower affinity to antigens compared to IgG (Muthana et al., 2015). However, the lower affinity can be compensated for by the greater avidity of IgM. Avidity can present challenges in measuring binding affinity with traditional immobilization techniques, such as SPR and BLI, because the density of immobilized protein can greatly increase avidity effects which can lead to an increase in apparent binding affinity. Finally, avidity can assist in coating a target cell which can enhance Fc-mediated effector functions.

1.2.6 Fc-mediated effector functions

Antibody effector functions effectively link adaptive and innate immune responses to eliminate pathogens and target cells. The most common effector functions are antibody-dependent cell-mediated cytotoxicity (ADCC), antibody-dependent cellular phagocytosis (ADCP), and complement-dependent cytotoxicity (CDC) (Van Erp et al., 2019). Activation of these pathways involve antigen bound antibodies interacting with specialized Fc receptors and complement proteins in their constant domains below the hinge region. Antibody coated targets are subsequently eliminated via downstream processes that lead to cytolysis, phagocytosis, or osmosis. There are several types of FcRs (FcγRI, FcγRIIA, FcγRIIB, FcγRIIC, FcγRIIIA, FcγRIIIB, FcεRI, FcαRI, and FcμR). FcRs are presented on a variety of immune cells and bind either IgA (FcαRI),

IgE (FcεRI), or IgG (FcγRs) to activate ADCC and ADCP (Goulet & Atkins, 2020; Mancardi & Daëron, 2014). Aside from FcγRI, which binds monomeric IgG with high affinity, most stimulatory FcγRs require immune complex formation to elicit effector functions (R. Liu et al., 2020). While most FcγRs are stimulatory, FcγRIIB is inhibitory. Therefore, binding both inhibitory FcγRIIB and stimulatory FcγRs on the same cell can reduce effector function. FcγRIIB exhibits low expression on natural killer (NK) cells involved in ADCC and higher expression on immune cells involved in ADCP (macrophages, neutrophils, etc.). Therefore, ADCC is a potent effector function of many market IgG therapeutics.

The ADCC mechanism involves release of cytotoxic granules from FcR-presenting effector cells that lyse and eliminate antibody-coated target cells via cytolysis. IgA, IgE, and IgG can induce ADCC by binding FcαRI (neutrophils), FcεRI (Basophils and mast cells), and FcγRIIIa (NK cells), respectively. IgG and IgA antibodies can also eliminate cells through phagocytosis via binding stimulatory FcγRs presented on monocytes, macrophages, and neutrophils. In contrast, the CDC effector function is elicited by IgG and IgM antibodies. Fc-mediated interactions with C1q triggers a cascade of proteolytic complement proteins that attack and lyse cell membranes, effectively eliminating target cells via osmosis (Goulet & Atkins, 2020). The complement cascade can also indirectly eliminate complement coated target cells through phagocytic clearance (Van Erp et al., 2019). IgM induces strong CDC functions due to the hexameric structure of C1q. Although IgG also induces CDC, it requires hexamerization of individual IgG monomers at the cell surface for activation (Goulet & Atkins, 2020).

1.2.7 Neonatal Fc receptor (FcRn)

IgG Fc also mediates interactions with neonatal Fc receptor (FcRn) but such interactions are not involved in effector functions. In fact, the function and structure of FcRn is significantly

different than FcγRs (R. Liu et al., 2020). FcRn exhibits structural similarity to the major histocompatibility complex (MHC) and functions inside endosomes in multiple cell types (Blumberg et al., 2019; R. Liu et al., 2020). As the name suggests, it was first recognized for placental transport of IgG antibodies from mother to fetus during pregnancy (R. Liu et al., 2020). It was later established that FcRn also prolongs the circulating half-lives of IgG antibodies. IgGs, including therapeutics, are continuously endocytosed into monocytes and endothelial cells, where they bind FcRn in the mildly acidic condition of early endosomes. The endosomes are subsequently transferred back to the cell surface where FcRn releases IgGs back into the bloodstream at neutral pH. In doing so, FcRn recycles IgGs and effectively rescues them from lysosomal degradation (Roopenian & Akilesh, 2007) which prolongs their half-lives (~23 days for IgG1, IgG2, and IgG4 isotypes) (Saxena & Wu, 2016). This is often termed the endocytic salvage pathway and is a major contributor to the development of IgG-based therapeutics. This allows for longer dosing intervals, which is particularly beneficial since therapeutic antibodies require subcutaneous or intravenous administration.

1.3 Therapeutic antibody properties and optimization strategies

1.3.1 Overview

Collaboration across a team of scientists from various disciplines is required to carry an antibody from discovery to approval (Dunlap & Cao, 2022). In early stages of discovery and lead candidate selection, antibodies are generated for specific molecular targets and validated based on target affinity, specificity, and biological function. A lead candidate undergoes extensive optimization to enhance efficacy, developability, and safety (B. Wang et al., 2021). There are many properties of therapeutic antibodies that require consideration during development, including antigen affinity and specificity, Fc effector function, isoelectric point, post translational

modifications, aggregation, immunogenicity, and PK/PD. Addressing issues associated with one property often leads to issues in another, therefore antibody properties require characterization in parallel throughout the development process. This is both time consuming and labor intensive, requiring a plethora of *in vitro*, *in vivo,* and *in silico* approaches. This chapter covers many of the important properties and optimization strategies of therapeutic antibodies, some of which are summarized in **Figure 1.3** (Ulitzka et al., 2020; B. Wang et al., 2021)**.**

1.3.2 IgG-based therapeutics

Marketed therapeutics are exclusively IgG-based. Most marketed mAbs are IgG1 (74%) and to a lesser extent IgG2 and IgG4 (~13% each) isotypes (Tang et al., 2021). Although IgG3 antibodies display high affinity to Fcγ receptors, they are not developed as therapeutics. This is mainly due to instability associated with the extended hinge region, increased tendency to aggregate, and lower half-life (~7 days compared to ~21 days for the other subclasses) due to lower affinity to FcRn (Kretschmer et al., 2017). IgG1 antibodies dominate the pool of therapeutic mAbs due to greater stability, lower aggregation propensity, and higher affinity to Fcγ receptors and C1q that mediate ADCC, ADCP, and CDC pathways, respectively. This is especially important in many cancers where the objective is to eliminate malignant cells. The IgG2 isotype is selected when target neutralization and reduced effector function is desired. Common indications are therapeutics that target growth receptors (EGFR, HER2, etc.) to block signaling associated with disease progression. Similarly, IgG4 antibodies are selected when no effector function is desired, such as in the case of immunotherapy checkpoint blockade inhibitors (Kretschmer et al., 2017).

1.3.3 Optimizing antigen binding affinity

Antigen binding is critical for therapeutic efficacy. Therefore, binding kinetics, epitope specificity, and binding affinity are heavily characterized during development. *In vitro* binding data in early stages of development informs lead candidate selection, PK/PD modeling, and optimization strategies (X. Wang et al., 2020). There are many *in vitro* assays used to characterize binding properties such as SPR, BLI, enzyme-linked immunoassay (ELISA), biolayer and isothermal titration calorimetry (ITC). In addition, nuclear magnetic resonance (NMR) and hydrogen-deuterium exchange mass spectrometry (HDX-MS), are useful tools for epitope mapping.

Affinity maturation of lead antibody candidates is a routine method aimed at improving antigen binding. This typically involves mutagenesis in the variable domains of antibodies (B. Wang et al., 2021). For example, substitution with charged residues has been reported to significantly increase affinity (Kiyoshi et al., 2014). Several *in silico* approaches aid in designing variants that are then produced and subject to validation assays. However, mutagenesis aimed at increasing antigen affinity can also increase the propensity for undesirable cross-reactivity to other antigens. Therefore, additional mutagenesis steps that optimize specificity are often required (B. Wang et al., 2021). Although early development focuses on high antigen affinity to model durable target coverage, optimal affinity depends on the MoA. In some contexts, high affinity is not necessarily optimal . For example, increased affinity to growth factor receptors does not always translate into increased signaling suppression. In this case, optimal affinity relies on the rate of internalization of the antibody-receptor complex and the association rate (k_{on}) (Tang & Cao, 2021; Tiwari et al., 2017). Furthermore, elimination rate of free drug from the target environment is an important consideration as well as local phenomena, such as diffusion and interactions with

surrounding proteins (Vauquelin & Charlton, 2010). Therefore, factors related to MoA, pharmacokinetics, and macromolecular crowding should be considered when optimizing antigen binding.

1.3.4 Fc engineering

Extensive research focused on elucidating structure-function relationships in the Fc domains of antibodies and has led to interest in Fc engineering strategies aimed at improving therapeutic efficacy (R. Liu et al., 2020). To date, marketed antibodies are of the IgG class. Therefore, many studies have focused on IgG Fc domains. However, other antibody classes are entering the clinic which will prompt further characterization given differences in their heavy chains and glycosylation profiles. Identifying specific amino acids responsible for Fc-binding and the role of glycosylation has prompted development of Fc engineered antibodies for specific mechanisms of action and therapeutic processes. As discussed in section 1.2, IgG Fc domains induce effector functions via binding specialized Fcγ receptors and complement initiator, C1q. The Fc also mediates interactions with FcRn to achieve long circulating half-lives of therapeutic antibodies. Furthermore, glycosylation is important for structural conformation of the Fc and modulates interactions with Fc-binding proteins. Therefore, Fc engineering strategies have focused on glycoengineering and amino acid mutagenesis in the Fc to alter effector functions and enhance binding to FcRn (R. Liu et al., 2020). High resolution mapping via alanine scanning mutagenesis has been used to determined specific amino acids in the lower hinge and C_H2 regions of IgG1 antibodies that bind FcγRs and FcRn (Shields et al., 2001). This has led to further mutational studies, often using computational structure-based modeling and high throughput screening, to produce variants with altered effector functions and enhanced half-lives (R. Liu et al., 2020).

Incorporating mutations that enhance binding affinity to FcγR1, FcγRIIa, FcγRIIIa and reduce affinity to inhibitory FcγRIIB have shown enhanced ADCP and ADCC (R. Liu et al., 2020). There are also several CDC-enhancing Fc variants reported in the literature (Idusogie et al., 2001; Natsume et al., 2008). However, CDC is complicated by specific molecular target requirements and less explored in clinical settings. This is largely because IgG antibodies have to hexamerize to engage C1q (Diebolder et al., 2014), which in turn requires high antigen density at cell surfaces. Glycoengineering is an additional strategy used to enhance Fc-mediated effector functions (predominantly ADCC). The conserved N-glycan at Asn 297 on IgG1 antibodies has been shown to stabilize the Fc at the FcγRIIIa binding interface (Subedi & Barb, 2015). However, fucose residues are reported to lead to steric repulsion that can lower affinity to FcγRIIIa (Arnold et al., 2007). Therefore, elimination of fucose is a strategy used to enhance ADCC (R. Liu et al., 2020). The most promising clinical indication of the above-mentioned Fc engineering strategies is for solid tumor cancers, where antibodies often elicit effector functions to eliminate target cells. In some contexts, decreased effector function is desired, such as with check-point inhibitors for immunotherapy. In this case, therapeutic antibodies are used to block interactions between T-cell receptors and ligands on cancer cells to essentially reactivate tumor specific T-cells. In contrast to the examples above, specific Fc amino acid mutations can also decrease affinity to FcγRs and C1q to reduce effector function. In addition, producing aglycosylated variants to silence the Fc domain is a glycoengineering approach that can also effectively reduce effector functions. Finally Fc engineering strategies are also implemented to prolong the half-life of antibodies by incorporating mutations that increase interactions with FcRn (R. Liu et al., 2020). In addition, Fc engineering has also been used to covalently attach IgG Fc domains to therapeutic proteins to increase half-life and provide additional biological functions (Czajkowsky et al., 2012).

1.3.5 Charge and Isoelectric point

The isoelectric point (PI) is the pH at which a therapeutic antibody has no net charge and is typically characterized by capillary isoelectric focusing (icIEF). Surface charge and charge distribution can impact antibody solubility, viscosity, off-target interactions, and clearance. Like endogenous IgG1s, most therapeutic antibodies have a PI ≥ 8, resulting in slight positive charge at physiological pH. This is desirable for biodistribution given the negative charge of most cell surfaces. Higher PI has also been associated with decreased risk of self-association due to repulsion in high concentration therapeutic formulations (which are typically at pH 5-6) (Yang et al., 2019). Hydrophobic patches serve as hot spots for aggregation (Li et al., 2016), and so engineering strategies that incorporate basic amino acids to raise PI also distribute them between hydrophobic residues. Furthermore, basic charge variants have also demonstrated greater affinity to FcγRIIIa and enhanced ADCC responses (Hintersteiner et al., 2016). Despite the advantages associated with PI ≥ 8, positive net charge has been found to increase risk or nonspecific tissue uptake, clearance (Gupta et al., 2022), and propensity for interactions with many serum proteins, including some immunoglobulins, which carry negative charge at physiological pH (Filoti et al., 2015; Yang et al., 2019). Therefore, it is challenging to find a balance in charge that ensures both safety and efficacy of the therapeutic product.

1.3.6 Immunogenicity

Given that therapeutic antibodies are exogenous proteins, they can trigger an immune reaction that can compromise both safety and efficacy. This immune response involves the production of anti-drug antibodies (ADAs). Neuralization by ADAs can reduce or abolish drug efficacy and the side effects associated with immunogenicity can range from mild (headache, nausea, etc.) to severe (infection, cardiotoxicity, severe allergic reaction). Non-human sequences

are common inducers of ADA responses (Ulitzka et al., 2020). Therefore, antibody humanization is a common optimization strategy (B. Wang et al., 2021). This typically involves generating a chimeric antibody via fusing a non-human variable domain to the constant region of a human antibody. The variable domain of the chimeric antibody is often further modified at certain residues to increase similarity to natural antibodies. Common approaches for humanization include computer-aided design, yeast display, and phage display (B. Wang et al., 2021). Post translational modifications and other factors that increase aggregation can also induce immunogenicity and will be further discussed in subsequent sections.

1.3.7 Post translational modifications

Post translational modifications contribute significantly to heterogeneity in the final antibody product. These modifications can occur at various stages of development (i.e., manufacturing, storage, etc.) (Ulitzka et al., 2020). Some of the most common PTMs that can negatively influence antibody stability and efficacy are free cysteine residues, glycosylation, glycation, oxidation (methionine, tryptophan, and histidine), glutamine (Gln) and deamidation (asparagine and glutamine), aspartate (Asp) isomerization (**Figure 1.3**). Free cysteines and glycation have been linked to increased aggregation propensity (Huh et al., 2013; Ulitzka et al., 2020). In contrast to antibody glycosylation, glycation results from non-enzymatic addition of free sugars to lysine residues, which can occur during cell culture, formulation, and storage (H. Liu et al., 2014). High mannose groups in antibody glycosylation profiles have been associated with decreased effector function and increased clearance (Goetze et al., 2011). Oxidation in CH_2 domains has been linked to decreased biological function, half-life, and stability (D. Liu et al., 2008; W. Wang et al., 2011; Wei et al., 2007). Finally, deamidation and isomerization in Fab domains have been linked to decreased antigen affinity (Cacia et al., 1996; Yan et al., 2009). Many

PTMs are shared between endogenous and recombinant IgGs and are considered low risk for immunogenicity (H. Liu et al., 2014). However, PTMs that increase aggregation propensity and PTMs unique to therapeutic antibodies increase risk. Therefore, extensive characterization and optimization of PTMs is required during development. Mass spectrometry-based approaches coupled to UV-based chromatographic (ion exchange, hydrophobic, or reverse-phase) techniques are commonly used to monitor PTMs, while optimization typically requires removal of modified sites via targeted site mutagenesis (B. Wang et al., 2021).

1.3.8 Aggregation – colloidal and conformational stability

Antibody aggregation is recognized as a risk factor for immunogenicity, increased drug clearance, and decreased efficacy. Antibodies experience many stresses during manufacturing (temperature, pH, ionic strength, etc.) and are formulated to high concentrations (>50 mg/mL) that can drive aggregation (Dobson et al., 2016). Therefore, aggregation is a major obstacle during development that requires extensive characterization. Size-exclusion chromatography (SEC) is a common technique used to characterize aggregation during development. Alternative techniques are also used to determine aggregation propensity. Although there is no single aggregation pathway, colloidal and conformational stability are two properties correlated to aggregation propensity (Lundahl et al., 2021). Conformational stability is defined as the Gibbs free energy between native and denatured states (Oyama et al., 2020). Partial unfolding, for example, can lead to exposure of hydrophobic regions that are susceptible to attractive protein-protein interactions between antibodies. The aggregation temperature (T_{agg}) and melting temperature (T_m) are parameters used to measure conformational stability. T_{agg} is the temperature at which particle size increases compared to monomer and is typically measured by light scattering. T_m represents the midpoint of thermal unfolding, typically characterized by differential scanning calorimetry (DSC)

(Oyama et al., 2020). Lower T_{agg} and T_m values correspond to lower conformational stability and great aggregation propensity. These parameters are particularly important to account for stress during manufacturing and storage. However, since unfolding rates are strongly correlated with aggregation (Džupponová et al., 2020), measuring kinetic changes in conformational stability are also important and likely more relevant *in vivo*. Common approaches used to measure protein folding kinetics are time-resolved circular dichroism (CD), stopped flow, and H/D exchange methods (Bengt, 2006).

In contrast, colloidal stability refers to the ability of monomers to remain separated in solution, which can be influenced by a variety of factors including concentration, solubility, and repulsive interactions (Lundahl et al., 2021). A common parameter used to measure colloidal stability is the second osmotic virial coefficient (B_{22}) or interaction parameter, k_{diff} which indicates the propensity for either repulsive or attractive interactions between antibodies in solution. Positive values indicate net repulsion, whereas negative values indicate attraction. The more negative the value, the higher the aggregation propensity. We discuss below how similar ideas can also be used to quantify interactions between antibodies and diverse co-solutes. Characterization is typically carried out in either formulation buffer or in ideal buffer systems such as PBS. However, characterization in biological fluids is out of the scope of many analytical techniques, which dramatically hinders our understanding of antibody stability and aggregation propensity *in vivo*.

1.3.9 Pharmacokinetics (PK) and Pharmacodynamics (PD)

The PD of a drug substance refers to biochemical and physiological effects (MoA). As previously discussed, this includes target neutralization, signaling suppression, and effector functions. In contrast, PK refers to the drug-concentration time course in biological fluids, which is governed by absorption, distribution, metabolism, and excretion (ADME). As a result, PK

directly impacts the magnitude and duration of PD (Tang & Cao, 2021). PK/PD analyses are critical to antibody development (Tang & Cao, 2021; Van Der Graaf & Gabrielsson, 2009). However, modeling PK/PD of therapeutic antibodies is incredibly difficult. Well-established approaches that correlate *in vitro* and *in vivo* ADME in small molecule drug development do not translate to therapeutic antibodies. This is largely attributed to the complexity of protein-based therapeutics and many unique considerations compared to small molecule drugs, such as clearance, drug exposure, biotransformation, and target engagement in tissue and vascular spaces (Lee, 2013). Typical PK studies focus on system persistence and target distribution. As a result, physiologically based pharmacokinetic (PBPK) models are often used to describe *in vivo* behavior, including FcRn recycling, tissue uptake and target binding in specific tissues. However there are still major shortcomings in the ability to adequately model complex and dynamic physiological environments. High PK/PD variability, low tissue distribution, flat dose responses, and high treatment resistance are continued challenges in antibody PK/PD characterization (Tang & Cao, 2021). Furthermore, the major gaps in our understanding of antibody PK/PD in traditional monoclonal antibody platforms dramatically hinders the development of alternative antibody platforms.

1.3.10 Alternative antibody platforms

There is increased interest in developing derivatives of mAbs to optimize mechanisms of action (MoAs) for specific disease indications. Two of the most popular gaining clinical approval are antibody-drug conjugates (ADCs) and bispecific antibodies (BsAbs). These platforms have demonstrated enhanced therapeutic effects compared to traditional mAbs for some cancers and other disease areas. This section will focus on ADCs and BsAbs but it should be noted that there

are several other emerging platforms, such as Fab fragments, nanobodies, and Fc-fusion proteins that are excluded from this discussion.

ADCs target cancer cells by tethering a cytotoxic payload to a monoclonal antibody via a chemical linker. The MoA of ADCs involves mAbs binding a target antigens, followed by internalization and subsequent release of the cytotoxic payloads to kill target cells (Yu et al., 2020). The targeted delivery of the payload improves toxicity associated with many traditional chemotherapy agents. This requires unique expression of target antigen on malignant cells, minimal expression on normal cells, receptor-mediated endocytosis, and linker stability. There are currently 14 approved antibody-drug conjugates for the treatment of solid tumor cancers and hematological malignancies (Fu et al., 2022). First-generation ADCs (early 2000s) focused on utilizing the mAb as a vehicle and were therefore IgG4-based due to the absence of effector function. However, effector function is now considered a secondary MoA by which ADCs can improve therapeutic efficacy (Yu et al., 2020). For this reason, IgG1-based ADCs dominate the pool of approved therapeutics. IgG2-based ADCs have not made it to the market due to aggregation and increased clearance compared to IgG1 and IgG4-based ADCs (Zhang et al., 2018). Furthermore, conjugating payloads to mAb scaffolds presents many unique developmental challenges.

BsAbs contain different binding sites on each Fab arm toward either two different antigens or two different epitopes on the same antigen. Complex signaling pathways in many cancers and other diseases often lead to drug resistance with traditional mAbs. Therefore, combinatorial mAb treatment approaches are becoming increasingly important. However, the dual targeting ability of BsAbs decreases resistance compared to mAbs while also achieving superior cytotoxic effects with a single therapeutic agent. The majority of marketed BsAbs treat cancer. For immunotherapy, a

common MoA is dual targeting of immune checkpoint inhibitors presented on T-cells, such as PD1, CTL-4, and LAG-3 as well as tumor associated antigens such as CD23 and PDL-1. This effectively reactivates suppressed tumor targeting T-cells. In addition to immune cells, BsAbs also target tumor antigens, such as HER2, HER3, and EGFR, effectively blocking dual signaling pathways (Ma et al., 2021). While the majority of bsAbs target cancer, there are also MoAs for the treatment of hemophilia A, Alzheimer's disease, diabetes, and macular degeneration. The main challenge associated with BsAb development is mismatching of heavy and light chains (Brinkmann & Kontermann, 2017; Q. Wang et al., 2019). However, this has been improved by major advancements in technology and protein engineering strategies. This has led to a variety of different BsAb formats, which are divided into two main groups, IgG-like and non-IgG-like. IgG-like BsAbs contains the full antibody structure, therefore retain long half-life, greater stability, and effector functions. In contrast, non-IgG-like bsAbs are easier to produce but do not contain the Fc domain. Ma et al., 2021 provides a detailed description of the different bsAb formats and required technologies. There are currently 6 FDA approved bsAbs (*Antibody Society. In: Approved Antibodies*, 2022), with over 100 in the development pipeline. Although the majority of approved and developing BsAbs are for tumor immunotherapy but there are several other emerging indications. In addition to therapy, BsAbs are also being used as diagnostic agents (Ma et al., 2021).

1.4 The impact of crowded physiological environments on therapeutic antibodies

1.4.1 Overview

Macromolecular crowding is a well-established phenomenon in physiological environments. The impact of crowding on protein thermodynamics has been heavily studied and related to many biological processes. However, investigating the impact of crowding on

therapeutic antibodies has only recently started gaining interest (Kim et al., 2019; Larsen et al., 2021; Wright et al., 2018). Given that therapeutic antibodies are proteins, it is surprising that more consideration is not given to the potential for weak, nonspecific interactions between therapeutic antibodies and the various proteins in physiological environments. Such interactions may lead to changes in biophysical properties of antibodies resulting in detrimental effects to safety and efficacy of the therapeutic product. Developing *in vitro* approaches that characterize therapeutic antibodies in biological fluids may better inform protein engineering strategies and aid in further optimizing the development process. Important topics related to macromolecular crowding and potential implications in therapeutic antibody development with be further discussed in this section.

1.4.2 The evolution of macromolecular crowding theory

It is well-established that physiological environments, such as serum and cells, contain high concentrations of macromolecules (proteins, lipids, nucleic acids, etc.). Protein concentration alone in serum is 60-80 mg/mL and even higher in intracellular compartments (200-300 mg/mL) (Leeman et al., 2018). Given the inability of molecules to occupy the same space at the same time, crowding results in steric repulsion between solutes that generates excluded volume in solution. It has been hypothesized that excluded volume effects enhance the thermodynamics equilibria of proteins (folding stability, binding affinity). Excluded volume effects alone can enhance protein stability by favoring more compact structures and increase binding affinity due to an increase in apparent protein concentration.

Many traditional studies aimed at characterizing the effects of macromolecular crowding utilized various protein and polymer-based (PEG, Dextran, etc.) crowding agents. Studies have demonstrated that excluded volume effects enhance the thermodynamics and increase kinetics of

many important biological processes such as protein folding, binding, and transport (via diffusion) (Cheung et al., 2005; A. P. Minton & Wilf, 1981; Allen P. Minton, 1983; Van Den Berg et al., 2000; Y.-L. Zhou et al., 2006). This may have a range of implications *in vivo* such as facilitating transcription, translation, enzymatic reactions, and signaling. However, crowding can also facilitate unwanted processes, such as driving formation of pathological complexes and protein aggregation associated with amyloid formation (Hatters et al., 2002; Z. Zhou et al., 2009). There are assumptions in the theory behind excluded volume that complicate *in vitro* studies. The main assumptions of excluded volume are that crowder molecules are spherical and inert. However, crowder agents are neither. In addition, the size and shape of the crowder can also greatly influence excluded volume effects. For example, large molecules will exclude more volume compared to small molecules, while branched molecules (i.e., PEGs) are not spherical and can perturb diffusion differently than globular proteins. Finally, crowder molecules can participate in enthalpically-driven weak protein-protein interactions with target proteins (Sukenik et al., 2013). Such interactions can be repulsive or attractive in nature which can either contribute or compete with stabilizing entropy driven excluded volume effects. Attractive interactions between crowders and proteins have been demonstrated to destabilize the formation of protein complexes, which opposes the stabilizing effects of excluded volume (Bhattacharya et al., 2013; Jiao et al., 2010; Phillip et al., 2012).

Traditional macromolecular crowding theory was solely explained by excluded volume effects. However, this does fully capture the effects of crowding *in vivo* because physiological environments contain heterogenous populations of macromolecules. This encompasses molecules of various sizes, shapes, and chemical compositions. Furthermore, many are proteins and can participate in enthalpically-driven weak, nonspecific interactions. As mentioned above,

enthalpically driven interactions between target proteins and crowder molecules can be both stabilizing (repulsive) and destabilizing (attractive). For example, Sukenik et al. observed concentration dependent mechanisms of stabilization of a 16-amino acid peptide folding into a β-harpin in the presence of various crowder molecules (PEGs, dextran, etc.). At low concentrations of crowders, stabilization was driven by entropically driven excluded volume effects. However, they observed increasing enthalpic contributions to stabilization with increasing crowder concentration, suggesting a balance between excluded volume effects and enthalpically driven weak interaction between target proteins and commonly used crowder agents (Sukenik et al., 2013). While this complicates studies that utilize these systems to elucidate the effects of excluded volume, it likely highlights true effects of crowding *in vivo*. That said, modeling macromolecular crowding with proteins and polymer-based crowding molecules does not likely capture the true effects of crowding *in vivo*. The studies presented in this dissertation probe weak, nonspecific interactions between antibodies and serum proteins directly in serum. This provides a more representative model compared to many traditional systems to capture the global effects of crowding on target proteins.

1.4.3 Nonideality and the second virial coefficient

Molecules in dilute buffer systems are typically far enough apart in solution that they do not interact. Therefore, dilute buffer systems are considered ideal compared to concentrated solutions where there can be a variety of forces acting between molecules. Proteins in crowded environments, for example, can participate in hydrogen bonding, electrostatic, and hydrophobic interactions that can influence structure and function (as discussed above). However, these effects are difficult to probe. The complexity of biological fluids complicates measurements with many traditional analytical techniques. Therefore, most protein characterization, including that of

therapeutic antibodies, is carried out in ideal buffer systems. This dramatically hinders the ability to characterize protein behavior *in vivo*. The main goals of the research presented in this dissertation are to probe nonideality between antibodies and serum proteins directly in undilute serum and to further investigate the impact of the interactions on protein-target affinity. This required the development and validation of a novel approach capable of measuring second osmotic virial coefficients directly in biological fluids.

Second osmotic virial coefficients B_{22} and B_{23} are the parameters used to describe weak, nonspecific interactions between two of the same or different molecules, respectively. The sign of the coefficient informs on the nature of the interactions, where positive and negative values indicate repulsion or attraction between molecules, respectively. There are many analytical techniques used to measure traditional second osmotic virial coefficients in buffer systems. However, we present a novel fluorescence correlation spectroscopy (FCS) approach capable of probing serum-induced nonideality effects directly in serum through measurements of apparent second virial coefficients ($B_{2,app}$). The theory, methodology, and important comparisons to traditional approaches are presented in our previous publication (Larsen et al., 2021; Chapter 2). Briefly, these measurements probe weak, nonspecific interactions between labeled antibodies and serum proteins as a measure of global nonideality effects in serum. This provides an advantage over many traditional approaches that are confined to buffer systems. The in-serum FCS approach effectively probes interactions between labeled antibodies and various serum proteins simultaneously while also capturing the effects that serum proteins have on each other. This provides a more relevant representation of the effects of nonideality *in vivo* compared to many tradition approaches that use individual proteins or crowding agents (Kim et al., 2019; Wright et

al., 2018). This ultimately delivers unprecedented insight into therapeutic antibody behavior *in vivo* and may have applications in the therapeutic antibody industry.

1.4.4 Applications of the second virial coefficient in therapeutic antibody development

The second osmotic virial coefficient has been implemented in therapeutic antibody development. Self-term virial coefficient (B_{22}) measurements are used to probe aggregation propensity in high antibody formulations, which typically exceed 50 mg/mL to accommodate high dosing regimens (Baek & Zydney, 2018). Cross-term viral coefficient (B_{23}) measurements are less common but are also used during formulation development to monitor protein-excipient (i.e., sucrose, trehalose, mannitol, and sorbitol) interactions (Kamerzell et al., 2011). Although these measurements are useful in formulating the final therapeutic product, they provide no information on aggregation propensity *in vivo*. That said, methods that probe *in vivo* behavior of therapeutic antibodies are not well-established in general. Following administration, therapeutic antibodies are delivered directly into the bloodstream through the lymphatic system. Given the long-serum half-lives of therapeutic antibodies, exposure to serum proteins can persist for several weeks. As previously discussed, the crowded environment in serum can increase the propensity for weak interactions between therapeutic antibodies and serum proteins. However, approaches capable of probing these interactions are not established and as a result the consequences of nonideality on the biophysical properties of therapeutic antibodies remains unknown. In serum FCS $B_{2,app}$ measurements may aid in furthering our understanding of the effects of serum-induced nonideality on therapeutic antibody stability and efficacy. This could prove useful during various stages of therapeutic antibody development. Perhaps implementing $B_{2,app}$ in the early stages of discovery and lead candidate selection could dramatically advance the development process .

1.5 Summary

One major consideration often overlooked in therapeutic antibody development is that *in vitro* assays utilize dilute buffer systems that are vastly different from crowded biological fluids. In early stages of development, *in vitro* assays are used to estimate target (antigen, Fc receptors, FcRn, etc.) affinity, which informs lead candidate selection and PK/PD modeling. In addition to binding assays, many orthogonal analytical techniques are used throughout the remainder of development to monitor biophysical properties of lead candidates through various process changes and optimization steps. Although antibody-based PK/PD studies are useful tools for predicting *in vivo* behavior, they are ultimately insufficient. The many shortcomings of *in vivo* and *in silico* approaches to estimate *in vivo* properties has led to major gaps in our understanding of antibody PK/PD. Therefore, the inefficient development process is largely attributed to many limitations in our ability to model and predict complex, crowded physiological environments. The purpose of this dissertation is to address this issue directly by developing and characterizing nonideality of antibodies directly in serum. In Chapter 2, I present the development and validation of the in-serum FCS approach for $B_{2,app}$ determination. In chapter 3, I complete $B_{2,app}$ measurements for a panel of antibodies and fragments in the presence of serum and isolated serum proteins to determine the origins of nonideality. Finally, in Chapter 4, I compare antibody-target affinity in buffer and serum (via FCS measurements). I also investigate correlations between changes in affinity and $B_{2,app}$ values to explore functional consequences of nonideality *in vivo*.

FIGURES

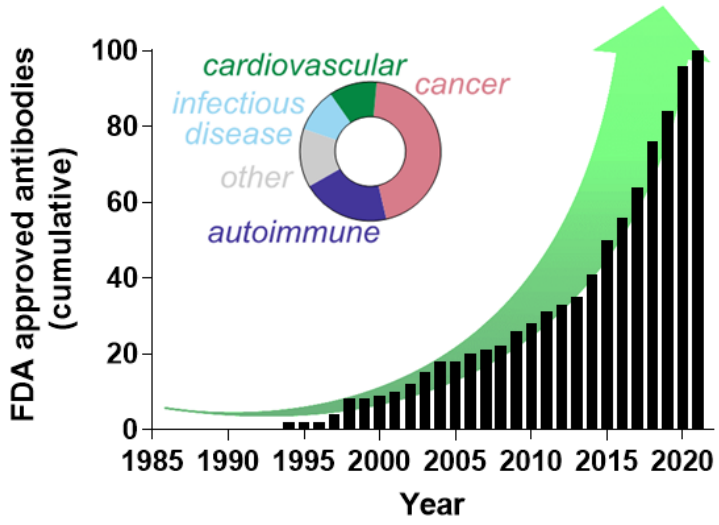

Figure 1.1: FDA approved therapeutic antibodies: The antibody industry has experienced exponential growth in the number of approved therapeutic antibodies since the first in 1985 for a wide range of indication, with the majority treating cancers and autoimmune disorders.

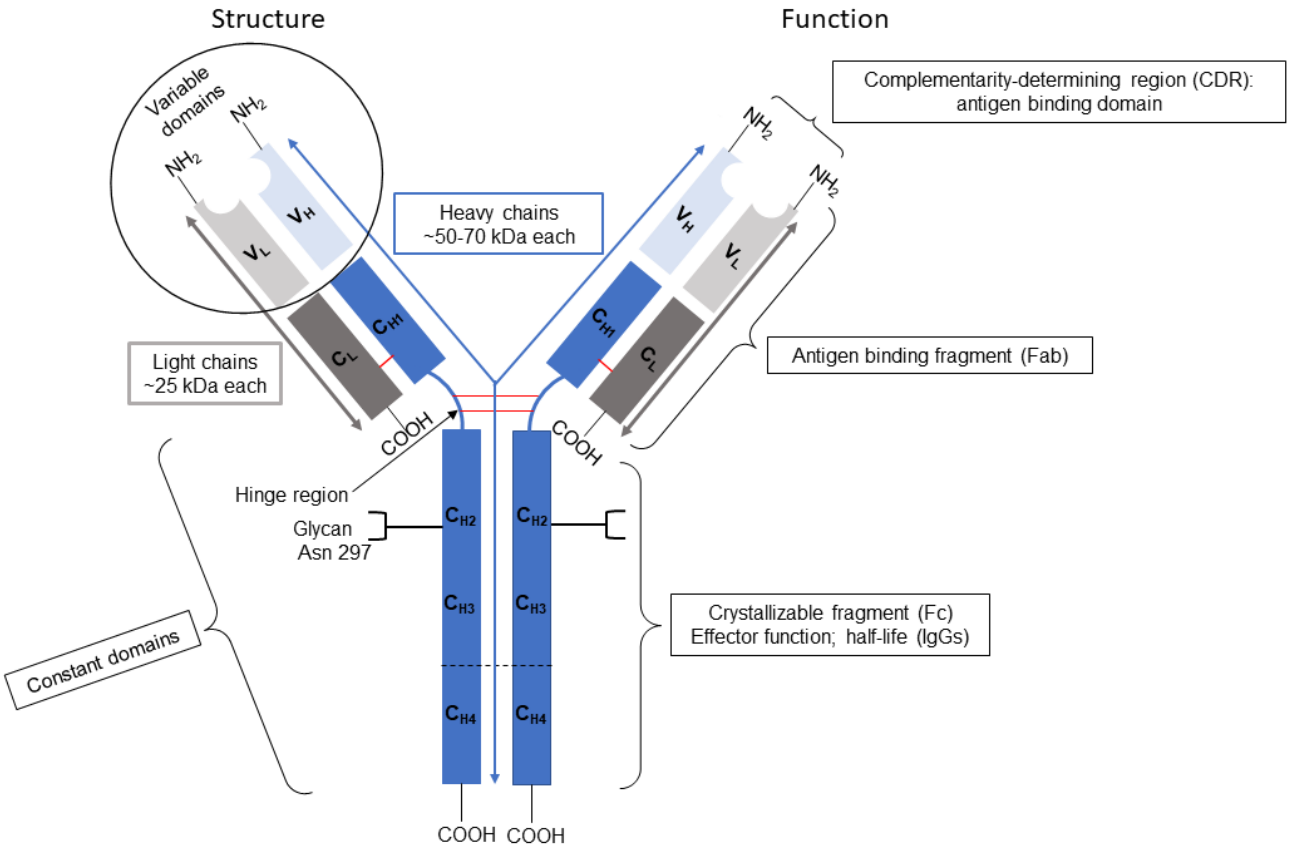

Figure 1.2: Structural and functional domains of an Ig monomer. Antibodies contain two light chains and two heavy chains. Each Ig domain contains a disulfide bond (not shown), while interchain disulfide bonds link the heavy chains in the flexible hinge region and the light chain to the heavy chain (red lines). The constant region of the antibody is referred to as the crystallizable fragment (Fc) which mediates effector function and interactions with FcRn. The two Fab arms contain the antigen binding site (CDR) in the variable domains of the heavy (V_H) and light (V_L) chains. Finally, the antibody is decorated with glycans. The number and sites depend on isotype. As an example, glycans are added at Asn 297 which is the conserved glycan for IgG antibodies.

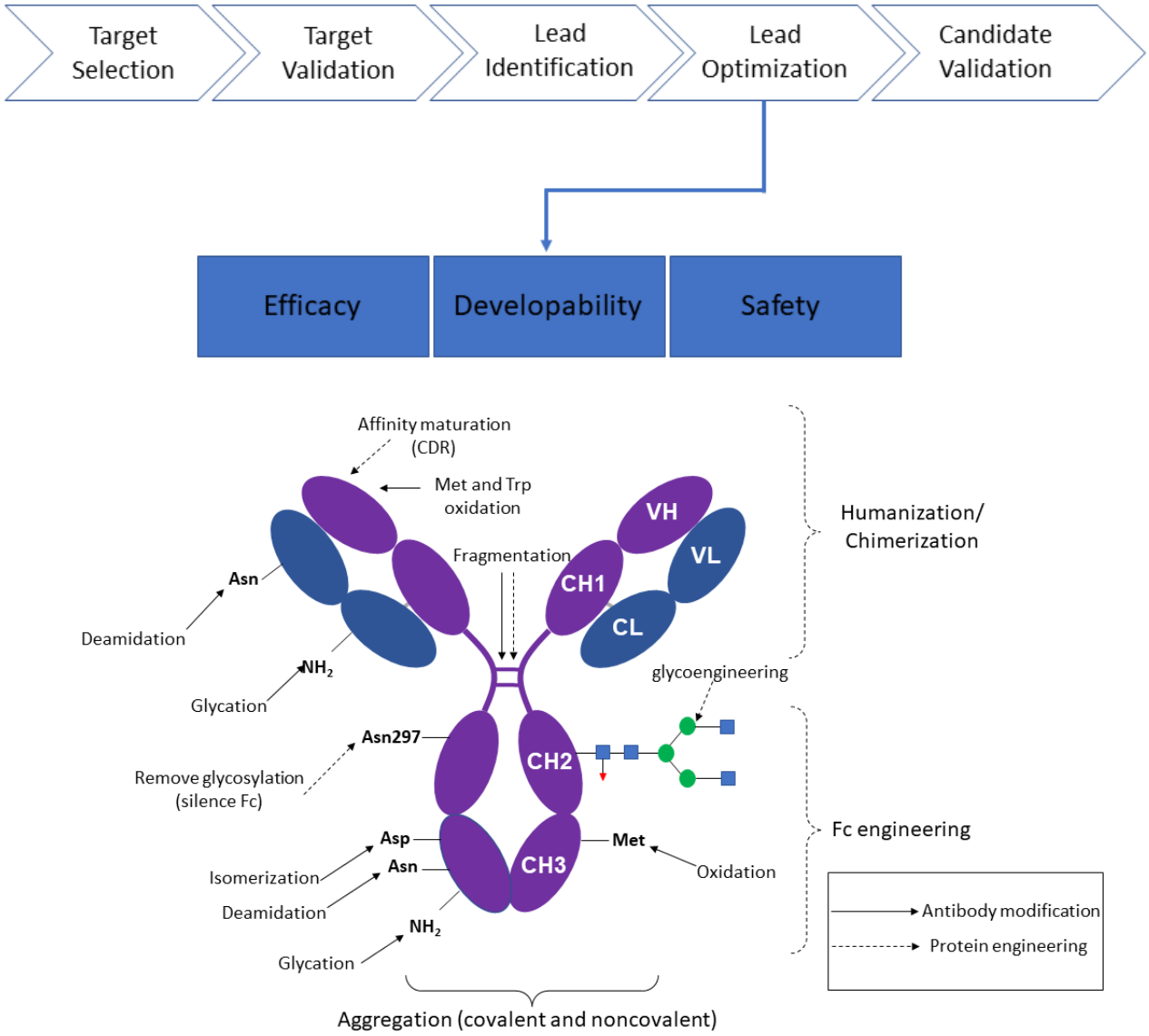

Figure 1.3: Antibody modifications and protein engineering strategies: Optimizing various properties of lead antibody candidates involves various protein engineering strategies some of which are related to post translational modifications.

TABLES

Table 1.1: Properties of human antibody classes

Property	IgA	IgD	IgE	IgG	IgM
Heavy chain	α	δ	ε	γ	μ
subclasses	2	0	0	4	0
Heavy chain Ig domains	4	4	5	4	5
Molecular weight of monomer (kDa)	160	184	188	146-165[a]	194
Oligomeric forms	1-4	1	1	1-2[b]	5-6
Heavy chain N-glycan sites	2-5[c]	3	7	1	5
Heavy chain O-glycan sites	0-9[d]	5	0	0-3[e]	0
Serum level (g/L)	0.5-3[f]	0.03	0.00005	0.5-9[g]	1.5
Serum half-life (days)	6	3	2	7-21[h]	10

[a] IgG1, IgG2, and IgG4 are 146 kDa while IgG3 is 165 kDa.
[b] IgG2 can form monomers and dimers while the other three isotypes form monomers.
[c] IgA1 HC contains 2 N-glycan sites while IgA2 contains 4-5 based on allotype (not discussed).
[d] IgA1 HC contains 9 O-glycan sites (less than 6 are typically occupied) and IgA2 contains zero.
[e] There are no O-glycan sites in IgG1, IgG2, and IgG4 HCs while IgG3 HC contains 3 sites.
[f] There is 3 g/L IgA1 and 0.5 g/L IgA2 in serum.
[g] Serum level (9 g/L, 3 g/L, 1 g/L, 0.5 g/L) depends on subclass where IgG1>IgG2>IgG3>IgG4.
[h] The half-life of IgG1 and IgG4 is 21 days, IgG2 20 days, and IgG3 7 days.

Note: Adapted from "Considerations for the Design of Antibody-based Therapeutics" by Goulet, DR., Atkins, WM, 2020, J of Pharm Sci, 109(1), p.74-103 (doi: 10.1016/j.xphs.2019.05.031).

References

Antibody Society. In: Approved Antibodies. (2022). https://www.antibodysociety.org/resources/approved-antibodies/

Arnold, J. N., Wormald, M. R., Sim, R. B., Rudd, P. M., & Dwek, R. A. (2007). The impact of glycosylation on the biological function and structure of human immunoglobulins. In *Annual Review of Immunology*. https://doi.org/10.1146/annurev.immunol.25.022106.141702

Baek, Y., & Zydney, A. L. (2018). Intermolecular interactions in highly concentrated formulations of recombinant therapeutic proteins. *Current Opinion in Biotechnology*, *53*, 59–64. https://doi.org/10.1016/j.copbio.2017.12.016

Bengt, N. (2006). *Protein Folding Kinetics* (2nd ed.). Springer-Verlag. https://doi.org/10.1007/b138868

Bhattacharya, A., Kim, Y. C., & Mittal, J. (2013). Protein–protein interactions in a crowded environment. *Biophysical Reviews*, *5*(2), 99–108. https://doi.org/10.1007/s12551-013-0111-5

Blumberg, L. J., Humphries, J. E., Jones, S. D., Pearce, L. B., Holgate, R., Hearn, A., Cheung, J., Mahmood, A., Del Tito, B., Graydon, J. S., Stolz, L. E., Bitonti, A., Purohit, S., de Graaf, D., Kacena, K., Andersen, J. T., Christianson, G. J., Roopenian, D. C., Hubbard, J. J., … Blumberg, R. S. (2019). Blocking FcRn in humans reduces circulating IgG levels and inhibits IgG immune complex–mediated immune responses. *Science Advances*. https://doi.org/10.1126/sciadv.aax9586

Brinkmann, U., & Kontermann, R. E. (2017). The making of bispecific antibodies. In *mAbs*. https://doi.org/10.1080/19420862.2016.1268307

Cacia, J., Keck, R., Presta, L. G., & Frenz, J. (1996). Isomerization of an Aspartic Acid Residue in the Complementarity-Determining Regions of a Recombinant Antibody to Human IgE: Identification and Effect on Binding Affinity. *Biochemistry*, *35*(6), 1897–1903. https://doi.org/10.1021/bi951526c

Cheung, M. S., Klimov, D., & Thirumalai, D. (2005). Molecular crowding enhances native state stability and refolding rates of globular proteins. *Proceedings of the National Academy of Sciences of the United States of America*. https://doi.org/10.1073/pnas.0409630102

Czajkowsky, D. M., Hu, J., Shao, Z., & Pleass, R. J. (2012). Fc-fusion proteins: New developments and future perspectives. In *EMBO Molecular Medicine*. https://doi.org/10.1002/emmm.201201379

Dam, T. K., Torres, M., Brewer, C. F., & Casadevall, A. (2008). Isothermal titration calorimetry reveals differential binding thermodynamics of variable region-identical antibodies differing in constant region for a univalent ligand. *Journal of Biological Chemistry*. https://doi.org/10.1074/jbc.M806473200

Diebolder, C. A., Beurskens, F. J., de Jong, R. N., Koning, R. I., Strumane, K., Lindorfer, M. A., Voorhorst, M., Ugurlar, D., Rosati, S., Heck, A. J. R., van de Winkel, J. G. J., Wilson, I. A., Koster, A. J., Taylor, R. P., Ollmann Saphire, E., Burton, D. R., Schuurman, J., Gros, P., & Parren, P. W. H. I. (2014). Complement Is Activated by IgG Hexamers Assembled at the Cell Surface. *Science*, *343*(6176), 1260–1263. https://doi.org/10.1126/science.1248943

Dobson, C. L., Devine, P. W. A., Phillips, J. J., Higazi, D. R., Lloyd, C., Popovic, B., Arnold, J., Buchanan, A., Lewis, A., Goodman, J., Van Der Walle, C. F., Thornton, P., Vinall, L., Lowne, D., Aagaard, A., Olsson, L. L., Wollberg, A. R., Welsh, F., Karamanos, T. K., … Lowe, D. C. (2016). Engineering the surface properties of a human monoclonal antibody prevents self-

association and rapid clearance in vivo. *Scientific Reports*. https://doi.org/10.1038/srep38644
Dunlap, T., & Cao, Y. (2022). Physiological Considerations for Modeling in vivo Antibody-Target Interactions. *Frontiers in Pharmacology*, *13*. https://doi.org/10.3389/fphar.2022.856961
Džupponová, V., Huntošová, V., & Žoldák, G. (2020). A kinetic coupling between protein unfolding and aggregation controls time-dependent solubility of the human myeloma antibody light chain. *Protein Science*, *29*(12), 2408–2421. https://doi.org/10.1002/pro.3968
Farid, S. S., Baron, M., Stamatis, C., Nie, W., & Coffman, J. (2020). Benchmarking biopharmaceutical process development and manufacturing cost contributions to R&D. *MAbs*, *12*(1). https://doi.org/10.1080/19420862.2020.1754999
Filoti, D. I., Shire, S. J., Yadav, S., & Laue, T. M. (2015). Comparative Study of Analytical Techniques for Determining Protein Charge. In *Journal of Pharmaceutical Sciences*. https://doi.org/10.1002/jps.24454
Frutiger, A., Tanno, A., Hwu, S., Tiefenauer, R. F., Vörös, J., & Nakatsuka, N. (2021). Nonspecific Binding - Fundamental Concepts and Consequences for Biosensing Applications. In *Chemical Reviews*. https://doi.org/10.1021/acs.chemrev.1c00044
Fu, Z., Li, S., Han, S., Shi, C., & Zhang, Y. (2022). Antibody drug conjugate: the "biological missile" for targeted cancer therapy. In *Signal Transduction and Targeted Therapy*. https://doi.org/10.1038/s41392-022-00947-7
Goetze, A. M., Liu, Y. D., Zhang, Z., Shah, B., Lee, E., Bondarenko, P. V., & Flynn, G. C. (2011). High-mannose glycans on the Fc region of therapeutic IgG antibodies increase serum clearance in humans. *Glycobiology*. https://doi.org/10.1093/glycob/cwr027
Goulet, D. R., & Atkins, W. M. (2020). Considerations for the Design of Antibody-Based Therapeutics. *Journal of Pharmaceutical Sciences*, *109*(1), 74–103. https://doi.org/10.1016/j.xphs.2019.05.031
Gupta, P., Makowski, E. K., Kumar, S., Zhang, Y., Scheer, J. M., & Tessier, P. M. (2022). Antibodies with Weakly Basic Isoelectric Points Minimize Trade-offs between Formulation and Physiological Colloidal Properties. *Molecular Pharmaceutics*. https://doi.org/10.1021/acs.molpharmaceut.1c00373
Hatters, D. M., Minton, A. P., & Howlett, G. J. (2002). Macromolecular Crowding Accelerates Amyloid Formation by Human Apolipoprotein C-II. *Journal of Biological Chemistry*, *277*(10), 7824–7830. https://doi.org/10.1074/jbc.M110429200
Hay, M., Thomas, D. W., Craighead, J. L., Economides, C., & Rosenthal, J. (2014). Clinical development success rates for investigational drugs. *Nature Biotechnology*, *32*(1), 40–51. https://doi.org/10.1038/nbt.2786
Hintersteiner, B., Lingg, N., Zhang, P., Woen, S., Hoi, K. M., Stranner, S., Wiederkum, S., Mutschlechner, O., Schuster, M., Loibner, H., & Jungbauer, A. (2016). Charge heterogeneity: Basic antibody charge variants with increased binding to Fc receptors. *MAbs*. https://doi.org/10.1080/19420862.2016.1225642
Huh, J. H., White, A. J., Brych, S. R., Franey, H., & Matsumura, M. (2013). The identification of free cysteine residues within antibodies and a potential role for free cysteine residues in covalent aggregation because of agitation stress. *Journal of Pharmaceutical Sciences*. https://doi.org/10.1002/jps.23505
Idusogie, E. E., Wong, P. Y., Presta, L. G., Gazzano-Santoro, H., Totpal, K., Ultsch, M., & Mulkerrin, M. G. (2001). Engineered Antibodies with Increased Activity to Recruit Complement. *The Journal of Immunology*. https://doi.org/10.4049/jimmunol.166.4.2571
Janeway, C. J., Travers, P., & M., W. (2001). *Immunobiology: The Immune System in Health and*

Disease: The interaction of the antibody molecule with spec (5th ed.). Garland Science. https://www.ncbi.nlm.nih.gov/books/NBK27160/

Jiao, M., Li, H.-T., Chen, J., Minton, A. P., & Liang, Y. (2010). Attractive Protein-Polymer Interactions Markedly Alter the Effect of Macromolecular Crowding on Protein Association Equilibria. *Biophysical Journal*, *99*(3), 914–923. https://doi.org/10.1016/j.bpj.2010.05.013

Kamerzell, T. J., Esfandiary, R., Joshi, S. B., Middaugh, C. R., & Volkin, D. B. (2011). Protein–excipient interactions: Mechanisms and biophysical characterization applied to protein formulation development. *Advanced Drug Delivery Reviews*, *63*(13), 1118–1159. https://doi.org/10.1016/j.addr.2011.07.006

Kaplon, H., Chenoweth, A., Crescioli, S., & Reichert, J. M. (2022). Antibodies to watch in 2022. *MAbs*, *14*(1). https://doi.org/10.1080/19420862.2021.2014296

Kim, D. M., Yao, X., Vanam, R. P., & Marlow, M. S. (2019). Measuring the effects of macromolecular crowding on antibody function with biolayer interferometry. *MAbs*, *11*(7), 1319–1330. https://doi.org/10.1080/19420862.2019.1647744

Kiyoshi, M., Caaveiro, J. M. M., Miura, E., Nagatoishi, S., Nakakido, M., Soga, S., Shirai, H., Kawabata, S., & Tsumoto, K. (2014). Affinity improvement of a therapeutic antibody by structure-based computational design: Generation of electrostatic interactions in the transition state stabilizes the antibody-antigen complex. *PLoS ONE*. https://doi.org/10.1371/journal.pone.0087099

Kretschmer, A., Schwanbeck, R., Valerius, T., & Rösner, T. (2017). Antibody Isotypes for Tumor Immunotherapy. In *Transfusion Medicine and Hemotherapy*. https://doi.org/10.1159/000479240

Larsen, H. A., Atkins, W. M., & Nath, A. (2021). Probing interactions of therapeutic antibodies with serum via second virial coefficient measurements. *Biophysical Journal*, *120*(18), 4067–4078. https://doi.org/10.1016/j.bpj.2021.08.007

Lee, J. W. (2013). ADME of monoclonal antibody biotherapeutics: Knowledge gaps and emerging tools. In *Bioanalysis*. https://doi.org/10.4155/bio.13.144

Leeman, M., Choi, J., Hansson, S., Storm, M. U., & Nilsson, L. (2018). Proteins and antibodies in serum, plasma, and whole blood—size characterization using asymmetrical flow field-flow fractionation (AF4). *Analytical and Bioanalytical Chemistry*, *410*(20), 4867–4873. https://doi.org/10.1007/s00216-018-1127-2

Lefranc, M. P., & Lefranc, G. (2020). Immunoglobulins or antibodies: IMGT® bridging genes, structures and functions. In *Biomedicines*. https://doi.org/10.3390/biomedicines8090319

Li, W., Prabakaran, P., Chen, W., Zhu, Z., Feng, Y., & Dimitrov, D. (2016). Antibody Aggregation: Insights from Sequence and Structure. *Antibodies*, *5*(3), 19. https://doi.org/10.3390/antib5030019

Liu, D., Ren, D., Huang, H., Dankberg, J., Rosenfeld, R., Cocco, M. J., Li, L., Brems, D. N., & Remmele, R. L. (2008). Structure and stability changes of human IgG1 Fc as a consequence of methionine oxidation. *Biochemistry*. https://doi.org/10.1021/bi702238b

Liu, H., Ponniah, G., Zhang, H. M., Nowak, C., Neill, A., Gonzalez-Lopez, N., Patel, R., Cheng, G., Kita, A. Z., & Andrien, B. (2014). In vitro and in vivo modifications of recombinant and human IgG antibodies. In *mAbs*. https://doi.org/10.4161/mabs.29883

Liu, R., Oldham, R., Teal, E., Beers, S., & Cragg, M. (2020). Fc-Engineering for Modulated Effector Functions—Improving Antibodies for Cancer Treatment. *Antibodies*, *9*(4), 64. https://doi.org/10.3390/antib9040064

Lu, R. M., Hwang, Y. C., Liu, I. J., Lee, C. C., Tsai, H. Z., Li, H. J., & Wu, H. C. (2020).

Development of therapeutic antibodies for the treatment of diseases. In *Journal of Biomedical Science*. https://doi.org/10.1186/s12929-019-0592-z

Lundahl, M. L. E., Fogli, S., Colavita, P. E., & Scanlan, E. M. (2021). Aggregation of protein therapeutics enhances their immunogenicity: Causes and mitigation strategies. In *RSC Chemical Biology*. https://doi.org/10.1039/d1cb00067e

Ma, J., Mo, Y., Tang, M., Shen, J., Qi, Y., Zhao, W., Huang, Y., Xu, Y., & Qian, C. (2021). Bispecific Antibodies: From Research to Clinical Application. *Frontiers in Immunology*, *12*. https://doi.org/10.3389/fimmu.2021.626616

Mancardi, D., & Daëron, M. (2014). Fc Receptors in Immune Responses. In *Reference Module in Biomedical Sciences*. Elsevier. https://doi.org/10.1016/B978-0-12-801238-3.00119-7

Minton, A. P., & Wilf, J. (1981). Effect of Macromolecular Crowding upon the Structure and Function of an Enzyme: Glyceraldehyde-3-phosphate Dehydrogenase. *Biochemistry*. https://doi.org/10.1021/bi00520a003

Minton, Allen P. (1983). The effect of volume occupancy upon the thermodynamic activity of proteins: some biochemical consequences. *Molecular and Cellular Biochemistry*, *55*(2), 119–140. https://doi.org/10.1007/BF00673707

Muthana, S. M., Xia, L., Campbell, C. T., Zhang, Y., & Gildersleeve, J. C. (2015). Competition between Serum IgG, IgM, and IgA anti-glycan antibodies. *PLoS ONE*. https://doi.org/10.1371/journal.pone.0119298

Natsume, A., In, M., Takamura, H., Nakagawa, T., Shimizu, Y., Kitajima, K., Wakitani, M., Ohta, S., Satoh, M., Shitara, K., & Niwa, R. (2008). Engineered antibodies of IgG1/IgG3 mixed isotype with enhanced cytotoxic activities. *Cancer Research*. https://doi.org/10.1158/0008-5472.CAN-07-6297

Oyama, H., Koga, H., Tadokoro, T., Maenaka, K., Shiota, A., Yokoyama, M., Noda, M., Torisu, T., & Uchiyama, S. (2020). Relation of Colloidal and Conformational Stabilities to Aggregate Formation in a Monoclonal Antibody. *Journal of Pharmaceutical Sciences*, *109*(1), 308–315. https://doi.org/10.1016/j.xphs.2019.10.038

Phillip, Y., Kiss, V., & Schreiber, G. (2012). Protein-binding dynamics imaged in a living cell. *Proceedings of the National Academy of Sciences*, *109*(5), 1461–1466. https://doi.org/10.1073/pnas.1112171109

Pritsch, O., Hudry-Clergeon, G., Buckle, M., Pétillot, Y., Bouvet, J. P., Gagnon, J., & Dighiero, G. (1996). Can immunoglobulin C(H)1 constant region domain modulate antigen binding affinity of antibodies? *Journal of Clinical Investigation*. https://doi.org/10.1172/JCI119033

Reichert, J. (2020). *Bispecific antibodies come to the force*. https://www.antibodysociety.org/antibody-therapeutics-pipeline/bispecific-antibodies-come-to-the-fore/

Roopenian, D. C., & Akilesh, S. (2007). FcRn: The neonatal Fc receptor comes of age. In *Nature Reviews Immunology*. https://doi.org/10.1038/nri2155

Saxena, A., & Wu, D. (2016). Advances in Therapeutic Fc Engineering – Modulation of IgG-Associated Effector Functions and Serum Half-life. *Frontiers in Immunology*, *7*. https://doi.org/10.3389/fimmu.2016.00580

Schroeder, H. W., & Cavacini, L. (2010). Structure and function of immunoglobulins. *Journal of Allergy and Clinical Immunology*. https://doi.org/10.1016/j.jaci.2009.09.046

Sedrak, P., Hsu, K., & Mohan, C. (2003). Molecular signatures of anti-nuclear antibodies - Contribution of heavy chain framework residues. *Molecular Immunology*. https://doi.org/10.1016/S0161-5890(03)00223-2

Sela-Culang, I., Kunik, V., & Ofran, Y. (2013). The structural basis of antibody-antigen recognition. *Frontiers in Immunology*. https://doi.org/10.3389/fimmu.2013.00302

Shields, R. L., Namenuk, A. K., Hong, K., Meng, Y. G., Rae, J., Briggs, J., Xie, D., Lai, J., Stadlen, A., Li, B., Fox, J. A., & Presta, L. G. (2001). High Resolution Mapping of the Binding Site on Human IgG1 for FcγRI, FcγRII, FcγRIII, and FcRn and Design of IgG1 Variants with Improved Binding to the FcγR. *Journal of Biological Chemistry*. https://doi.org/10.1074/jbc.M009483200

Subedi, G. P., & Barb, A. W. (2015). The Structural Role of Antibody N-Glycosylation in Receptor Interactions. *Structure*. https://doi.org/10.1016/j.str.2015.06.015

Sukenik, S., Sapir, L., Gilman-Politi, R., & Harries, D. (2013). Diversity in the mechanisms of cosolute action on biomolecular processes. *Faraday Discussions*. https://doi.org/10.1039/c2fd20101a

Tang, Y., Cain, P., Anguiano, V., Shih, J. J., Chai, Q., & Feng, Y. (2021). Impact of IgG subclass on molecular properties of monoclonal antibodies. *MAbs*, *13*(1). https://doi.org/10.1080/19420862.2021.1993768

Tang, Y., & Cao, Y. (2021). Modeling pharmacokinetics and pharmacodynamics of therapeutic antibodies: Progress, challenges, and future directions. *Pharmaceutics*. https://doi.org/10.3390/pharmaceutics13030422

Tiwari, A., Abraham, A. K., Harrold, J. M., Zutshi, A., & Singh, P. (2017). Optimal Affinity of a Monoclonal Antibody: Guiding Principles Using Mechanistic Modeling. *AAPS Journal*. https://doi.org/10.1208/s12248-016-0004-1

Torres, M., Fernández-Fuentes, N., Fiser, A., & Casadevall, A. (2007). The immunoglobulin heavy chain constant region affects kinetic and thermodynamic parameters of antibody variable region interactions with antigen. *Journal of Biological Chemistry*. https://doi.org/10.1074/jbc.M700661200

Ulitzka, M., Carrara, S., Grzeschik, J., Kornmann, H., Hock, B., & Kolmar, H. (2020). Engineering therapeutic antibodies for patient safety: Tackling the immunogenicity problem. In *Protein Engineering, Design and Selection*. https://doi.org/10.1093/protein/gzaa025

Van Den Berg, B., Wain, R., Dobson, C. M., & Ellis, R. J. (2000). Macromolecular crowding perturbs protein refolding kinetics: Implications for folding inside the cell. *EMBO Journal*. https://doi.org/10.1093/emboj/19.15.3870

Van Der Graaf, P. H., & Gabrielsson, J. (2009). Pharmacokinetic-pharmacodynamic reasoning in drug discovery and early development. In *Future Medicinal Chemistry*. https://doi.org/10.4155/fmc.09.124

van der Horst, H. J., Nijhof, I. S., Mutis, T., & Chamuleau, M. E. D. (2020). Fc-engineered antibodies with enhanced fc-effector function for the treatment of b-cell malignancies. In *Cancers*. https://doi.org/10.3390/cancers12103041

Van Erp, E. A., Luytjes, W., Ferwerda, G., & Van Kasteren, P. B. (2019). Fc-mediated antibody effector functions during respiratory syncytial virus infection and disease. In *Frontiers in Immunology*. https://doi.org/10.3389/fimmu.2019.00548

Vauquelin, G., & Charlton, S. J. (2010). Long-lasting target binding and rebinding as mechanisms to prolong in vivo drug action. *British Journal of Pharmacology*, *161*(3), 488–508. https://doi.org/10.1111/j.1476-5381.2010.00936.x

Vidarsson, G., Dekkers, G., & Rispens, T. (2014). IgG Subclasses and Allotypes: From Structure to Effector Functions. *Frontiers in Immunology*, *5*. https://doi.org/10.3389/fimmu.2014.00520

Wang, B., Kankanamalage, S. G., Dong, J., & Liu, Y. (2021). Optomization of therapeutic antibodies. *Antibody Therapeutics*, *4*(1), 45–54. https://doi.org/doi:10.1093/abt/tbab003

Wang, Q., Chen, Y., Park, J., Liu, X., Hu, Y., Wang, T., McFarland, K., & Betenbaugh, M. J. (2019). Design and Production of Bispecific Antibodies. *Antibodies*, *8*(3), 43. https://doi.org/10.3390/antib8030043

Wang, W., Vlasak, J., Li, Y., Pristatsky, P., Fang, Y., Pittman, T., Roman, J., Wang, Y., Prueksaritanont, T., & Ionescu, R. (2011). Impact of methionine oxidation in human IgG1 Fc on serum half-life of monoclonal antibodies. *Molecular Immunology*. https://doi.org/10.1016/j.molimm.2010.12.009

Wang, X., Phan, M. M., Li, J., Gill, H., Williams, S., Gupta, N., Quarmby, V., & Yang, J. (2020). Molecular Interaction Characterization Strategies for the Development of New Biotherapeutic Antibody Modalities. *Antibodies*, *9*(2), 7. https://doi.org/10.3390/antib9020007

Wei, Z., Feng, J., Lin, H.-Y., Mullapudi, S., Bishop, E., Tous, G. I., Casas-Finet, J., Hakki, F., Strouse, R., & Schenerman, M. A. (2007). Identification of a Single Tryptophan Residue as Critical for Binding Activity in a Humanized Monoclonal Antibody against Respiratory Syncytial Virus. *Analytical Chemistry*, *79*(7), 2797–2805. https://doi.org/10.1021/ac062311j

Wright, R. T., Hayes, D. B., Stafford, W. F., Sherwood, P. J., & Correia, J. J. (2018). Characterization of therapeutic antibodies in the presence of human serum proteins by AU-FDS analytical ultracentrifugation. *Analytical Biochemistry*, *550*, 72–83. https://doi.org/10.1016/j.ab.2018.04.002

Xiang, J., Sha, Y., Jia, Z., Prasad, L., & Delbaere, L. T. J. (1995). Framework Residues 71 and 93 of the Chimeric B72.3 Antibody are Major Determinants of the Conformation of Heavy-chain Hypervariable Loops. In *Journal of Molecular Biology*. https://doi.org/10.1006/jmbi.1995.0560

Yan, B., Steen, S., Hambly, D., Valliere-Douglass, J., Vanden Bos, T., Smallwood, S., Yates, Z., Arroll, T., Han, Y., Gadgil, H., Latypov, R. F., Wallace, A., Lim, A., Kleemann, G. R., Wang, W., & Balland, A. (2009). Succinimide formation at Asn 55 in the complementarity determining region of a recombinant monoclonal antibody IgG1 heavy chain. *Journal of Pharmaceutical Sciences*. https://doi.org/10.1002/jps.21655

Yang, D., Kroe-Barrett, R., Singh, S., & Laue, T. (2019). IgG Charge: Practical and Biological Implications. *Antibodies*, *8*(1), 24. https://doi.org/10.3390/antib8010024

Yu, J., Song, Y., & Tian, W. (2020). How to select IgG subclasses in developing anti-tumor therapeutic antibodies. *Journal of Hematology & Oncology*, *13*(1), 45. https://doi.org/10.1186/s13045-020-00876-4

Zhang, J., Woods, C., He, F., Han, M., Treuheit, M. J., & Volkin, D. B. (2018). Structural Changes and Aggregation Mechanisms of Two Different Dimers of an IgG2 Monoclonal Antibody. *Biochemistry*. https://doi.org/10.1021/acs.biochem.8b00575

Zhou, Y.-L., Liao, J.-M., Chen, J., & Liang, Y. (2006). Macromolecular crowding enhances the binding of superoxide dismutase to xanthine oxidase: Implications for protein–protein interactions in intracellular environments. *The International Journal of Biochemistry & Cell Biology*, *38*(11), 1986–1994. https://doi.org/10.1016/j.biocel.2006.05.012

Zhou, Z., Fan, J. B., Zhu, H. L., Shewmaker, F., Yan, X., Chen, X., Chen, J., Xiao, G. F., Guo, L., & Liang, Y. (2009). Crowded cell-like environment accelerates the nucleation step of amyloidogenic protein misfolding. *Journal of Biological Chemistry*. https://doi.org/10.1074/jbc.M109.002832

CHAPTER 2

Probing Interactions of Therapeutic Antibodies with Serum via Second Virial Coefficient Measurements

Note: This chapter was adapted with permission from:
Larsen HA, Atkins WM, Nath A. Probing interactions of therapeutic antibodies with serum via second virial coefficient measurements **2021**, 120(18):4067-4078. © 2021 Biophysical Journal

2.1 Introduction

Biologics, or protein-based therapeutics, show great promise in treating aggressive cancers, chronic autoimmune conditions, and many other disease states (Lu et al., 2020). Antibody-based therapeutics, which are a subset of biologics, have emerged as the fastest growing drug class on the market, and often display superior versatility, specificity, and affinity (Goulet & Atkins, 2020). Platforms including conventional monoclonal antibodies (mAbs), bispecific Abs (bsAbs), antibody-drug conjugates (ADCs), Fab fragments, and Fc-fusion proteins have been used successfully in the clinic (AlDeghaither et al., 2015; Lambour et al., 2016; Leal et al., 2014). However, new variations of biologics appear in the literature or in pharmaceutical pipelines much more frequently than they reach the clinic or market (Hay et al., 2014). The inefficient commercial development of biologics reflects the inherent complexity of proteins. Furthermore, our understanding of factors controlling the pharmacokinetics (PK) and disposition of these drugs is extremely limited in comparison to small molecule drugs (Shi, 2014). Biologics interact with their targets and receptors in complex, crowded biological environments such as serum and the endosomal lumen. These biological fluids are not adequately represented in ideal buffer systems used for *in vitro* characterization, which may contribute to the gaps in our knowledge surrounding

PK and disposition. One approach to understanding these effects is to investigate how crowded environments affect the biophysical properties of therapeutic antibodies.

Macromolecular crowding is a phenomenon that has been studied extensively and traditionally explained by entropy-driven excluded volume effects (Ellis, 2001). Many studies aimed at investigating these effects have utilized various polymers, PEGs, or proteins as crowding molecules to mimic biological environments (Minton, 1983, 1998; Wills et al., 1995; Zhou & Dill, 2001). These approaches have many shortcomings, because biological environments are highly concentrated with diverse macromolecules (proteins, lipids, nucleic acids, polysaccharides, etc.). Typical biochemical studies that explore macromolecular crowding are carried out in dilute solutions (1–10 g/L), which are drastically different from biological macromolecular concentrations (50–400 g/L) (Biswas et al., 2018). Excluded volume effects alone enhance stability of proteins by shifting the conformational equilibrium to a more compact state. The equilibrium affinity of proteins for their binding partners may also increase as a result of crowding (Minton, 1983, 1998; Zhou & Dill, 2001). However, these proposed effects do not address the possibility of enthalpically-based weak interactions between proteins and other solutes, which have the potential to negatively impact binding affinity and stability. The complex effects of crowding on therapeutic efficacy and disposition of protein-based therapeutics have not been documented.

The framework of thermodynamic nonideality is often used to describe the weak interactions a protein may encounter in solution (Saluja & Kalonia, 2008). Strong interactions are routinely probed using a variety of techniques capable of measuring equilibrium binding constants, while weak interactions are less studied and can be more difficult to probe. The second virial coefficient (B_2) parameter quantifies such weak interactions and has been used to understand many biophysical properties of proteins in solution such as crystallization, solubility, stability,

aggregation, and diffusion (George & Wilson, 1994; Quigley & Williams, 2015; Velev et al., 1998; Wilson & DeLucas, 2014; Yadav, Scherer, et al., 2011). In general, negative values of second virial coefficients indicate attractive interactions between particles in solution, and positive values indicate repulsive interactions. Self- and cross-term second virial coefficients are used to describe homo- or hetero-interactions, respectively. Methods to determine second virial coefficients include various light scattering techniques (SLS, DLS, CG-MALS) (Ma et al., 2015; Velev et al., 1998; Yadav, Scherer, et al., 2011), self-interaction chromatography (SIC) (Quigley & Williams, 2015), size-exclusion chromatography (SEC) (Bloustine et al., 2003), membrane osmometry (MO) (Moon et al., 2000), and analytical ultracentrifugation (AUC) (Behlke & Ristau, 1999). Each of these techniques has its advantages and limitations. For example, DLS is rapid and well-established, but is highly sensitive to aggregates and impurities and is limited to measuring self-term nonideality, while AUC is capable of measuring both self- and cross-term nonideality but is expensive and time consuming.

Because aggregation is a common obstacle in biologics development, many studies have focused on self-term virial coefficients as a predictor of aggregation propensity (Quigley & Williams, 2015; Saito et al., 2012). Cross-interactions of mAbs in solution are not as commonly studied. In this study, we present fluorescence correlation spectroscopy (FCS) as an orthogonal method for calculating both self- and cross-term second virial coefficients. FCS is relatively simple to implement and has the capability of measuring the diffusive properties of molecules in complex media. Recently, AUC measurements have been used to investigate weak interactions between mAbs and serum components through the determination of cross-term virial coefficients for isolated components (Wright et al., 2018). However, our findings suggest that this reductionist approach may fail to provide a complete representation of the nonideal behavior of mAbs in

biological environments. FCS provides an alternative approach to measure an apparent second virial coefficient, $B_{2,app}$, for the "bulk environment" for six different mAbs in fetal bovine serum (FBS). These measurements serve to probe the global nonideality of mAbs in serum, rather than cross-terms between specific components, to better understand the forces acting on therapeutics once introduced into a patient. The advantage of this approach is that it incorporates the net entropic and enthalpic effect of all solution components, rather than the effects of single pair-wise interactions. While this study investigates mAbs in serum, this approach has the potential to be expanded to other antibody platforms, protein systems, and biological fluids. The ability to probe nonideality directly in biological fluids could help reveal the impacts of weak interactions on the biophysical properties of biologics in relevant environments.

2.2 Theory

2.2.1 Second virial coefficient (B_2) and interaction parameter (k_D)

The virial coefficients describe deviations from ideal behavior in fluids due to pair-wise or higher-order interactions among the constituent molecules. So, for example, pressure P can be expressed as a virial equation in terms of a power series in the number density ρ (n/V):

$$P = RT(\rho + B_2(T)\rho^2 + B_3(T)\rho^3 + \cdots) \quad (1)$$

where R is the gas constant, T is temperature, and B_n is the nth virial coefficient which corresponds to interactions between n molecules (Saluja & Kalonia, 2008). Similarly, the virial coefficients capture deviations from ideality in osmotic pressure Π:

$$\Pi = \frac{RT}{M}(c_p + B_2c_p^2 + B_3c_p^3 + \cdots + B_ic_p^i + \cdots) \quad (2)$$

Here, c_p is the mass concentration and M is the molecular weight. The sign of the virial coefficient indicates whether pressure is higher or lower than an ideal fluid. For example, if B_2 is positive,

then the pressure is higher than an ideal fluid due to repulsive pairwise intermolecular interactions between molecules. Conversely, a negative B_2 indicates attractive pairwise interactions between molecules. For the remainder of this paper, we neglect the third- and higher-order terms, which are in general much smaller than the second-order term at biologically relevant concentrations.

Virial coefficients also affect the diffusion of molecules, since repulsive and attractive interactions result in greater and less displacement, respectively, in a given time period. The diffusive properties of molecules can therefore be used to determine second virial coefficients, following the derivation of Harding and Johnston (Harding & Johnson, 1985). In ideal, dilute solutions, the diffusion coefficient is related to the hydrodynamic radius R_H as expressed by the Stokes-Einstein equation:

$$D^0 = \frac{k_B T}{6\pi\eta R_H} \quad \text{.....(3)}$$

where k_B is Boltzmann's constant, T is absolute temperature, and η is viscosity. The diffusion coefficient in the presence of higher concentrations of solute or co-solutes is also related to the concentration gradient of the osmotic pressure, and hence the virial coefficients, as follows:

$$D = D^0\left(\frac{M(1-\bar{V}c_p)}{RT}\frac{\partial \Pi}{\partial c_p}\right) \quad \text{.....(4)}$$

Here, $\bar{V}$ represents the partial specific volume, which is usually assumed to be a constant equal to ~0.7 mL/g for globular proteins. Differentiating **Equation 2** with respect to concentration yields:

$$\frac{\partial \Pi}{\partial c_p} = \frac{RT}{M}(1 + 2B_2 M c_p + \cdots) \quad \text{.....(5)}$$

Substituting **Equation 5** into **Equation 4** and simplifying then results in the following relationship, which is accurate to the first order:

$$D = D^0(1 + (2B_2M - \bar{V})c_p) = D^0(1 + k_D c_p) \quad \text{.....(6)}$$

To reiterate, here D is the diffusion coefficient observed at a given concentration of solute or co-solutes (corrected for changes in the bulk viscosity of the solution), D^0 is the diffusion coefficient in dilute solution, M is molecular weight of unlabeled species, B_2 is the second osmotic virial coefficient, c_p is the concentration of the unlabeled species (g/ml), and k_D is the diffusion interaction parameter defined by:

$$k_D = 2B_2M - \bar{V} \approx 2B_2M \quad \text{.....(7)}$$

With a complex mixture such as serum, the appropriate value of M (i.e., the effective molecular weight of the various interacting species) is not clear. Reporting results in terms of k_D or $2B_2M$, rather than B_2, avoids this problem.

Note that k_D is distinct from the equilibrium dissociation constant K_D or the dissociation rate constant k_d. Furthermore, our definition of k_D differs from many earlier works (Chaturvedi et al., 2018; Saluja et al., 2010; Wright et al., 2018) that also include a sedimentation interaction parameter k_s. Our correction for changes in bulk solvent viscosity, described in the FCS section below, removes the need to include or estimate this parameter explicitly. This is advantageous because k_s determination typically requires time-consuming and expensive SV-AUC experiments. We and others (Blanco et al., 2014; Connolly et al., 2012; Lehermayr et al., 2011) therefore report k_D values, which are proportional to $2B_2M$ and can conveniently quantify thermodynamic nonideality.

As can be seen from **Equation 6**, when the diffusion coefficient is plotted against solute or co-solute concentration, the slope of the line divided by the y-intercept (D^0) yields k_D. FCS and DLS are very similar in that they both measure changes in intensity over time to determine

translational diffusion coefficients. DLS monitors changes in the intensity of scattered light while FCS monitors changes in fluorescence intensity, but determination of the second virial coefficient from measured diffusion coefficients is essentially the same. Depending on whether the molecule of interest is monitored in the presence of increasing concentrations of itself or of other co-solutes, the diffusion interaction parameter represents self-term nonideality (denoted as k_{22} or B_{22}), or cross-term nonideality (denoted as k_{12} or B_{12}) respectively to represent intermolecular interactions between two of the same molecules or two different types of molecules, respectively. When measuring k_{12}, intermolecular interactions between two labeled molecules (denoted as k_{11}) are considered negligible due to the low concentration of tracer (<100 nM).

2.2.2 Dynamic light scattering (DLS)

Particles in solution are in Brownian motion and this constant, random motion causes the intensity of scattered light to fluctuate as a function of time. For a single diffusing species, DLS intensity time traces can be fit to the following correlation function (Stetefeld et al., 2016):

$$G_{DLS}(\tau) = \langle I(t)I(t+\tau)\rangle = A\left[1 + Be^{2D_T q^2 \tau}\right] \quad (8)$$

where τ is the autocorrelation lag time of the correlator, q^2 is the Bragg wave vector, D is the translational diffusion constant, and A and B respectively represent the baseline and intercept of the correlation function. For a monodisperse system, q^2 depends on the solvent refractive index n, wavelength of incident light λ, and scattering angle θ as follows:

$$q = \frac{4\pi n}{\lambda} \sin(\theta/2) \quad (9)$$

However for polydisperse samples, a variety of analytical approaches have been developed to account for unimodal or multimodal particle size distributions (Stetefeld et al., 2016). Using such approaches, it is possible to estimate the diffusion coefficient of the species of interest.

2.2.3 Fluorescence correlation spectroscopy (FCS)

FCS measures the diffusive properties of low concentrations of fluorescent molecules as they move through a well-defined, confocal detection volume. FCS relies on understanding how the fluorescence intensity fluctuates over time. From an intensity time trace, an autocorrelation is calculated and may be fit to yield the diffusion time, τ_D using the following equation (Haustein & Schwille, 2007):

$$G_{FCS}(\tau) = \frac{\langle \delta F(t) \delta F(t+\tau) \rangle}{\langle F(t) \rangle^2} = \frac{1}{N}\left(\frac{1}{1+{}^{\tau}/_{\tau_D}}\right)\sqrt{\frac{1}{1+{}^{s^2\tau}/_{\tau_D}}} \quad \text{.....(10)}$$

where N is the mean number of molecules in observation volume, τ_D is the correlation decay time due to translational diffusion, and *s* is the axial ratio of the detection volume (0.2 for our instrument). The diffusion time obtained from fitting FCS traces relate to the diffusion coefficients as follows:

$$D = \frac{\omega^2}{4\tau_D} \quad \text{.....(11)}$$

where ω is the radius of the confocal volume in the radial direction. In this study, ω^2 was experimentally determined based on the diffusion time of a dye standard (see Experimental Procedures) with known Stokes radius in buffer, using the following equation:

$$\omega^2 = 4D\tau_D = \frac{4k_B T \tau_D}{6\pi\eta R_H} \quad \text{.....(12)}$$

In order to measure k_D using a D vs. c plot (**Equation 6**), it is necessary to correct for changes in bulk solution viscosity, so that the observed dependence of diffusion time of labeled protein (at a constant, low nM concentration) depends solely on the second virial interactions with unlabeled carrier proteins (the identical protein for B_{22} measurements, a different protein for B_{12} measurements, or a complex mixture such as serum for $B_{2,app}$ measurements). Therefore, the

viscosity of carrier protein stocks were measured by FCS using a dye standard. Viscosity was measured at each carrier protein concentration used in this study, and varied linearly with concentration over the experimental range (see **Figure 2.1**). This is consistent with trends in the literature under the same concentration regime for BSA (Yadav, Shire, et al., 2011). Importantly, this approach also simultaneously corrects for changes in refractive index in the carrier protein solutions. Diffusion times were then scaled by the fold change in viscosity:

$$\tau_{D,adj} = \tau_D \eta / \eta' \quad \text{.....(13)}$$

where τ_D is the observed diffusion time, η is the buffer viscosity, and η' is the viscosity of the carrier protein solution. These adjusted diffusion times measured over a range of carrier protein concentrations were used to calculate diffusion coefficients using **Equation 11**, which were then fit to **Equation 6** to yield a k_D (or $2B_2M$) value.

2.3 Experimental procedures

2.3.1 Protein samples and other materials

Bovine serum albumin (factor V and protease free) was purchased as a lyophilized powder from GoldBio (St. Louis, MO). Recombinant human serum albumin (HSA) was purchased from Albumin Bioscience (Huntsville, AL). Materials were reconstituted according to the manufacturer's suggestions. The NIST mAb humanized IgG1 antibody (10 mg/mL) was purchased from the National Institutes of Standards and Technology (RM 8617). Tocilizumab (35 mg/mL) and Carlumab (4 mg/mL) IgG antibodies were provided by the Genentech Outgoing Materials Transfer Agreement program and by Janssen Pharmaceuticals, respectively.

Transient expression of Human anti-respiratory syncytial virus F405L and anti-gp120 K409R IgG1 mAbs was carried out in Expi293F cells (Thermo Fisher A14635) using a 1:3 ratio

of heavy chain (HC) to light chain (LC) DNA according to the manufacturer's protocol. Purification was performed via Protein A column in 1x phosphate buffered saline (PBS: 150 mM NaCl, 2.7 mM KCl, 10 mM Na_2HPO_4) pH 7.2. Briefly, supernatant was loaded onto the protein A column, washed with PBS, and eluted with 100 mM sodium citrate, pH 3.5 into 1.0-mL fractions. Ab-containing fractions (based on A280 UV-signal) were pooled and immediately buffer exchanged into 1x PBS using Zeba Spin Desalting columns (Thermo Scientific), following the manufacturer's protocol.

FCS and DLS experiments were run in phosphate-buffered saline (PBS: 150 mM NaCl, 2.7 mM KCl, 10 mM Na_2HPO_4, and 1.8 mM KH_2PO_4, pH 7.4 or 6.0). The antibodies and HSA were stored at 4°C in PBS pH 7.4, while BSA was stored in PBS pH 7.4 or 6.0 depending on the experiment. Fetal bovine serum (FBS) was purchased from Thermo Scientific (A3160401) and was stored in 1 mL aliquots at -20°C until use. The serum was thawed at 4°C before each experiment and used no more than 24h after thawing.

2.3.2 Generation of bispecific antibody (bsAb)

Parental antibodies, anti-RSV F405L and anti-gp120 K409R, containing complementary mutations, were used to generate the bsAb through controlled Fab-arm exchange (cFAE). Briefly, 0.5 mg of each mAb were co-incubated with 75 mM mercaptoethylamine (MEA) for five hours at room temperature with mixing (300 rpm in a ThermoMixer), followed by dialysis into PBS to remove MEA and allow re-oxidation of hinge disulfide bonds. The bsAb product was verified via hydrophobic interaction chromatography (HIC), where the bsAb resolved as a single peak between the two parental mAb peaks.

2.3.3 Protein labeling

Following the Thermo Scientific labeling protocol, the NIST mAb, tocilizumab, carlumab, anti-gp120 mAb, anti-RSV mAb, bsAb, and BSA were labeled with Alexa Fluor 488 carboxylic acid, succinimidyl ester (A488; Thermo Scientific). Desalting was carried out using Zeba Spin Desalting Columns (Thermo Scientific), following the manufacturer's protocol. Typically, 1–2 A488 molecules covalently attached to each mAb, while 0.7–1 molecule of A488 covalently attached to BSA. Labeling efficiency was determined through UV-Vis spectroscopy (at 280 nm and 494 nm) on a Nanodrop One Microvolume Uv-Vis spectrometer (Thermo Scientific, ND-ONE-W) as well as through diffusion time (change from free dye to protein-bound dye) (see example below). A488-mAbs and A488-BSA were stored in 1x PBS pH 7.4 at 4°C.

2.3.4 Determination of fluorescent dye labeling efficiency for BSA model system

The concentration of Alexa Fluor 488 SE and A488-labeled BSA (A488-BSA) were determined via absorbance measurements to determine the labeling ratio from the following relationships:

$$[Alexa488\ SE] = \frac{A_{494} \times dilution\ factor}{\ell \times \varepsilon_{A488\ SE}}$$

$$[labeled\ BSA] = \frac{(A_{280} - 0.11(A_{494})) \times dilution\ factor}{\ell \times \varepsilon_{BSA}}$$

$$labeling\ ratio\ (dye{:}protein) = \frac{[A488\ SE]}{[labeled\ BSA]}$$

where A represents the absorbance at either 280 nm or 494 nm, ℓ represents the path length (1 cm), and ε represents the extinction coefficient of either BSA (280 nm) or Alexa488 SE (494 nm). A correction factor of 0.11 is used to account for the contribution of Alexa488 SE to the absorbance at 280 nm based on extinction coefficients provided by the manufacturer (Johnson, 2010).

The change in diffusion time between Alexa488 SE and A488-labeled BSA was also used to support labeling efficiency determination by comparing the observed change to the expected fold change in diffusion time. The expected fold change in diffusion time can be estimated as follows:

$$\frac{\tau_{D,BSA}}{\tau_{D,dye}} = \sqrt[3]{\frac{MW_{BSA}}{MW_{dye}}} = \sqrt[3]{\frac{66{,}463\ Da}{643.4\ Da}} \approx 4.7$$

where $\Delta\tau_D$ represents the change in diffusion time and ΔMW represents the change in molecular weight, in this case between Alexa488 SE and BSA (**Table 2.1**).

2.3.5 Fluorescence correlation spectroscopy (FCS)

All experiments were carried out at room temperature on a home-built instrument based on a Zeiss Axio Observer D1 microscope equipped with Hydra-Harp 400 detection electronics, Tau-SPAD photon counting detector, and pulsed 485 nm laser line driven by a PicoQuant PDL 828 Sepia II driver (PicoQuant GmbH, Berlin, Germany). Sample aliquots of 50 µL were placed on a 22x22 cover glass (VWR 48366-067). Five 30 s measurements of 10 nM A488 were used to calibrate the instrument at the start of each experiment. The average diffusion time was used to determine the ω^2 parameter needed for second virial coefficient calculations. Antibody and BSA measurements (n=5) were carried out for 60s each.

A488-labeled antibodies or BSA were diluted to ~20 nM in varying concentrations of carrier protein (FBS, HSA, or BSA), ranging from 0% to 100%, where the 100% condition ranged from 36–46 mg/mL depending on the experiment. FCS traces were imported into Prism Graphpad software and fit to a single component FCS equation to yield the average diffusion times at each carrier concentration. These diffusion times were then used to calculate the translational diffusion coefficients at each carrier concentration. Diffusion coefficients D were corrected for changes in viscosity and plotted against carrier protein concentration c. D vs. c plots were fit to **Equation 6** to determine k_D and D^0. Standard deviations were calculated based on three independent experiments (apart from bsAb, n=2) with fresh samples.

2.3.6 Viscosity determination of carrier protein solutions using linear interpolation

The density and viscosity of PBS were measured using an Anton Paar (DMA50000M) densitometer and Anton Paar Automated micro viscometer (AMVn). The viscosity of carrier protein stocks (BSA, HSA, and FBS) was measured by FCS, using A488 (R_H = 5.80 x 10^{-8} cm (Heyman & Burt, 2008)) as a standard. A stock of A488 was diluted 1000-fold into 150 mM Tris HCl pH 7.4, so that the tris buffer passivated the succinimidyl ester moiety to prevent interaction with other amines present in carrier solutions. This passivated A488 was further diluted to 10nM in PBS or carrier protein solutions. The diffusion time of A488 in PBS was used to determine ω^2 from the previously determined viscosity value using **Equation 12** as described in the above Theory section.

To determine the viscosity of carrier protein solutions, the radial dimension of the FCS observation volume (ω^2 parameter) was first determined from the diffusion time of Alexa488 SE with known Stokes radius (R_H) in 1x phosphate-buffered saline (PBS) pH 7.4 with predetermined

viscosity (via densitometer and viscometer measurements as outlined above) (η) through the following relationship:

$$\omega^2 = 4D\tau_D = \frac{4k_BT\tau_D}{6\pi\eta R_H}$$

Since the ω^2 value does not significantly change over the relevant concentration ranges of carrier protein (Sherman et al., 2008), the same value can be used to determine the viscosity of carrier protein solutions (BSA, HSA, and FBS) at varying concentrations ranging from 0% (PBS) to 100% using the Stokes-Einstein equation:

$$D = \frac{\omega^2}{4\tau_D}$$

$$\eta = \frac{k_BT}{6\pi D R_H}$$

To verify linearity in the viscosity, solutions of BSA (40 mg/mL), HSA (34 mg/mL), and FBS (38 mg/mL) were prepared in PBS pH 7.4 at concentrations similar to experimental conditions. Intermediate concentrations of carrier (25%, 50%, and 75%) were prepared by diluting neat protein solutions in PBS pH 7.4. Ten 30 sec FCS measurements of passivated Alexa Fluor 488 (~20nM) were carried out at each carrier concentration. The average diffusion time of Alexa Fluor 488 in PBS, with predetermined viscosity, was used to determine the ω^2 parameter, which was also used to determine the viscosity at all other conditions as described above. In each case, the viscosity was determined to be linear (**Figure 2.1**). Therefore, the viscosity values in subsequent FCS and DLS experiments were determined from linear interpolation of the above data based on neat carrier protein concentrations.

2.3.7 Brightness per particle calculation for BSA model system

Brightness per particle was calculated (**Table 2.2**) by measuring the average intensity <*I*> over the course of an FCS measurement and dividing by the number of molecules, *N*, obtained by least-squares fitting of the autocorrelation to the following equation:

$$G_{FCS}(\tau) = \frac{1}{N}\left(\frac{1}{1 + {}^{\tau}/_{\tau_D}}\right)\sqrt{\frac{1}{1 + {}^{s^2\tau}/_{\tau_D}}}$$

where τ_D is the translational diffusion time and *s* is the axial ratio of the detection volume (fixed to 0.2).

2.3.8 Dynamic light scattering (DLS)

All DLS experiments were carried out on a DynaPro Nanostar analyzer (Wyatt Technology) equipped with Dynamics V7 software. BSA samples (100 µL) were spun at 14,000 RPM for 25 minutes at 25°C on an Eppendorf 5415C centrifuge (Brinkmann Instrument Inc) to avoid dust in samples. A quartz cuvette was loaded with ~10 µL of sample directly from the centrifuge tube. Diffusion coefficient measurements (n=20) were carried out at 25°C with a 5 s acquisition time. Viscosity corrections were carried out automatically in the DLS software by adding predetermined viscosity values into the sample parameters for each sample. Data were fit using the regularization analysis in Dynamics V7 (Wyatt Technology) software to generate an intensity versus diffusion coefficient histogram. The average diffusion coefficient of the most intense peak (which represents the monomeric species) was used to calculate k_D or $B_{22}M$. Using the average diffusion coefficient of the complete distribution had only a minor effect on the k_D values (**Figure 2.2**). Experiments were repeated three times, and averaged *D* values were plotted against carrier concentration and fit to **Equation 6** to determine k_D and D^0 values ± SD over three repeats.

2.4 Results

2.4.1 Validation of FCS-based virial coefficient measurements

In order to validate the use of FCS for the measurement of virial coefficient values, we first compared B_{22} values (i.e., the self-interaction term) for the model protein BSA at pH 7.4 and 6.0 obtained by FCS and by a widely-used dynamic light scattering (DLS) approach. BSA has been extensively studied, and B_{22} values have been reported over a range of different ionic strength and pH conditions. FCS and DLS are related techniques that involve the autocorrelation of a signal from particles in solution to infer their hydrodynamic properties. The key difference is that DLS relies on light scattered by the sample, while FCS relies on fluorescence emitted by the sample. The two techniques each have their advantages and drawbacks: DLS does not require the sample to be labeled but cannot be used to monitor a particular species of interest in a complex mixture. On the other hand, FCS does require the species of interest to be labeled (generally at quite low concentrations, $\leq$ 100 nM), but can be used with much more challenging samples to answer questions about complex mixtures that are intractable by DLS.

Because FCS and DLS are related, we could employ parallel approaches to obtain B_{22} values by each method as described in the Theory section. FCS and DLS measurements were carried out over a range of concentrations of BSA from 0.38 mg/mL to 38 mg/mL. Autocorrelation curves, generated via either technique, were fit to single-component models (**Figure 2.3A and Figure 2.3B**), which treat the relevant signal as originating from a single homogenous species, to obtain diffusion coefficients of BSA at each concentration. Minimal shifts in FCS autocorrelation data were observed for the BSA model system due to opposing viscosity and nonideality effects. The repulsion between BSA molecules speeds up the diffusion while the increase in viscosity with increasing BSA concentration results in slower diffusion. This can be demonstrated by plotting the

expected change in autocorrelation due to viscosity alone, which results in a more significant difference (**Figure 2.4**). Note that the rightward shift in FCS autocorrelation is smaller than would be expected from the increase in viscosity alone, due to the opposing effect of nonideality.

Residual free dye in the sample can result in a second, faster-diffusing component in FCS measurements, but based on the calculated labeling efficiency and model comparison calculations (see Experimental Procedures section), this does not appear to be a concern for our samples. Another potential concern is the formation of homo-dimers or small soluble oligomers of the protein of interest, which can bias the diffusion times to higher values. While accounting for such species using diffusion times alone can be challenging, FCS also yields a brightness per particle parameter that can be obtained by dividing the average intensity by the average particle count (N from **Equation 10**) for a given measurement. Increases in the brightness per particle would indicate homo-aggregation between two labeled molecules. Although this is unlikely at the low nM concentrations used here, homo-aggregation would impact our results and is important to rule out. Brightness per particle did not vary systematically as a function of carrier protein concentration, and our diffusion coefficients are very similar to those expected of monomeric BSA or antibodies, together suggesting that homo-dimerization or -oligomerization do not impact our finding (**Table 2.2**). As described in the Theory section, B_{22} values can be calculated by fitting to **Equation 6**. Note that the diffusion coefficients are scaled based on the bulk viscosity of the solution at each concentration of BSA based on separate viscosity measurements as described in the Theory section.

Figure 2.3B and Figure 2.3C shows FCS and DLS comparison of diffusion coefficients for BSA at pH 7.4. The second virial coefficient, $2B_{22}M$ (represented by the interaction parameter k_D) and D^0 values obtained by FCS (3.8 ± 0.1 mL/g and 5.45 ± 0.15 x 10^{-7} cm^2/s respectively) were

comparable to values obtained by DLS (3.3 ± 0.1 mL/g and 5.35 ± 0.10 x 10^{-7} cm^2/s respectively). The corresponding $2B_{22}M$ and D^0 values obtained at pH 6.0 (**Figure 2.3D**) by FCS (3.2 ± 0.5 mL/g and 5.60 ± 0.07 x 10^{-7} cm^2/s respectively) were also comparable to DLS values (3.4 ± 0.3 mL/g and 5.21 ± 0.04 x 10^{-7} cm^2/s respectively). These measurements are highly sensitive to buffer conditions resulting in a wide range of second virial coefficient values in the literature, but our results are well within the range of previously reported values (Ma et al., 2015; Tanford, 1961). The positive virial coefficients in both cases indicate weak repulsive interactions between BSA molecules. An important consideration with any fluorescence-detected technique, including FCS, is whether dye labeling perturbs the system of interest. We employed conditions that yielded a relatively low dye:protein ratio in the 1–2 range (see Experimental Procedures section). At least under these conditions, the agreement between DLS and FCS results suggests that the A488 moiety is not having a major effect on B_{22} values. However, other dyes or higher dye:protein ratios could well affect self- or cross-term virial coefficients. For further method validation, FCS measurements of the self-term virial coefficient were also conducted at two additional ionic strength conditions (25 mM NaCl and 750 mM NaCl, pH 7.4) for further method validation (**Figure 2.5**). As expected, the lower ionic strength condition resulted in an increase in k_D (6.5 ± 0.1 mL/g), while the higher ionic strength condition resulted in decrease in k_D (-0.5 ± 0.1 mL/g) compared to the original condition (3.8 ± 0.1 mL/g at 150 mM NaCl pH 7.4). Together, these results suggest that FCS can be used as an orthogonal method for calculating self-term nonideality.

2.4.2 NIST mAb cross-term interactions with albumin

NIST mAb with human serum albumin (HSA) as carrier protein was used as the model system to validate cross-term nonideality measurements by FCS. **Figure 2.6A** shows diffusion coefficients for NIST mAb in solutions containing between 0 and 46 mg/mL HSA. Second virial

coefficient $2B_{12}M$, and D^0 values obtained by FCS (3.3 ± 0.4 mL/g and 4.07 ± 0.09 x 10^{-7} cm^2/s respectively) were comparable to AUC values (3.2 ± 0.3 mL/g and 4.17 ± 0.03 x 10^{-7} cm^2/s) reported by Wright et al. (Wright et al., 2018). This result suggests that FCS can be used as an alternative method to calculate cross-term nonideality in addition to self-term nonideality. The positive virial coefficient indicates repulsive interactions between NIST mAb and HSA. Cross-interactions between NIST mAb and bovine serum albumin (BSA) were also measured, for comparison with subsequent measurements in fetal bovine serum (FBS). **Figure 2.6B** shows diffusion coefficients for NIST mAb in solutions containing between 0 and 42 mg/mL BSA. At 3.8 ± 0.4 mL/g, the k_D value with BSA was slightly higher than with HSA, while the D^0 value was similar at 4.22 ± 0.02 x 10^{-7} cm^2/s. The increased k_D suggests there may be slightly stronger repulsive interactions between NIST mAb and BSA than for HSA.

Albumin is the most abundant protein in serum, making it a good carrier protein to investigate cross-term nonideality for protein-based therapeutics (Busher, 1990). The repulsive interactions observed between NIST mAb and HSA could shift the folding equilibrium of the antibody to favor more compact structures, thus enhancing folding stability. Further assessment needs to be completed with a broader panel of antibodies to determine potential trends; however, these effects could be antibody dependent. Despite the abundance of albumin in serum, there are many other components to consider that could have opposing effects. Therefore, cross-term measurements with albumin alone may be an incomplete representation of the nonideality exhibited by a protein-based therapeutic in serum.

2.4.3 mAb cross-term interactions with serum

We introduce an apparent second virial coefficient, $B_{2,app}$, which measures global nonideality between a labeled species and serum components. By labeling antibodies and diluting

them in varying concentrations of serum, we were able to probe nonideality in complex media. In this approach, we are unable to specify which component(s) in serum are interacting with our labeled antibodies. It is worth noting that a k_D value of 0 mL/g does not necessarily indicate a lack of interactions with serum components but could instead reflect a balance of both attractive and repulsive interactions. The positive and negative values resulting from repulsive interactions with one component in the medium and attractive interactions with another component would cancel each other out. A value deviating from 0 mL/g would indicate that either repulsive or attractive interactions dominate but does not exclude the possibility of opposing interactions occurring simultaneously. In theory, $B_{2,app}$ could also be applied to other complex multicomponent systems such as plasma, endosomal lysate, etc.

$B_{2,app}$ values in serum were determined for six antibodies: NIST mAb, Carlumab, Tocilizumab, anti-gp120 mAb, anti-RSV mAb, and bsAb. NIST mAb served as a reference mAb, anti-gp120 mAb, anti-RSV mAb, and bsAb as research mAbs, while Tocilizumab is a clinically approved therapeutic (an interleukin-6 receptor inhibitor used to treat autoimmune diseases) and Carlumab is a discontinued therapeutic candidate. Measurements of A488-NIST mAb, A488-Tocilizumab, A488-Carlumab, A488-anti-gp120 mAb, A488-anti-RSV mAb, and A488-bsAb with fetal bovine serum (FBS) as the carrier solution were used to calculate apparent second virial coefficients as shown in **Figure 2.7**. FCS traces (not shown) were fit to a single-component FCS equation to yield diffusion time (τ_d) values at each FBS concentration. Adjusted diffusion coefficients, D_{adj}, were calculated from diffusion times that were adjusted based on separately determined solution viscosity data. D_{adj} values were plotted against FBS concentration and data were fit to yield k_D or $2B_{2,app}M$ values.

A488-NIST mAb yielded a k_D value of -0.8 ± 0.3 mL/g and a D^0 value of 4.04 ± 0.12 x 10^{-7} cm^2/s (**Figure 2.7A**). A488-Tocilizumab yielded a similar result with k_D value of -0.4 ± 0.5 mL/g and a D^0 value of 4.42 ± 0.26 x 10^{-7} cm^2/s (**Figure 2.7B**). In both cases, k_D values did not significantly deviate from 0 mL/g. A488-Carlumab exhibited a k_D value of -10.9 ± 0.8 mL/g and a D^0 value of 4.56 ± 0.15 x 10^{-7} cm^2/s (**Figure 2.7C**), suggesting weak attractive interactions with serum components. The possible curvature and the magnitude of the change observed in the D_{adj} vs. concentration plot of A488-Carlumab vs. FBS could indicate the presence of more complex or higher-order interactions with serum components, but this needs further investigation. A488-anti-gp120 mAb and anti-RSV mAb yielded slightly negative k_D values of -1.6 ± 0.3 mL/g and -2.2 ± 0.3 mL/g, with comparable D^0 values of 4.04 ± 0.37 x 10^{-7} cm^2/s and 4.04 ± 0.25 x 10^{-7} cm^2/s, respectively (**Figure 2.7D and Figure 2.7E**). A488-bsAb exhibited a slightly more negative k_D value of -3.7 ± 0.4 mL/g with a similar D^0 value of 4.0 ± 0.02 x 10^{-7} cm^2/s (**Figure 2.7F**). In all three cases, the slightly negative k_D value suggests weak attractive interactions with serum components, albeit to a lesser extent than Carlumab. The bsAb exhibited greater attraction to serum than the parental mAbs, potentially rendering it less stable in serum, however this needs further investigation. Interestingly, Carlumab, the discontinued therapeutic, displays markedly different behavior than the other mAbs, with (on balance) much stronger attractive interactions with serum components.

2.4.4 Summary of self- and cross-term nonideality parameters

Table 1 summarizes both self and cross-term nonideality parameters obtained from DLS and FCS measurements. Validation of our FCS method was accomplished with BSA and NIST mAb model systems. Determination of the diffusion interaction parameter k_D for BSA at pH 7.4 and 6.0 yielded comparable results between FCS and DLS methods. In addition, the low and high

ionic strength conditions at pH 7.4 exhibited expected trends in k_D by FCS. Similarly, NIST mAb and HSA, our model system for cross-term nonideality, yielded results comparable to the AUC literature value. We introduced an apparent second virial coefficient as a determinant of global nonideality in complex media and successfully measured k_D values for six mAbs (NIST mAb, Tocilizumab, Carlumab, anti-gp120 mAb, anti-RSV mAb, and bsAb) in FBS. The variability in k_D values across this panel of IgG1 antibodies suggests that nonideality effects are antibody dependent (**Figure 2.8**).

2.5 Discussion

Studies of the second virial coefficient date back over a century, and their original application to gases has broadened to encompass many other systems. Although derived from the ideal gas law, similar deviations from ideality apply to diffusion and sedimentation behavior, making it possible to measure second virial coefficients with many analytical techniques. The second virial coefficient in protein systems has been extensively studied in terms of the effects of solution conditions, such as pH and ionic strength, as well as of weak protein interactions. Methods used include AUC (Behlke & Ristau, 1999; Saito et al., 2012; Wright et al., 2018), size-exclusion chromatography (SEC) (Bloustine et al., 2003), membrane osmometry (MO) (Moon et al., 2000), cross-interaction chromatography (SIC) (Quigley & Williams, 2015), and various light scattering techniques such as DLS (Yadav, Scherer, et al., 2011), static light scattering (SLS) (Alford et al., 2008; Velev et al., 1998), and composition-gradient multi-angle light scattering (CG-MALS) (Ma et al., 2015). There are disadvantages associated with each of these methods. For example, chromatography methods often consume a lot of protein and immobilization conditions can be challenging to establish. Membrane osmometry is complex and requires determination of specific properties for the individual proteins prior to analysis. Light scattering measurements such as DLS

are highly sensitive to impurities and, as previously mentioned, cannot measure cross-term nonideality. AUC requires costly instrumentation as well as expertise in running experiments and analyzing sedimentation data. The capability of fluorescence detection in AUC measurements (AU-FDS) allows AUC to be applied to complex media, but the analysis is complicated by the fact that the concentration and viscosity of the medium varies over the sample. Sedimentation and diffusion coefficients are system properties that depend on the concentration of other solutes present in solution. Furthermore, the viscosity of the samples varies depending on position in the sample cell during centrifugation. As a result, AUC requires analysis of both sedimentation and diffusion interaction parameters, k_S and k_D respectively, to determine the second virial coefficient. While second virial coefficient determination has been reported by AUC in buffer systems, determination in complex biological fluids has not been reported. The interpretation of such data is complicated, requiring a more detailed analysis than currently available. The correction for changes in bulk viscosity in our FCS measurements, as discussed in the above Theory section, eliminates the need to estimate the k_S parameter, thus simplifying our analysis. We have successfully validated FCS as an orthogonal method for calculating both self and cross-term virial coefficients. FCS experiments are relatively fast and do not consume large quantities of protein. One major downfall of this technique, as discussed in the Results section, is that FCS does require the species of interest to be labeled. However, A488 labeling of mAbs and BSA in this study was efficient and does not appear to have perturbed interactions with co-solutes. FCS is relatively inexpensive and easy to implement, making it an attractive alternative to other methods.

The second virial coefficient is finding applications in the biopharmaceutical industry as a tool to better understand protein aggregation. The self-term virial coefficient (B_{22}) and diffusion interaction parameter (k_D) have demonstrated applicability (Baek & Zydney, 2018; Kamerzell et

al., 2011; Le Brun et al., 2010; Obrezanova et al., 2015; Saluja et al., 2010) in relating intermolecular interactions to various biophysical properties of proteins, including aggregation. Biologics are subject to a range of stresses during manufacturing such as variations in ionic strength, pH, temperature, and high protein concentrations that can drive aggregation. The negative impacts of aggregation are not limited to manufacturing but can also be detrimental to half-life, efficacy, and the safety profiles of therapeutic products (Le Basle et al., 2020). As a result, the biopharmaceutical industry has shown increasing interest in utilizing B_{22} as a predictor of aggregation propensity. In contrast, measurements of cross-term second virial coefficients (B_{12}) have been underutilized. Perhaps the most common application of cross-term virial coefficient determination is to probe protein-excipient interactions during formulation development (Kamerzell et al., 2011). There is, however, an emerging movement towards studying weak interactions in crowded conditions. While macromolecular crowding has traditionally focused on excluded volume effects, there is increasing agreement that weak interactions in crowded conditions have the potential to overcome the (generally stabilizing) excluded volume effect. Thus, our understanding of nonideality has seen a paradigm shift. In recent years there has been increasing interest in exploring cross-interactions between therapeutic antibodies and serum proteins. Wright, et al. (Wright et al., 2018) proposed a preclinical AUC method to measure weak interactions between mAbs and serum components such as HSA and IgG through determination of second virial coefficients and sedimentation interaction parameters. Kim, et al. (Kim et al., 2019) used CG-MALS to probe cross-term interactions between mAbs and HSA, but also used biolayer interferometry (BLI) to explore the functional consequence of this nonideality on antigen binding. While these studies relied on HSA alone as a model system to determine cross-term

nonideality of mAbs in serum, our results caution that such an approach may fail to qualitatively or quantitatively capture the true effects of serum.

Our second virial coefficient results for NIST mAb with BSA (k_D = 3.8 mL/g) and for NIST mAb with serum (k_D = –0.8 mL/g) differ in a particularly interesting way. Because albumin is the most abundant component of serum, one might expect its effects to predominate serum-induced nonideality. Instead, the lower k_D value in FBS suggests that repulsive interactions with BSA and attractive interactions with some other component(s) are occurring simultaneously in serum. Furthermore, this suggests that the approach of isolating specific components and completing independent cross-term virial coefficient measurements may be an incomplete representation of nonideality in serum. The ability to directly measure diffusion coefficients in complex media gives FCS an important advantage over existing methods in probing global nonideality in relevant biological fluids. Implementing these measurements into biologics development could prove beneficial on several levels from candidate selection to formulation development. For example, comparing $B_{2,app}$ values for a panel of mAbs during candidate selection could facilitate elimination or selection of certain candidates. Additionally, implementing $B_{2,app}$ measurements during characterization could serve as a complementary tool to various analytical techniques for assessing the impacts of process changes during recovery, purification, and formulation development. In theory, this approach has the potential to be applied to other biological fluids and protein systems. For example, $B_{2,app}$ measurements could be conducted in plasma or endosomal lysate to better understand nonideality following internalization. $B_{2,app}$ could be measured in interstitial fluids to model tumor microenvironments or in a solution mocking the serum formulation interface during administration. This approach can potentially be applied to different antibody platforms such as

antibody-drug conjugates, Fab fragments, bispecific antibodies, and Fc-fusion proteins, as well many other therapeutic proteins, vaccine platforms and diagnostics.

Serum is a complex solution comprising albumin (roughly two-thirds of the protein content), IgG (~20%), IgA (~4%), IgM (~2%), as well as numerous other lipoproteins, complement factors, transport proteins and smaller osmolytes (Anderson et al., 2004; Gonzalez-Quintela et al., 2008; Leeman et al., 2018). **Figure 2.9** depicts the increasingly crowded environment that a labeled antibody samples when going from 10% (**Figure 2.9A**) to neat (**Figure 2.9C**) serum, while **Figure 2.9B** represents the intermediate condition of 50% serum. Due to short intermolecular distances in the crowded environment, serum components can experience weak, nonspecific interactions with labeled antibodies and with each other. As previously discussed, repulsive interactions occur between NIST mAb and BSA (**Figure 2.9D**). While our apparent second virial coefficient results cannot identify the various interacting species in serum, they do suggest that these repulsive interactions with BSA are counteracted by attractive interactions with other, non-albumin serum components (**Figure 2.9E).** In the case of Carlumab, attractive interactions with as-yet unidentified serum components dominate, as illustrated in **Figure 2.9F**. It is also possible that Carlumab could be experiencing both weak self-association and association with serum components simultaneously, but further investigation is needed.

We hypothesize that there may be biophysical consequences of nonideality in crowded biological environments that could impact important properties of biologics (i.e., binding affinity, stability, half-life, etc.). The approach presented here will enable future studies on the effects of serum-induced nonideality on other IgG isotypes, antibody platforms and fragments. Moreover, a component assessment of serum and comparative studies of sera from humans and preclinical species could prove informative. Our comparison of k_D values in BSA and FBS is a preliminary

step along this path. Our work also enables mechanistic studies focused on understanding the biophysical basis of nonideality exhibited by mAbs.

2.6 Conclusion

In this study, we have validated FCS as an orthogonal method for determining both self and cross-term second virial coefficients via diffusion time measurements and the concentration dependence of corresponding translation diffusion coefficients. Plots of diffusion coefficients against carrier protein concentration were fit to yield diffusion interaction parameter (k_D) values, which are proportional to the second osmotic virial coefficient, $2B_2M$. Furthermore, the capability of FCS measurements in complex media allowed for determination of an apparent second virial coefficient ($B_{2,app}$) for six mAbs in FBS to probe global nonideality effects in serum. These results reveal that multiple forces may be acting on mAbs simultaneously in biological environments, where repulsive or attractive interactions can dominate or balance one another. Further investigation into the biophysical significance of these $B_{2,app}$ values is needed. This approach may be useful in areas of biologics development such as candidate selection, characterization, and formulation development, as well as in understanding other biological fluids and protein systems.

FIGURES

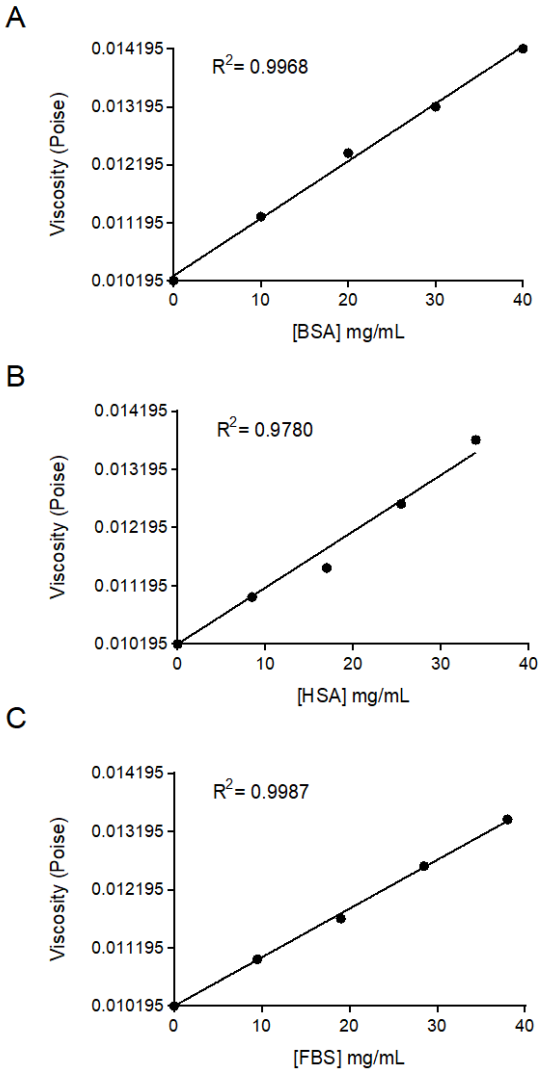

Figure 2.1: Viscosity vs. carrier concentration for BSA (A), HSA (B), and FBS (C). The viscosity at each carrier concentration was determined from the diffusion time of Alexa 488 SE and predetermined PBS pH 7.4 viscosity. In each case, the viscosity is linear over the experimental concentration range with R^2 values ≥ 0.97.

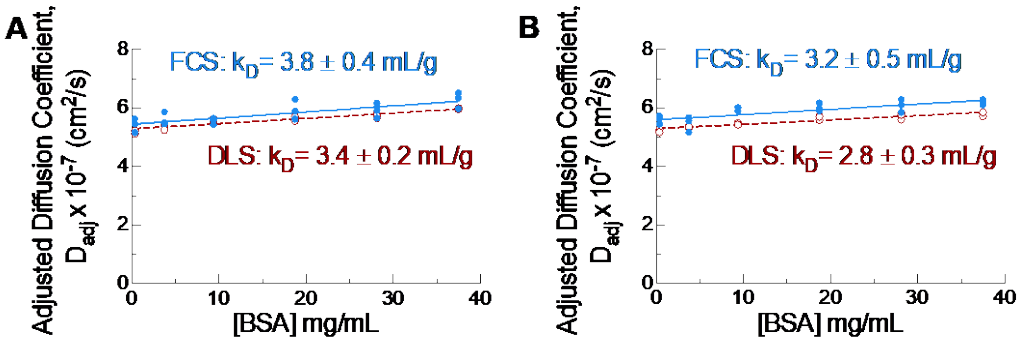

Figure 2.2: DLS virial coefficient measurements for BSA model system from complete diffusion coefficient distributions. Comparison of diffusion coefficients determined by FCS and DLS for BSA at pH 7.4 (A) and pH 6.0 (B). The second virial coefficient, $B_{22}M$ (or k_D) for DLS measurements were obtained using the average diffusion coefficient from a complete distribution. This had only a minor effect on k_D measured at pH 7.4 (3.4 ± 0.2 mL/g) compared to the value (3.3 ± 0.1 mL/g) obtained from the average diffusion coefficient of the monomeric peak and reported in Table 1. Using the complete diffusion coefficient distribution also had a minor effect on the DLS k_D value measured at pH 6.0 (2.8 ± 0.3 mL/g) compared to our reported value (3.4 ± 0.3 mL/g). Regardless of the analysis method, DLS values are close to FCS values.

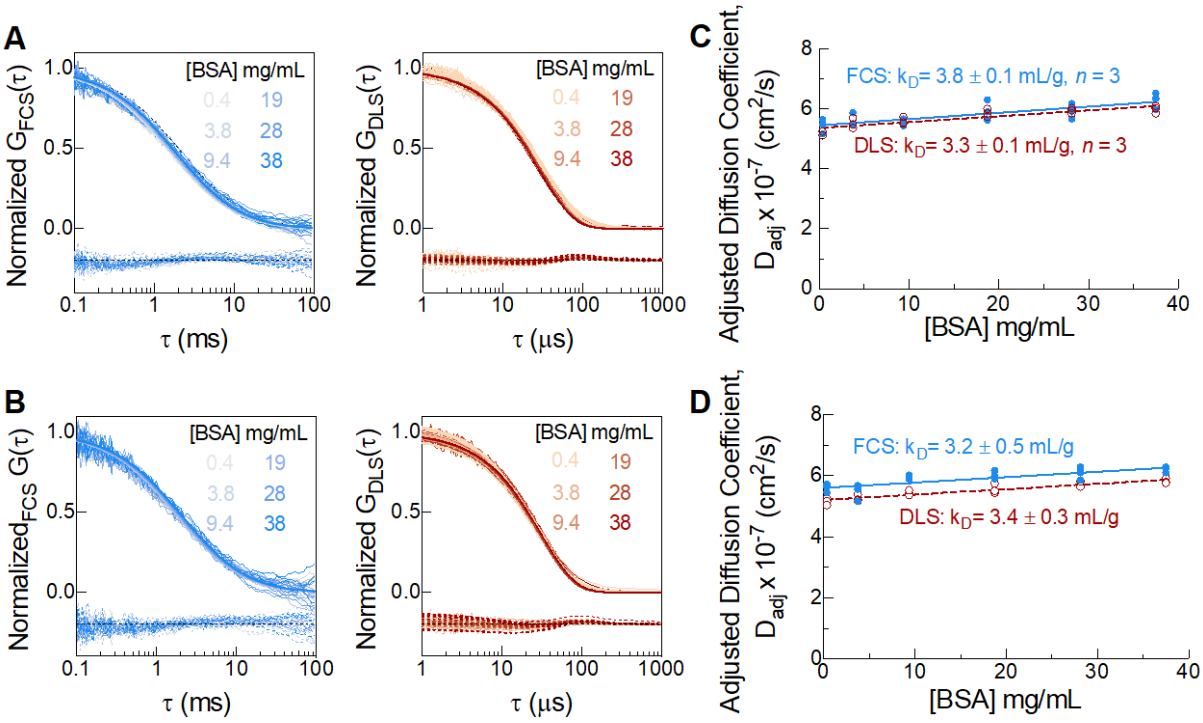

Figure 2.3: Self-term nonideality for BSA at pH 7.4 and 6.0 measured by FCS and DLS. FCS (left) and DLS (right) traces were collected over a range of BSA concentrations at pH 7.4 (A) and pH 6.0 (B). Residuals are shown in dashed lines and have been shifted downwards by 0.2 units for clarity. Diffusion coefficients were scaled based on sample viscosity and plotted against BSA concentration at pH 7.4 (C) and pH 6.0 (D). These plots were fit to the linear equation $D = D^0(1 + k_D c)$ to obtain k_D values, with results presented as mean ± S.D. from three replicates with independent sample preparations.

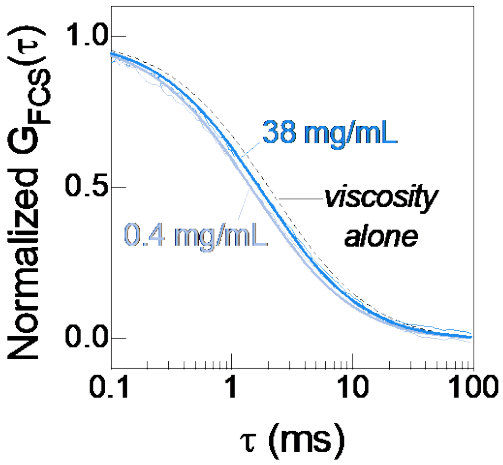

Figure 2.4: FCS autocorrelation traces of A488-BSA measured at a total BSA concentration of 0.4 mg/mL (light blue) and 38 mg/mL (blue). The viscosity alone line (dashed black line) shows the autocorrelation decay that would be seen with a solution of 38 mg/mL BSA in the absence of second virial effects. This illustrates the opposing effects of self-term interactions and viscosity in the case of BSA (at pH 7.4 and 150 mM NaCl).

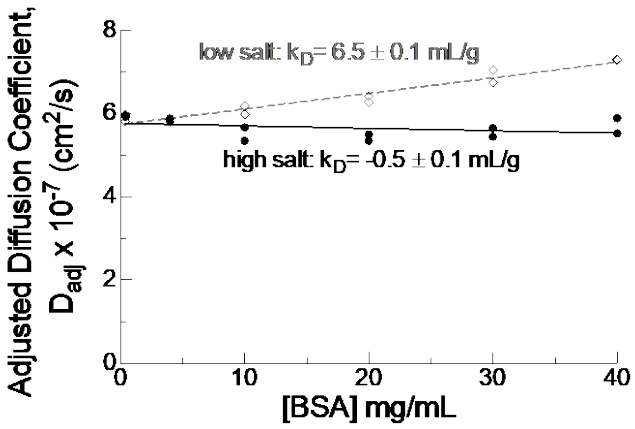

Figure 2.5: FCS-based virial coefficient measurements for BSA model system at different ionic strength conditions. Self-term virial coefficient measured for BSA at pH 7.4 by FCS at 25 nM NaCl (grey diamonds and dashed line) and 750 mM NaCl (black circles and solid line). These plots were fit to the linear equation $D = D^0(1 + k_D c)$ to obtain k_D values.

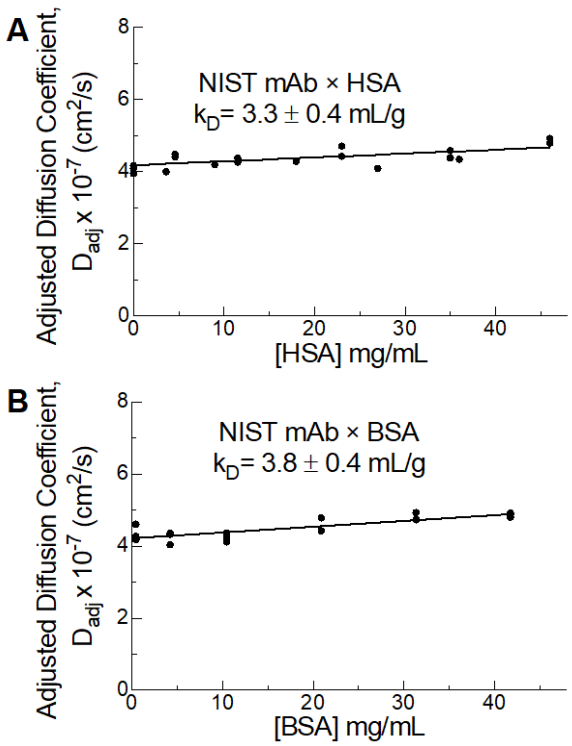

Figure 2.6: Cross-term nonideality of A488-NIST mAb and human serum albumin (A) or bovine serum albumin (B). Data were fit to the linear equation $D = D^0(1 + k_D c)$ to obtain k_D values. Both conditions yield positive k_D values, indicating repulsive interactions between NIST mAb and albumin. Points indicate data from three replicates with independent sample preparations, and results are presented as mean ± S.D. (Note that in panel A, one replicate measurement covered 0.4–36 mg/mL, while the other two replicates cover 0.5–46 mg/mL).

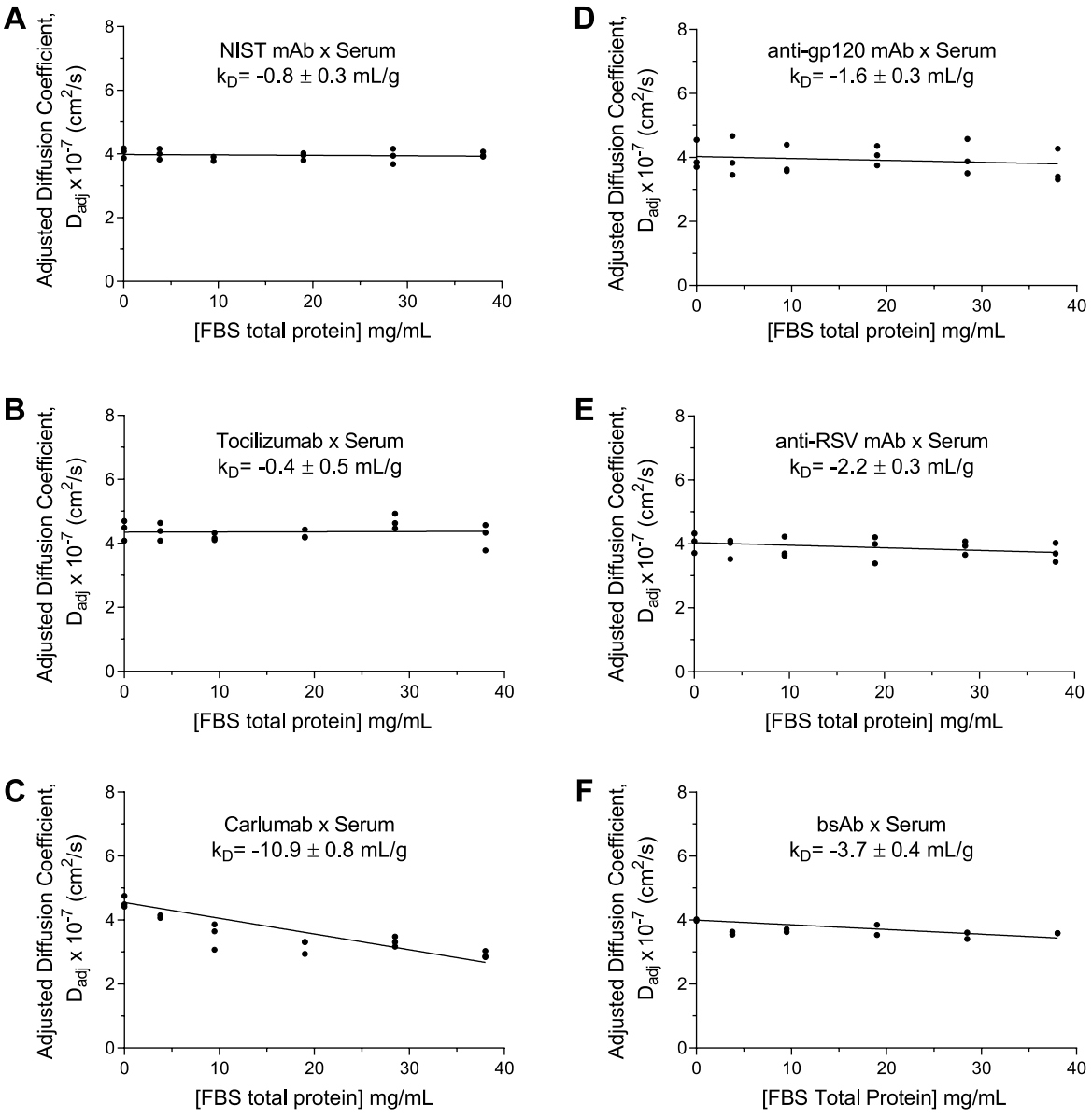

Figure 2.7: Apparent second virial coefficients for mAbs in FBS: Dadj vs. [FBS] for NIST mAb (A), Tocilizumab (B), Carlumab (C), anti-gp120 mAb (D), anti-RSV mAb (C), and bsAb (D). NIST mAb and Tocilizumab show negligible deviations from ideal behavior, while Carlumab shows a marked decrease in diffusion coefficient indicative of attractive interactions with one or more co-solutes in serum. Similarly. anti-gp120 mAb, anti-RSV mAb, and bsAb also show a decrease in diffusion coefficient, albeit to a lesser extent than Carlumab, indicative of slight attraction to serum. Points indicate data from three replicates (apart from bsAb which was n=2) with independent sample preparations, and results are presented as mean ± S.D

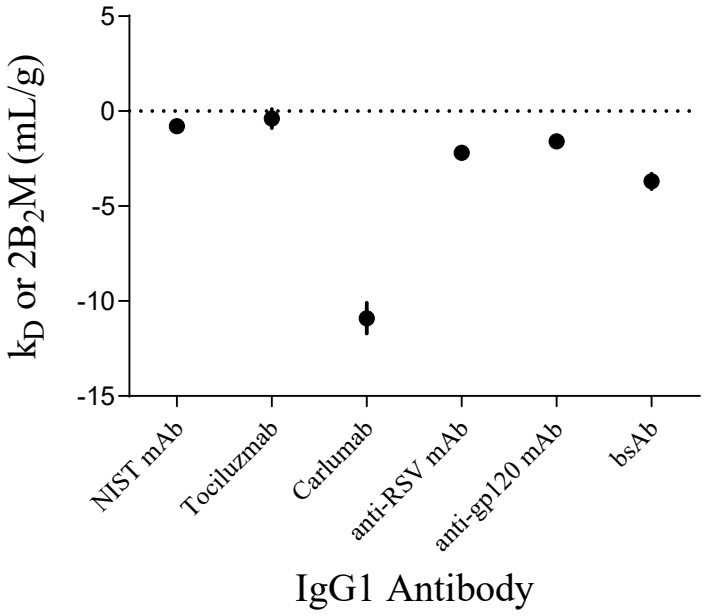

Figure 2.8: Comparison of interaction parameter k_D values for NIST mAb, tocilizumab, carlumab, anti-gp120 mAb, anti-RSV mAb, and bsAb. The variability in k_D for the panel of mAbs from the same isoptype (IgG1), suggests that nonideality effects in serum are antibody dependent. Points indicate data from three replicates (apart from bsAb which was n=2) with independent sample preparations, and results are presented as mean ± S.D

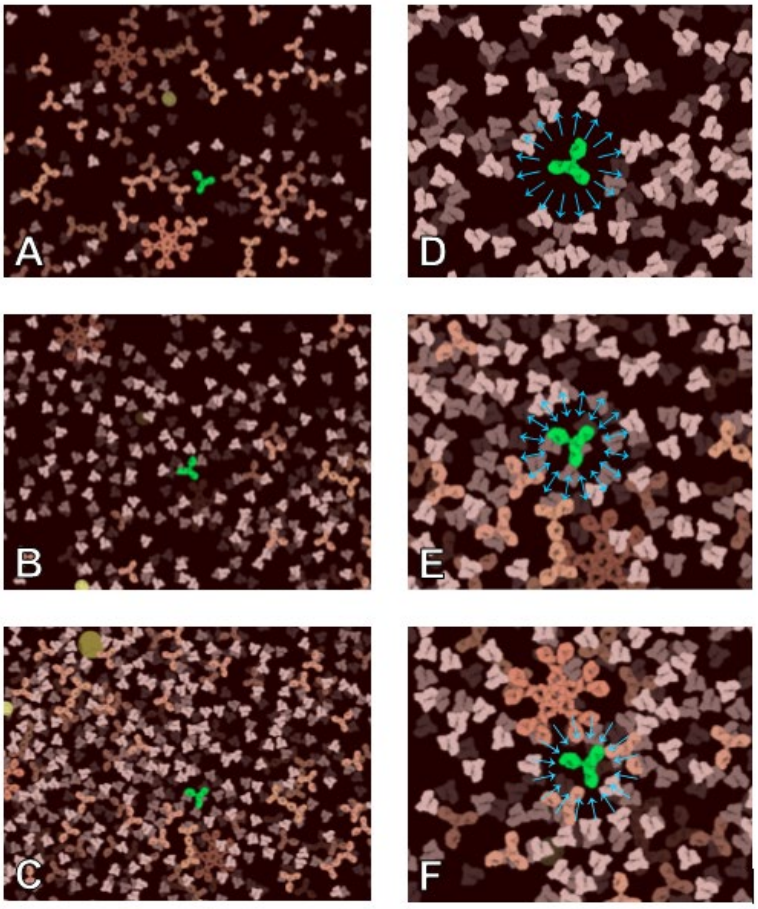

Figure 2.9: These illustrations, prepared in CellPAINT 2.0 (Gardner et al., 2018), depict the environments experienced by a probe mAb (green) in 10% (A), 50% (B) or 100% serum (C). Co-solutes such as serum albumin, other IgGs, IgAs, IgMs and lipoprotein particles (differing shades of pink) are shown to scale and in approximately the concentrations found in human serum. Molecules of interest may participate in predominantly repulsive interactions with co-solutes, as in the case of NIST mAb and BSA (D). Attractive and repulsive interactions may cancel each other out, as in the case of NIST mAb and serum (E). Finally, attractive interactions may predominate, as in the case of Carlumab and serum (F).

TABLES

Table 2.1: Diffusion time and labeling ratio estimates for BSA model system

Sample	τ_D (ms)		$\frac{\tau_{D,BSA}}{\tau_{D,dye}}$		Labeling ratio (dye:BSA)
	dye	BSA	Observed	Ideal	
BSA pH 6.0	0.23	1.5	6.4	4.7	1:1
BSA pH 7.4	0.25	1.5	6.1	4.7	1:1.5

Table 2.2: Brightness per particle calculations for BSA model system at pH 7.4 and 6.0. Note: pH 7.4 and pH 6.0 data were collected on different days with different laser powers, and so cannot be compared directly.

[BSA] (mg/mL)	$\langle I \rangle / N$ (Hz)	
	pH 7.4	pH 6.0
0.38	2676	1242
3.8	2527	1512
9.4	2437	1565
18.8	2230	1170
28	2257	1222
38	2156	1263

Table 2.3: Summary of self- and cross-term nonideality parameters. Values presented are mean ± S.D. from at least three independent replicates (apart from bsAb which was n=2).

Sample	Nonideality Coefficient	k_D or $2B_2M$ (mL/g)	$D^0 \times 10^{-7}$ (cm^2/s)
BSA pH 7.4	B_{22} self-interaction	3.8 ± 0.1[a]	5.45 ± 0.15[a]
(150 mM)		3.3 ± 0.1[b]	5.35 ± 0.10[b]
25 mM NaCl		6.5 ± 0.1[a]	5.74 ± 0.06[a]
750 mM NaCl		-0.5 ± 0.1[a]	6.11 ± 0.02[a]
BSA pH 6.0	B_{22} self-interaction	3.2 ± 0.5[a]	5.60 ± 0.07[a]
		3.4 ± 0.3[b]	5.21 ± 0.04[b]
NIST/HSA	B_{12} cross-interaction	3.3 ± 0.4[a]	4.07 ± 0.09[a]
		3.2 ± 0.3[c*]	4.17 ± 0.03[c*]
NIST/BSA	B_{12} cross-interaction	3.8 ± 0.4[a]	4.22 ± 0.02[a]
NIST/FBS	$B_{2,app}$ cross-interaction(s)	-0.8 ± 0.3[a]	4.04 ± 0.12[a]
Tocilizumab/FBS	$B_{2,app}$ cross-interaction(s)	-0.4 ± 0.5[a]	4.42 ± 0.26[a]
Carlumab/FBS	$B_{2,app}$ cross-interaction(s)	-10.9 ± 0.8[a]	4.56 ± 0.15[a]
anti-gp120 mAb	$B_{2,app}$ cross-interaction(s)	-1.6 ± 0.3[a]	4.04 ± 0.37[a]
anti-RSV mAb	$B_{2,app}$ cross-interaction(s)	-2.2 ± 0.3[a]	4.04 ± 0.25[a]
bsAb	$B_{2,app}$ cross-interaction(s)	-3.7 ± 0.4[a]	4.00 ± 0.02[a]

[a]FCS; [b]DLS; [c*]AUC literature value (for comparison)

2.7 References

AlDeghaither, D., Smaglo, B. G., & Weiner, L. M. (2015). Beyond peptides and mAbs-current status and future perspectives for biotherapeutics with novel constructs. *The Journal of Clinical Pharmacology*, *55*(S3), S4–S20. https://doi.org/10.1002/jcph.407

Alford, J. R., Kendrick, B. S., Carpenter, J. F., & Randolph, T. W. (2008). Measurement of the second osmotic virial coefficient for protein solutions exhibiting monomer–dimer equilibrium. *Analytical Biochemistry*, *377*(2), 128–133. https://doi.org/10.1016/j.ab.2008.03.032

Anderson, N. L., Polanski, M., Pieper, R., Gatlin, T., Tirumalai, R. S., Conrads, T. P., Veenstra, T. D., Adkins, J. N., Pounds, J. G., Fagan, R., & Lobley, A. (2004). The Human Plasma Proteome. *Molecular & Cellular Proteomics*, *3*(4), 311–326. https://doi.org/10.1074/mcp.M300127-MCP200

Baek, Y., & Zydney, A. L. (2018). Intermolecular interactions in highly concentrated formulations of recombinant therapeutic proteins. *Current Opinion in Biotechnology*, *53*, 59–64. https://doi.org/10.1016/j.copbio.2017.12.016

Behlke, J., & Ristau, O. (1999). Analysis of the thermodynamic non-ideality of proteins by sedimentation equilibrium experiments. *Biophysical Chemistry*, *76*(1), 13–23. https://doi.org/10.1016/S0301-4622(98)00212-9

Biswas, S., Kundu, J., Mukherjee, S. K., & Chowdhury, P. K. (2018). Mixed Macromolecular Crowding: A Protein and Solvent Perspective. *ACS Omega*, *3*(4), 4316–4330. https://doi.org/10.1021/acsomega.7b01864

Blanco, M. A., Perevozchikova, T., Martorana, V., Manno, M., & Roberts, C. J. (2014). Protein–Protein Interactions in Dilute to Concentrated Solutions: α-Chymotrypsinogen in Acidic Conditions. *The Journal of Physical Chemistry B*, *118*(22), 5817–5831. https://doi.org/10.1021/jp412301h

Bloustine, J., Berejnov, V., & Fraden, S. (2003). Measurements of Protein-Protein Interactions by Size Exclusion Chromatography. *Biophysical Journal*, *85*(4), 2619–2623. https://doi.org/10.1016/S0006-3495(03)74684-0

Busher, J. T. (1990). Serum Albumin and Globulin. In *Clinical Methods: The History, Physical, and Laboratory Examinations* (3rd ed.). Butterworths. https://doi.org/https://www.ncbi.nlm.nih.gov/books/NBK204/

Chaturvedi, S. K., Ma, J., Brown, P. H., Zhao, H., & Schuck, P. (2018). Measuring macromolecular size distributions and interactions at high concentrations by sedimentation velocity. *Nature Communications*, *9*(1), 4415. https://doi.org/10.1038/s41467-018-06902-x

Connolly, B. D., Petry, C., Yadav, S., Demeule, B., Ciaccio, N., Moore, J. M. R., Shire, S. J., & Gokarn, Y. R. (2012). Weak Interactions Govern the Viscosity of Concentrated Antibody Solutions: High-Throughput Analysis Using the Diffusion Interaction Parameter. *Biophysical Journal*, *103*(1), 69–78. https://doi.org/10.1016/j.bpj.2012.04.047

Ellis, R. J. (2001). Macromolecular crowding: obvious but underappreciated. *Trends in Biochemical Sciences*, *26*(10), 597–604. https://doi.org/10.1016/S0968-0004(01)01938-7

Gardner, A., Autin, L., Barbaro, B., Olson, A. J., & Goodsell, D. S. (2018). CellPAINT: Interactive Illustration of Dynamic Mesoscale Cellular Environments. *IEEE Computer Graphics and Applications*, *38*(6), 51–66. https://doi.org/10.1109/MCG.2018.2877076

George, A., & Wilson, W. W. (1994). Predicting protein crystallization from a dilute solution property. *Acta Crystallographica Section D Biological Crystallography*, *50*(4), 361–365.

https://doi.org/10.1107/S0907444994001216
Gonzalez-Quintela, A., Alende, R., Gude, F., Campos, J., Rey, J., Meijide, L. M., Fernandez-Merino, C., & Vidal, C. (2008). Serum levels of immunoglobulins (IgG, IgA, IgM) in a general adult population and their relationship with alcohol consumption, smoking and common metabolic abnormalities. *Clinical & Experimental Immunology*, *151*(1), 42–50. https://doi.org/10.1111/j.1365-2249.2007.03545.x
Goulet, D. R., & Atkins, W. M. (2020). Considerations for the Design of Antibody-Based Therapeutics. *Journal of Pharmaceutical Sciences*, *109*(1), 74–103. https://doi.org/10.1016/j.xphs.2019.05.031
Harding, S. E., & Johnson, P. (1985). The concentration-dependence of macromolecular parameters. *Biochemical Journal*, *231*(3), 543–547. https://doi.org/10.1042/bj2310543
Haustein, E., & Schwille, P. (2007). Fluorescence Correlation Spectroscopy: Novel Variations of an Established Technique. *Annual Review of Biophysics and Biomolecular Structure*, *36*(1), 151–169. https://doi.org/10.1146/annurev.biophys.36.040306.132612
Hay, M., Thomas, D. W., Craighead, J. L., Economides, C., & Rosenthal, J. (2014). Clinical development success rates for investigational drugs. *Nature Biotechnology*, *32*(1), 40–51. https://doi.org/10.1038/nbt.2786
Heyman, N. S., & Burt, J. M. (2008). Hindered Diffusion through an Aqueous Pore Describes Invariant Dye Selectivity of Cx43 Junctions. *Biophysical Journal*, *94*(3), 840–854. https://doi.org/10.1529/biophysj.107.115634
Johnson, I. D. (Ed.). (2010). *Molecular Probes Handbook: A Guide to Fluorescent Probes and Labeling Technologies*. Life Technologies Corporation.
Kamerzell, T. J., Esfandiary, R., Joshi, S. B., Middaugh, C. R., & Volkin, D. B. (2011). Protein–excipient interactions: Mechanisms and biophysical characterization applied to protein formulation development. *Advanced Drug Delivery Reviews*, *63*(13), 1118–1159. https://doi.org/10.1016/j.addr.2011.07.006
Kim, D. M., Yao, X., Vanam, R. P., & Marlow, M. S. (2019). Measuring the effects of macromolecular crowding on antibody function with biolayer interferometry. *MAbs*, *11*(7), 1319–1330. https://doi.org/10.1080/19420862.2019.1647744
Lambour, J., Naranjo-Gomez, M., Piechaczyk, M., & Pelegrin, M. (2016). Converting monoclonal antibody-based immunotherapies from passive to active: bringing immune complexes into play. *Emerging Microbes & Infections*, *5*(1), 1–9. https://doi.org/10.1038/emi.2016.97
Le Basle, Y., Chennell, P., Tokhadze, N., Astier, A., & Sautou, V. (2020). Physicochemical Stability of Monoclonal Antibodies: A Review. *Journal of Pharmaceutical Sciences*, *109*(1), 169–190. https://doi.org/10.1016/j.xphs.2019.08.009
Le Brun, V., Friess, W., Bassarab, S., Mühlau, S., & Garidel, P. (2010). A critical evaluation of self-interaction chromatography as a predictive tool for the assessment of protein–protein interactions in protein formulation development: A case study of a therapeutic monoclonal antibody. *European Journal of Pharmaceutics and Biopharmaceutics*, *75*(1), 16–25. https://doi.org/10.1016/j.ejpb.2010.01.009
Leal, M., Sapra, P., Hurvitz, S. A., Senter, P., Wahl, A., Schutten, M., Shah, D. K., Haddish-Berhane, N., & Kabbarah, O. (2014). Antibody-drug conjugates: an emerging modality for the treatment of cancer. *Annals of the New York Academy of Sciences*, *1321*(1), 41–54. https://doi.org/10.1111/nyas.12499
Leeman, M., Choi, J., Hansson, S., Storm, M. U., & Nilsson, L. (2018). Proteins and antibodies in serum, plasma, and whole blood—size characterization using asymmetrical flow field-flow

fractionation (AF4). *Analytical and Bioanalytical Chemistry*, *410*(20), 4867–4873. https://doi.org/10.1007/s00216-018-1127-2

Lehermayr, C., Mahler, H.-C., Mäder, K., & Fischer, S. (2011). Assessment of Net Charge and Protein–Protein Interactions of Different Monoclonal Antibodies. *Journal of Pharmaceutical Sciences*, *100*(7), 2551–2562. https://doi.org/10.1002/jps.22506

Lu, R.-M., Hwang, Y.-C., Liu, I.-J., Lee, C.-C., Tsai, H.-Z., Li, H.-J., & Wu, H.-C. (2020). Development of therapeutic antibodies for the treatment of diseases. *Journal of Biomedical Science*, *27*(1), 1. https://doi.org/10.1186/s12929-019-0592-z

Ma, Y., Acosta, D. M., Whitney, J. R., Podgornik, R., Steinmetz, N. F., French, R. H., & Parsegian, V. A. (2015). Determination of the second virial coefficient of bovine serum albumin under varying pH and ionic strength by composition-gradient multi-angle static light scattering. *Journal of Biological Physics*, *41*(1), 85–97. https://doi.org/10.1007/s10867-014-9367-7

Minton, A. P. (1983). The effect of volume occupancy upon the thermodynamic activity of proteins: some biochemical consequences. *Molecular and Cellular Biochemistry*, *55*(2), 119–140. https://doi.org/10.1007/BF00673707

Minton, A. P. (1998). [7] Molecular crowding: Analysis of effects of high concentrations of inert cosolutes on biochemical equilibria and rates in terms of volume exclusion. In *Methods in Enzymology* (pp. 127–149). https://doi.org/10.1016/S0076-6879(98)95038-8

Moon, Y. U., Curtis, R. A., Anderson, C. O., Blanch, H. W., & Prausnitz, J. M. (2000). Protein-protein interactions in aqueous ammonium sulfate solutions. Lysozyme and bovine serum albumin (BSA). *Journal of Solution Chemistry*, *29*, 699–718. https://doi.org/https://doi.org/10.1023/A:1005112927213

Obrezanova, O., Arnell, A., de la Cuesta, R. G., Berthelot, M. E., Gallagher, T. R. A., Zurdo, J., & Stallwood, Y. (2015). Aggregation risk prediction for antibodies and its application to biotherapeutic development. *MAbs*, *7*(2), 352–363. https://doi.org/10.1080/19420862.2015.1007828

Quigley, A., & Williams, D. R. (2015). The second virial coefficient as a predictor of protein aggregation propensity: A self-interaction chromatography study. *European Journal of Pharmaceutics and Biopharmaceutics*, *96*, 282–290. https://doi.org/10.1016/j.ejpb.2015.07.025

Saito, S., Hasegawa, J., Kobayashi, N., Kishi, N., Uchiyama, S., & Fukui, K. (2012). Behavior of Monoclonal Antibodies: Relation Between the Second Virial Coefficient (B 2) at Low Concentrations and Aggregation Propensity and Viscosity at High Concentrations. *Pharmaceutical Research*, *29*(2), 397–410. https://doi.org/10.1007/s11095-011-0563-x

Saluja, A., Fesinmeyer, R. M., Hogan, S., Brems, D. N., & Gokarn, Y. R. (2010). Diffusion and Sedimentation Interaction Parameters for Measuring the Second Virial Coefficient and Their Utility as Predictors of Protein Aggregation. *Biophysical Journal*, *99*(8), 2657–2665. https://doi.org/10.1016/j.bpj.2010.08.020

Saluja, A., & Kalonia, D. S. (2008). Nature and consequences of protein–protein interactions in high protein concentration solutions. *International Journal of Pharmaceutics*, *358*(1–2), 1–15. https://doi.org/10.1016/j.ijpharm.2008.03.041

Sherman, E., Itkin, A., Kuttner, Y. Y., Rhoades, E., Amir, D., Haas, E., & Haran, G. (2008). Using Fluorescence Correlation Spectroscopy to Study Conformational Changes in Denatured Proteins. *Biophysical Journal*, *94*(12), 4819–4827. https://doi.org/10.1529/biophysj.107.120220

Shi, S. (2014). Biologics: An Update and Challenge of Their Pharmacokinetics. *Current Drug*

Metabolism, *15*(3), 271–290. https://doi.org/10.2174/1389200215031404122129 05
Stetefeld, J., McKenna, S. A., & Patel, T. R. (2016). Dynamic light scattering: a practical guide and applications in biomedical sciences. *Biophysical Reviews*, *8*(4), 409–427. https://doi.org/10.1007/s12551-016-0218-6
Tanford, C. (1961). Physical chemistry of macromolecules. In *Journal of Pharmaceutical Sciences*. Wiley.
Velev, O. D., Kaler, E. W., & Lenhoff, A. M. (1998). Protein Interactions in Solution Characterized by Light and Neutron Scattering: Comparison of Lysozyme and Chymotrypsinogen. *Biophysical Journal*, *75*(6), 2682–2697. https://doi.org/10.1016/S0006-3495(98)77713-6
Wills, P. R., Georgalis, Y., Dijk, J., & Winzor, D. J. (1995). Measurement of thermodynamic nonideality arising from volume-exclusion interactions between proteins and polymers. *Biophysical Chemistry*, *57*(1), 37–46. https://doi.org/10.1016/0301-4622(95)00043-W
Wilson, W. W., & DeLucas, L. J. (2014). Applications of the second virial coefficient: protein crystallization and solubility. *Acta Crystallographica Section F Structural Biology Communications*, *70*(5), 543–554. https://doi.org/10.1107/S2053230X1400867X
Wright, R. T., Hayes, D., Sherwood, P. J., Stafford, W. F., & Correia, J. J. (2018). AUC measurements of diffusion coefficients of monoclonal antibodies in the presence of human serum proteins. *European Biophysics Journal*, *47*(7), 709–722. https://doi.org/10.1007/s00249-018-1319-x
Yadav, S., Scherer, T. M., Shire, S. J., & Kalonia, D. S. (2011). Use of dynamic light scattering to determine second virial coefficient in a semidilute concentration regime. *Analytical Biochemistry*, *411*(2), 292–296. https://doi.org/10.1016/j.ab.2010.12.014
Yadav, S., Shire, S. J., & Kalonia, D. S. (2011). Viscosity Analysis of High Concentration Bovine Serum Albumin Aqueous Solutions. *Pharmaceutical Research*, *28*(8), 1973–1983. https://doi.org/10.1007/s11095-011-0424-7
Zhou, H.-X., & Dill, K. A. (2001). Stabilization of Proteins in Confined Spaces †. *Biochemistry*, *40*(38), 11289–11293. https://doi.org/10.1021/bi0155504

CHAPTER 3

The Origins of Nonideality Exhibited by Monoclonal Antibodies and Fab Fragments in Human Serum

Note: This chapter was adapted from the manuscript: Larsen HA, Atkins WM, Nath A. The Origins of Nonideality Exhibited by Monoclonal Antibodies and Fab Fragments in Human Serum

3.1 Introduction

Therapeutic antibodies show significant clinical promise but are challenging molecules to study and develop. Antibody-derived therapeutics are rapidly becoming the predominant treatment modality for many cancers, autoimmune disorders, and other diseases (Hafeez et al., 2018; Kimiz-Gebologlu et al., 2018; Lu et al., 2020). As of 2021, 100 therapeutic antibodies have been FDA approved with 800 in the clinical pipeline and many more in earlier stages of development (Kaplon et al., 2022). Advances in protein engineering and optimization have also driven development of non-traditional antibody platforms – such as antibody-drug conjugates (ADCs), bispecific antibodies (bsAb), Fc-fusion proteins – that are also reaching the clinic, albeit in smaller numbers (Abdollahpour-Alitappeh et al., 2019; Godar et al., 2018; Mullard, 2021). While therapeutic antibodies are more targeted and potent than most traditional small molecule therapies, their development is challenging and consequently time consuming and expensive. This inefficiency reflects, in large part, major limitations in our understanding of the pharmacokinetics and pharmacodynamics of antibody-based therapeutics.

Therapeutic antibody development requires consideration of folding stability, aggregation propensity, and protein-protein interactions, all of which can be perturbed *in vivo* due to thermodynamic nonideality. In highly concentrated solutions of other macromolecules, proteins may experience macromolecular crowding as well as weak, nonspecific interactions with co-

solutes that lead to deviations from the ideal behaviors seen in dilute conditions. These nonideal effects can perturb stability and molecular recognition in ways that are challenging to predict and model (Bhattacharya et al., 2013; Kuznetsova et al., 2015; Rivas & Minton, 2022; Sarkar et al., 2013; Zhou et al., 2008).

Despite extensive characterization *in vitro*, little is known about the behavior of biopharmaceuticals in relevant physiological environments. Given the long circulating half-lives of therapeutic antibodies (typically several weeks), blood serum is the biological environment to which they are exposed the longest. For this reason, there is growing interest in understanding how therapeutic antibodies interact with serum proteins, and how serum impacts target or receptor binding (Chaturvedi et al., 2020; Demeule et al., 2009; Kim et al., 2019; Larsen et al., 2021; Wright, Hayes, Stafford, et al., 2018). Human serum is a concentrated, complex fluid whose composition varies with physiological or disease state, from one individual to another; in general, serum contains approximately 60-80 mg/mL protein, comprised of mainly albumin (60%) and immunoglobulin G, IgG (20%) with lower levels of other globulins, lipoproteins, transport proteins, complement factors, and smaller osmolytes (Anderson et al., 2004; Gonzalez-Quintela et al., 2008; Leeman et al., 2018).

In vitro methods capable of characterizing the properties of therapeutic antibodies directly in such complex media are limited. However, fluorescence correlation spectroscopy (FCS) is a single-molecule fluorescence technique capable of characterizing the diffusion of molecules directly in environments such as serum and plasma (Macháň & Wohland, 2014; Schmitt et al., 2022; L. Yu et al., 2021). This provides a key advantage over classical analytical techniques currently used during biologics development that are typically confined to dilute, ideal buffer systems. Techniques with fluorescence detection capabilities, such as analytical

ultracentrifugation (AUC-FDS) and size-exclusion chromatography (SEC-FL), can complete in-serum measurements. However, there are disadvantages associated with each technique. AUC is expensive and requires expertise in both running experiments and analyzing sedimentation data, while the stationary phase in SEC has many limitations that can lead to significant error in molecular weight estimates (Burgess, 2018). FCS does not require a stationary phase or large quantities of protein and is relatively cheap and easy to implement, making it an appealing alternative.

This works builds on our previously developed and validated in-serum FCS approach to probe serum-induced nonideality effects for IgG1 antibodies through apparent second virial coefficient ($B_{2,app}$) measurements (Larsen et al., 2021). Traditional self-term (B_{22}) and cross-term (B_{12}) second virial coefficients describe weak, nonspecific interactions between two of the same or different molecules, respectively. The sign of the coefficient informs on the nature of the interactions, where a positive value indicates repulsion, a negative value attraction, and a zero value no interaction between the molecules of interest. Conversely, the apparent second virial coefficient ($B_{2,app}$) probes weak, nonspecific interactions between a labeled species and the components in complex media (such as serum) as a measure of global nonideality. In this case, a positive value indicates net repulsion, a negative value net attraction, while a zero value likely indicates a balance between attraction and repulsion.

In our validation experiments, we used two model systems for traditional self- and cross-term virial coefficient measurements. BSA served as a model system to measure self-term second virial coefficient values at different pH and ionic strength conditions by comparing FCS results to those obtained via a well-established DLS approach. The cross-term virial coefficient value obtained by FCS for NIST mAb and albumin was also comparable to the published AUC value,

providing confidence in FCS for traditional virial coefficient measurements. $B_{2,app}$ measurements were completed for a panel of labeled IgG1 antibodies in fetal bovine serum (FBS) by monitoring the changes in diffusion coefficient over increasing concentrations of serum.

Briefly, the diffusion coefficient (D) of a labeled species (in our case determined by FCS) at a given concentration of unlabeled species (c_p) can be used to determine the second osmotic virial coefficient (B_2) through the following relationship:

$$D = D^0(1 + (2B_2M - \bar{V})c_p) = D^0(1 + k_{diff}c_p) \quad \text{.....(1)}$$

where D^0 is the diffusion coefficient in infinite dilution, M is the effective molecular weight of unlabeled species, $\bar{V}$ is the partial specific volume, and k_{diff} is the diffusion interaction parameter defined by:

$$k_{diff} = 2B_2M - \bar{V} \approx 2B_2M \quad \text{.....(2)}$$

In the case of complex mixtures such as serum, the appropriate molecular weight of the interacting species is unclear, reporting results in terms of k_{diff} ($2B_2M$), rather than B_2, avoids this problem. The complete theory behind our apparent second virial coefficient approach can be found in our previous publication (Larsen et al., 2021). Note the change in nomenclature: we denote the diffusion interaction parameter k_{diff} rather than k_D to avoid confusion with binding equilibrium constant, K_D.

Higher order virial terms are ignored in the approach outlined above due to their low and likely negligible contributions at concentrations relevant to serum and plasma. However, this analysis could be extended in the future following Kirkwood-Buff (KB) solution theory to account for higher-order interactions (Blanco et al., 2011, 2014). Accordingly, our current interpretation of $B_{2,app}$ focuses on the sign of the parameter and qualitative changes rather than the precise magnitude of the values. This approach trades formal rigor for the ability to compare our $B_{2,app}$

values with analogous B_2 values commonly determined in similar concentration regimes by academic and industry groups (Correia et al., 2018; Yang et al., 2018).

There are many well-established techniques used to determine traditional second virial coefficient values. Perhaps the most common are light scattering techniques, such as dynamic light scattering (DLS), static-light scattering (SLS), and composition-gradient multi-angle light scattering (Ma et al., 2015; Roberts et al., 2014; Yadav et al., 2011). The major disadvantage of DLS and SLS is the inability to complete measurements in multicomponent systems, limiting them to only self-term virial coefficient determination. CG-MALS is capable of measurements in multicomponent systems, albeit not as complex as serum. As previously mentioned, AUC is capable of measuring both self- and cross-term virial coefficient values (Correia et al., 2018) and has the potential to complete in-serum measurements, but methods to do so are not well-established due to the complexity of the technique. Although the above-mentioned methods can rigorously determine traditional second virial coefficient values, our FCS $B_{2,app}$ measurements that probe global nonideality effects sacrifice some rigor for easier and more physiologically relevant information.

Classic experiments investigating the effects of complex media on protein behavior have focused on either excluded volume effects by mimicking biological environments with crowding agents (i.e., PEGs, polymers, or proteins)(Minton, 1998; Wills et al., 1995), or nonideality by isolating specific components and characterizing their effects independently (Moreira et al., 2007; Quigley & Williams, 2015; Velev et al., 1998). More recent studies investigating the effects of serum-induced nonideality on therapeutic antibodies have taken the traditional approach of completing independent second virial coefficient measurements with isolated serum proteins (Kim et al., 2019; Wright, Hayes, Sherwood, et al., 2018). However, such approaches may not

effectively measure global nonideality in serum, because they cannot capture the effects that serum components have on each other. $B_{2,eff}$ measurements present an avenue to resolve this question directly.Furthermore, $B_{2,app}$ measurements can be expanded to other biological fluids to characterize nonideality effects in other biological environments.

Here, we characterize the contributions of albumin and serum IgG antibodies to serum-induced global nonideality effects for a panel of IgG1 antibodies. Cross-term virial coefficient measurements with IgG antibodies isolated from human serum, HSA, and IgG-depleted serum were compared to values obtained in pooled human serum. In addition, cross-term virial coefficient measurements were carried out with antibody Fab and Fc fragments to determine how these different domains mediate nonideal effects on mAbs. This comparison also highlights systematic differences between mAb- and Fab-based therapeutic platforms. Our studies provide unprecedented, detailed insight into the impacts of serum-induced nonideality on therapeutic antibodies and other protein-based therapeutics.

3.2 Experimental Procedures

3.2.1 Protein samples and other materials

The NIST mAb humanized IgG antibody (10 mg/mL) was purchased from the National Institute of Reference Standards and Technology (RM 8617). Tocilizumab (35 mg/mL) and anti-RSV mAb (10.91 mg/mL) IgG antibodies were provided by the Genentech Outgoing Materials Transfer Agreement program and Jannsen Pharmaceuticals, respectively. Albumin from human serum (lyophilized powder) and serum IgG antibodies were purchased from Sigma-Aldrich. Pooled human serum (34019) and IgG-depleted serum (34021) were purchased from Pel-Freeze Biologics. Recombinant Human IgG1 Fc Fragment was purchased from Thermo Scientific (A42561). Transient expression of Human anti-gp120 IgG1 mAb was carried out in Expi293F

cells (Thermo Fisher A14635) using a 1:3 ratio of heavy chain (HC) to light chain (LC) DNA according to the manufacturer's protocol. Purification was performed via Protein A column in 1x phosphate buffered saline (PBS: 150 mM NaCl, 2.7 mM KCl, 10 mM Na_2HPO_4) pH 7.2. Briefly, supernatant was loaded onto the protein A column, washed with PBS, and eluted with 100 mM sodium citrate, pH 3.5 into 1.0-mL fractions. Ab-containing fractions (based on A280 UV-signal) were pooled and immediately buffer exchanged into 1x PBS using Zeba Spin Desalting columns (Thermo Scientific), following the manufacturer's protocol. The antibodies and HSA were stored at 4°C in PBS pH 7.4. Serum and the Fc fragment were stored at -20°C until use and thawed at 4°C prior to experiments.

3.2.2 Protein labeling

Following the Thermo Scientific labeling protocol, NIST mAb, tocilizumab, anti-RSV mAb, anti-gp120 mAb, and the Fc fragment were labeled with Alexa-Fluor 488 carboxylic acid, succinimidyl ester (Thermo Scientific A20000; A488). Desalting was carried out using Zeba Spin Desalting Columns from Thermo Scientific (89882), following the Thermo Scientific protocol. Labeling efficiency was determined through UV-Vis spectroscopy (absorbance measurements at 280 nm and 494 nm) on a Nanodrop One Microvolume UV-Vis spectrometer (Thermo Scientific, ND-ONE-W). Additionally, diffusion time was used to verify the absence of free dye in solution by comparing observed changes to expected changes in diffusion from free dye to protein-bound dye. A488-mAbs were stored in 1x PBS pH 7.4 at 4°C. Typically, 1-2 A488 molecules covalently attached to each mAb or Fab fragment, while 0.5 molecules of A488 covalently attached to the Fc fragment.

3.2.3 Antibody deglycosylation

NIST mAb, tocilizumab, anti-RSV mAb and anti-gp120 mAb deglycosylation was carried out by adding 2 µL of PNGaseF (New England Biolabs P0711S) to 60 µg of antibody (in 1x PBS, pH 7.4) in a reaction volume of 20 µL following manufacturer's suggestions. After 2 hours at room temperature, PNGaseF was removed from samples using Zeba Spin Desalting Columns from Thermo Scientific (87766). Deglycosylation products were confirmed by SDS-PAGE using 4-20% polyacrylamide gels from Bio-Rad (4561094). Deglycosylated antibodies were labeled with Alexa Fluor 488 SE using the labeling protocol above. Samples were stored in 1x PBS, pH 7.4 at 4°C.

3.2.4 Antibody fragmentation

NIST mAb, tocilizumab, anti-RSV mAb, and anti-gp120 mAb were first labeled with Alexa Fluor 488 SE using the labeling protocol above. A488-labeled antibodies were fragmented following the Thermo Scientific protocol using a Pierce Fab Micro Preparation kit (Thermo Scientific 44685). Fab fragments were stored in 1x PBS pH 7.4 at 4°C and used within 48 hours of fragmentation. Fc fragments were not salvaged using this protocol due to low yield. Recombinant IgG1 Fc was ordered from Thermo Scientific for experiments.

3.2.5 FCS

All experiments were carried out at room temperature on a home-built instrument based on a Zeiss Axio Observer D1 microscope equipped with HydraHarp 400 detection electronics, Tau-SPAD photon counting detector, and pulsed 485 nm laser line driven by a PicoQuant PDL 828 Sepia II driver (PicoQuant GmbH, Berlin, Germany). Sample aliquots of 50 µL were placed on a 22x22 cover glass (VWR 48366-067). Five 30 s measurements of 10 nM A-488 were used to calibrate the instrument at the start of each experiment. The average diffusion time was used to

determine the ω^2 parameter needed for second virial coefficient calculations. Antibody and Fab fragment measurements (n=5) were carried out for 60s each.

A488-labeled antibodies or antibody fragments were diluted to ~20 nM in varying concentrations of carrier protein (HSA, pooled IgG antibodies from human serum, pooled human serum, or IgG-depleted human serum) ranging from 0% to 100%, where the 100% condition ranged from 10-62 mg/mL depending on the experiment.

FCS intensity time traces were imported into PRISM Graphpad software and fit to a single component FCS equation to yield diffusion time, τ_D, using the following equation (Haustein Schwille, 2007):

$$G_{FCS}(\tau) = \frac{1}{N}\left(\frac{1}{1+{}^{\tau}/_{\tau_D}}\right)\sqrt{\frac{1}{1+s^2{}^{\tau}/_{\tau_D}}} \quad \text{.....(1)}$$

where N is the mean number of molecules in observation volume, τ_D is the correlation decay time due to translational diffusion, and *s* is the axial ratio of the detection volume (0.2 for our instrument). Translational diffusion coefficients (*D)* were determined from diffusion times and used to calculate interaction parameters (k_{diff}), that are directly proportional to the second osmotic virial coefficient (B_2). The methodology and validation behind these measurements is outlined in our previous publication (Larsen et al., 2021).

3.3 Results

The ability of FCS to measure diffusion coefficients in complex media enables the quantification of global nonideality effects on therapeutic antibodies in biological environments such as serum. Using our previously established approach (Larsen et al., 2021), we have transitioned from measurements in fetal bovine serum to measurements in pooled human serum as a more representative physiological model. Here, we compare how the two most abundant serum proteins, human serum albumin (HSA) and serum IgG antibodies, contribute to serum-induced

nonideality for a panel of monoclonal antibodies and their corresponding Fab fragments. Second virial coefficients were measured in pooled human serum, IgG-depleted serum, IgG antibodies isolated from human serum, and HSA, as summarized in **Table 3.1**. This comparative approach provides insight into component effects in isolation and in the context of serum.

Figure 3.1 depicts the experimental setup for determining second virial coefficient values. Alexa Fluor 488 SE labeled antibodies are diluted into varying concentrations of carrier solutions (human serum, IgG-depleted serum, IgG antibodies isolated from human serum, or HSA) and the corresponding diffusion coefficients are determined from FCS diffusion time measurements. Diffusion coefficients were adjusted for bulk viscosity, plotted against total protein concentration of the carrier solution, and fit to **Equation 1**, where the slope over the y-intercept yields interactions parameter k_{diff} that is directly proportional to B_2 via the relationship in **Equation 2**.

Interpretation of cross-term interaction values in serum and HSA are slightly different. In the case of serum, values deviating away from zero in the positive and negative direction indicate either net repulsion or attraction, respectively, while a value of zero likely indicates a balance between attraction and repulsion. Conversely with HSA, positive and negative values indicate repulsive and attractive interactions, respectively, while a value of zero indicates there are no net interactions between IgG1 and HSA.

3.3.1 mAb interactions with serum and serum proteins

Apparent second virial coefficient measurements were carried out in pooled human serum to probe global nonideality between labeled antibodies and serum components. Values of k_{diff} in serum were determined for a panel of four antibodies: NIST mAb, tocilizumab, anti-gp120 mAb, and anti-RSV mAb. NIST mAb is a widely used reference standard mAb, tocilizumab is a clinically approved therapeutic (an interleukin-6 receptor inhibitor used to treat autoimmune

diseases), while anti-RSV mAb (targeting fusion (F) glycoprotein on respiratory syncytial virus) and anti-gp120 mAb (targeting envelop glycoprotein on human immunodeficiency virus) are research antibodies expressed in-house. NIST mAb (**Figure 3.2A**) and tocilizumab (**Figure 3.2B**) both displayed a balance of attractive and repulsive interactions with serum, with k_{diff} values (–1.1 ± 0.8 mL/g and –0.3 ± 0.3 mL/g respectively) not significantly different from zero. These results are comparable to those obtained previously in FBS for the same antibodies.(Larsen et al., 2021) In contrast, anti-gp120 mAb (**Figure 3.2C**) exhibited a k_{diff} value of –2.0 ± 0.1 mL/g, while anti-RSV mAb (**Figure 3.2D**) exhibited a k_{diff} value of –6.5 ± 0.7 mL/g, suggesting weak-to-moderately attractive interactions with serum components. It would be worth investigating whether there is a correlation between antibody light chain and k_{diff} values. While NIST mAb and tocilizumab have kappa light chains, the type of light chains in the anti-gp120 and anti-RSV mAbs expressed in-house are currently unknown. Therefore, anti-RSV mAb and anti-gp120 mAb should be sequenced in the future to determine the type of light chains they contain. Perhaps lambda light chains participate in attractive interactions with serum proteins given the negative k_{diff} values observed for anti-gp120 mAb and anti-RSV mAb compared values of ~0mL/g for the other two antibodies. If anti-gp120 mAb and anti-RSV mAb contain lambda light chains, this would suggest a correlation.

Upon depleting serum of IgG antibodies, k_{diff} values became positive, indicating net repulsion in the depleted serum. In all cases, the change from either a negative or zero value in pooled human serum to a positive value in the depleted serum indicates that serum IgG antibodies are primarily responsible for attractive interactions in serum. Values measured with HSA were very similar to IgG-depleted serum for all mAbs except anti-RSV. The decrease of 5.1 mL/g for anti-RSV mAb going from HSA to IgG-depleted serum suggests that some non-IgG components

of serum also interact with this mAb, but not the others in our panel. Interestingly, measurements with serum IgG antibodies isolated from pooled human serum produced negative k_{diff} values ranging from –12.5 mL/g to –16 mL/g, indicating much stronger attractive interactions with labeled antibodies. The discrepancy in the magnitude change in k_{diff} values with pooled human serum to those in IgG-depleted serum and serum IgG antibodies isolated from serum indicate that the approach of characterizing molecules of interest in the presence of isolated components is not an accurate representation of nonideality in serum. Complete D_{adj} vs. c plots are presented in **Figures 3.3-3.6.**

3.3.2 Fc fragment interactions with serum and serum proteins

The values of k_{diff} were measured for IgG1 Fc fragment with pooled human serum, IgG-depleted serum, and HSA (**Figure 3.7A**). In all cases, k_{diff} did not significantly deviate from 0 mL/g, indicating that there are no net interactions between IgG1 Fc and serum IgG antibodies, HSA, or whole serum. This suggests that nonideal interactions of mAbs are likely driven by differences in the Fab domain, while Fc domains may be evolutionarily optimized to avoid non-specific interactions with other constituents of serum. Complete D_{adj} vs. c plots are presented in **Figure 3.8.**

3.3.3 Deglycosylated mAb interactions with serum and serum proteins

Glycosylation of IgG1 mAbs, which occurs predominantly at specific sites in the Fc domain, can alter interactions with Fc receptors and consequent effector functions (Cobb, 2020). To test the effect of this functional modification on mAb interactions with serum components, k_{diff} values were measured for NIST mAb, tocilizumab, anti-gp120 mAb, and anti-RSV mAb in pooled human serum following deglycosylation (**Figure 3.7B**). In all cases, k_{diff} values were similar between deglycosylated and glycosylated mAbs, suggesting that glycans do not significantly

contribute to nonideal interactions with serum. While there is a trend of slightly more negative k_{diff} values for deglycosylated mAbs which could indicate increased propensity for interactions with serum, these shifts are not statistically significant. Taken together, these observations point to structural or dynamic differences in the Fab domains as drivers of nonideality in mAb/serum interactions. Complete D_{adj} vs. c plots are presented in **Figure 3.9** and a representative SDS-PAGE verifying deglycosylation products can be found in **Figure 3.10**.

3.3.4 Fab fragment interactions with serum and serum proteins

$B_{2,app}$ values for Fab fragments generated from NIST mAb, tocilizumab, anti-RSV mAb, and anti-gp120 mAbs were measured in pooled human serum, IgG-depleted serum, and HSA (**Figure 3.11**). In all cases, k_{diff} values were more negative in pooled human serum for Fab fragments than for the corresponding full-length antibodies. This indicates that Fab fragments experience greater net attraction to serum which could be attributed to loss of interactions between the Fab and Fc domains, exposing more potential sites for non-specific interactions. Since Fab fragments are known to be less stable than full-length antibodies, (Röthlisberger et al., 2005), experiments were carried out within 48 hours of fragmentation to avoid the risk of aggregation. Furthermore, observed diffusion times of Fab fragments were consistent with expected values, providing confidence that aggregation of A488-labeled Fab fragments was not occurring.

As with intact mAbs (**Figure 3.2**), IgG depletion decreased or eliminated attractive interactions with serum. Fab k_{diff} values in IgG-depleted serum were increased by 5–7 mL/g relative to pooled human serum, suggesting that serum IgGs are key mediators of attractive interactions for Fab fragments. However, for NIST mAb (**Figure 3.11A**) and anti-RSV mAb (**Figure 3.11D**), k_{diff} in IgG-depleted serum was significantly lower for Fabs than for the parental mAbs, indicating that non-IgG components were also playing a role in attraction. The overall

trends in the data suggest that Fab fragments display stronger attractive interactions with more diverse serum co-solutes and greater variability than intact mAbs, all of which could carry negative functional consequences.

The anti-gp120 Fab (**Figure 3.11C**) and anti-RSV Fab (**Figure 3.11D**) are modestly repelled by HSA (as evident by positive k_{diff} values), while NIST Fab (**Figure 3.11A**) and tocilizumab Fab fragment (**Figure 3.11B**) exhibit no interaction with albumin (k_{diff} values close to 0 mL/g). The latter result is striking, given that tocilizumab displays a positive k_{diff} value in IgG-depleted serum, which is predominantly HSA. It would seem that the minor fraction of non-HSA, non-IgG components may be able to increase the repulsion between HSA and the tocilizumab Fab fragment to generate the behavior observed in IgG-depleted serum. This further supports the idea that the net interaction with serum is not equal to the sum of the individual interactions with isolated serum components. Moreover, these non-additive effects can vary widely from one molecule to the next. Complete D_{adj} vs. c plots are presented in **Figures 3.12-3.15.**

3.4 Discussion

Our understanding of protein-protein interactions in biological environments is limited by the inability of most analytical techniques to complete measurements in complex media. For this reason, experiments aimed at investigating serum-induced nonideality through second virial coefficient (B_2) measurements have focused on independent cross-term (B_{12}) measurements with isolated serum components (Correia et al., 2018; Kim et al., 2019). Our results, however, suggest that this reductionist approach does not sufficiently model nonideality in serum. Second virial coefficient results for the panel of antibodies in **Figure 3.2** with serum, HSA, and pooled IgG antibodies isolated from serum clearly support this inference. Repulsion is observed with HSA (as evident by positive k_{diff} values), while either attraction or a balance between attraction and

repulsion is observed in serum (values ranging from 0 to –6.5 mL/g). The lower k_{diff} values in serum compared to HSA suggests that attractive interactions likely occur simultaneously in addition to the repulsion observed with albumin, a phenomenon that could not have been probed using measurements with individual components. When depleting serum of IgG antibodies, the k_{diff} values become positive indicating that the attraction observed in serum is likely due to serum IgG antibodies. However, IgG antibodies isolated from serum were very strongly attracted to mAbs, with k_{diff} values ranging from –12 to –16 mL/g, much greater than the change in k_{diff} when going from human serum to IgG-depleted serum. This is likely due to interactions amongst serum proteins that contribute to global nonideality but are lost when specific components are studied in isolation. These results mirror AUC studies (Yang et al., 2018) where weak attractive interactions were observed between mAbs and pooled serum IgGs. While the magnitude of k_{diff} values measured here differ from reported k_s values (as expected when comparing parameters based on sedimentation vs. diffusion), the trends and overall conclusion are consistent.

Our results may provide insight into the evolutionary pressures on nonideal behavior exhibited by mAbs in biological environments such as serum. Conserved Fc domains have likely evolved to optimize interactions with Fc-receptors and complement proteins that mediate effector functions, while simultaneously disfavoring nonspecific interactions with other constituents of serum. This is supported by our results for IgG1 Fc fragment in **Figure 3.7** which showed no net interactions with HSA, IgG-depleted serum, or whole serum, as evident by k_{diff} values that did not significantly deviate from 0 mL/g. Conversely, the hypervariable sequences in Fab domains are not subject to this selective pressure (particularly true of artificial or engineered mAbs) and therefore drive nonideal interactions with serum. Fab fragments for the panel of antibodies in **Figure 3.11** display attraction to serum IgG antibodies, as evident by the changes in k_{diff} from

negative values in pooled human serum to positive values in IgG-depleted serum. Furthermore, the more negative k_{diff} values observed for Fab fragments compared to corresponding full-length antibodies in **Figure 3.11** suggests that Fc domains essentially buffer nonideal interactions in the Fab domain, potentially highlighting a previously unappreciated advantage of mAbs over Fab fragments in therapeutic development.

While the second virial coefficient has found applications in the biopharmaceutical industry, our analysis provides a new use of this parameter in the drug development process. Current applications of the second virial coefficient in biologics development are predominantly focused on characterizing protein aggregation. During manufacturing, biologics are subject to a variety of stresses (i.e., temperature, pH, ionic strength, etc.) that can promote aggregation. In addition, highly concentrated antibody formulations are susceptible to aggregation that can negatively impact the overall efficacy, safety, and half-life of the therapeutic product (Le Basle et al., 2020). Therefore, aggregation continues to be a major obstacle and focus during the development process. As a result, self-term virial coefficient (B_{22}) measurements have been implemented in biologics development to probe aggregation propensity (Baek & Zydney, 2018; Le Brun et al., 2010; Obrezanova et al., 2015; Pham & Meng, 2020; Saluja et al., 2010). Conversely, cross-term virial coefficient measurements are not as common but have been used to probe protein-excipient interactions during formulation development (Kamerzell et al., 2011). Such applications of the second virial coefficient, albeit essential, only provide information on the behavior of the therapeutic prior to administration and little is known about the behavior of therapeutic proteins in biological environments. Our $B_{2,app}$ measurements provide a tool to better understand how therapeutic proteins interact with co-solutes in crowded, complex biological environments.

Better methods for early identification of proteins more likely to fail would make biologics development faster and more efficient. Although a variety of *in silico*, *in vitro*, and *in vivo* tools are currently used to de-risk molecules in development, the pharmacokinetics of therapeutic antibodies remains complex and difficult to predict (Dostalek et al., 2017). Many biochemical and biophysical properties have been shown to impact the pharmacokinetics of proteins, such as hydrophobicity (Sharma et al., 2014), net charge (Igawa et al., 2010), off-target binding (Hötzel et al., 2012), glycosylation (M. Yu et al., 2012), antigen binding (Shi, 2014), and interactions with Fc receptors, including neonatal Fc receptor (FcRn) (Liu, 2018; Wu et al., 2007). Although the impact of serum-induced nonideality on these properties has not yet been directly investigated, we have observed a case suggesting a potential correlation between net attraction in serum and lower *in vivo* binding affinity. In our previous study, Carlumab, a discontinued antibody from Janssen Therapeutics, exhibited more attraction (k_{diff} = –10.9 mL/g) to serum than clinical (tocilizumab) and reference standard (NIST mAb) antibodies (k_{diff} values = 0mL/g) (Larsen et al., 2021). Interestingly, Carlumab's failure during clinical trials was attributed to a discrepancy in the *in vitro* and *in vivo* binding affinity for its target, CCL2, that resulted in limited therapeutic efficacy (Majety et al., 2018). This directly supports the possibility that nonideal solutions can alter functional and therapeutic properties of biologics. However, the relationship between net attraction and discrepancies in antigen binding needs further investigation.

Further studies will reveal whether and how serum-induced nonideality can impact the overall efficacy of therapeutic antibodies. Results from this study suggest that serum IgG antibodies are responsible for attraction in serum, as evident by the change from negative or zero k_{diff} values in pooled human serum to positive k_{diff} values in IgG-depleted serum for four IgG1 antibodies. Interestingly, the attractive interactions were determined to occur in Fab domains,

which could have a negative impact on antigen binding. Attractive interactions are likely destabilizing in that they can lead to local unfolding in the antibody that can perturb binding. In effect, molecules that exhibit attractive interactions with serum are likely to be at greater risk of perturbation by the *in vivo* environment. Therefore, $B_{2,app}$ measurements have the potential to help de-risk therapeutic candidates during biologics development.

3.5 Conclusion

In this study, we used FCS-based second virial coefficient measurements to determine the contributions of albumin and IgG antibodies to global nonideality in serum for a panel of IgG1 antibodies. Apparent second virial coefficient measurements with pooled human serum, IgG-depleted serum, and in solutions of isolated serum proteins for a panel of full-length antibodies and their respective Fab fragments provided interesting insight into the origins of serum-induced nonideality. Differing results for the panel of IgG1 antibodies in pooled human serum supported our previous finding that nonideality effects are antibody dependent. Comparing interaction parameters across the different carrier solutions for each antibody revealed trends of attraction to serum IgG antibodies and repulsive interactions with albumin. Furthermore, attractive interactions were determined to occur in the Fab domain across the entire panel of antibodies, highlighting the potential for negative impacts to antigen binding. However, the significance of these measurements needs further investigation. Finally, comparing apparent second virial coefficient results in pooled human serum and IgG depleted serum to those obtained with HSA and pooled serum IgG antibodies, suggests that the classical approach of characterizing the contributions of isolated serum proteins, via independent cross-term virial coefficient measurements, does not adequately model nonideality in serum. $B_{2,app}$ measurements could provide an essential tool for understanding the behavior of therapeutic antibodies in physiological environments. Furthermore,

such measurements have the potential to enhance *in vitro* characterization used to de-risk therapeutic candidates during biologics development.

FIGURES

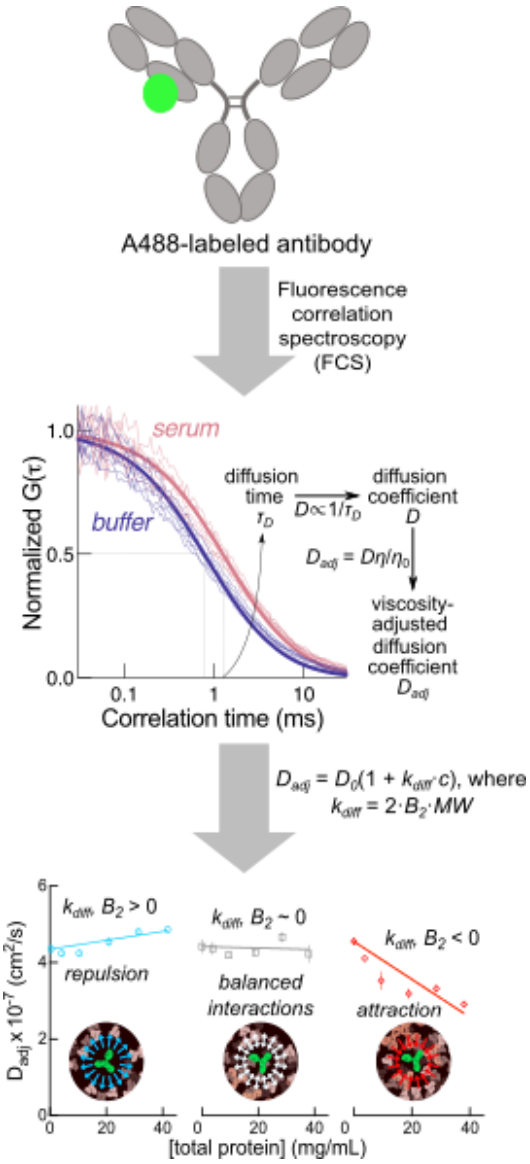

Figure 3.1: Model of k_{diff} (or $2B_2M$) determination: Alexa Fluor 488 SE labeled antibodies are diluted into varying concentrations of carrier solution (serum, depleted serum, isolated serum IgG antibodies, or HSA). The diffusion coefficient at each condition is determined via FCS diffusion time measurements. k_{diff} or B_2 values are determined by fitting plots of viscosity adjusted diffusion coefficients against carrier concentration to the linear equation $D = D^0(1 + k_{diff}c)$. Positive values indicate net repulsion in serum or repulsive interactions with isolated serum proteins, while negative values indicate net attraction in serum or attractive interactions with isolated serum proteins. A zero value likely indicates a balance between attraction and repulsion in serum as opposed to no interaction when measuring interactions with isolated proteins such as HSA.

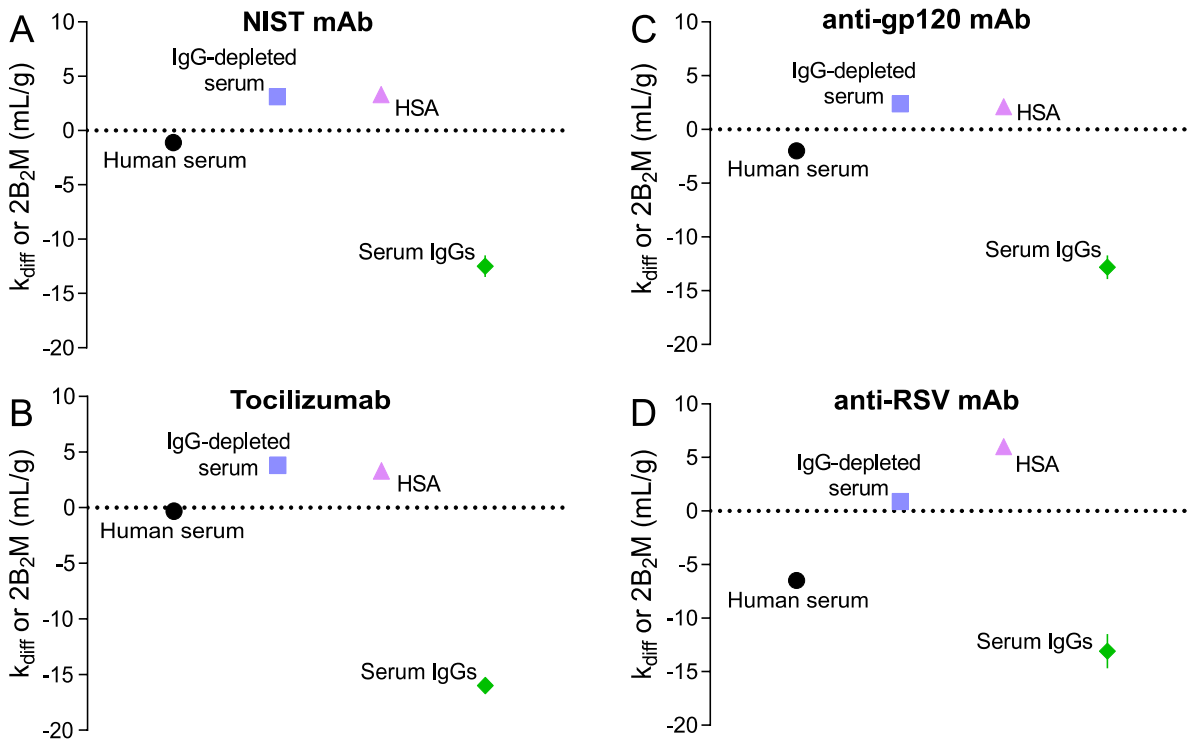

Figure 3.2: Comparison of cross-term interactions in human serum (black circles), IgG-depleted serum (blue squares), albumin (purple triangles), and IgG antibodies isolated form human serum (green diamonds) for NIST mAb (A), Tocilizumab (B), anti-gp120 mAb (C), and anti-RSV mAb (D). D_{adj} vs. c plots (Supplemental Figures S1–4) were fit to the linear equation $D = D^0(1 + k_{diff}c)$ to obtain k_{diff} values, with results presented as mean ± S.D. from three replicates with independent sample preparations.

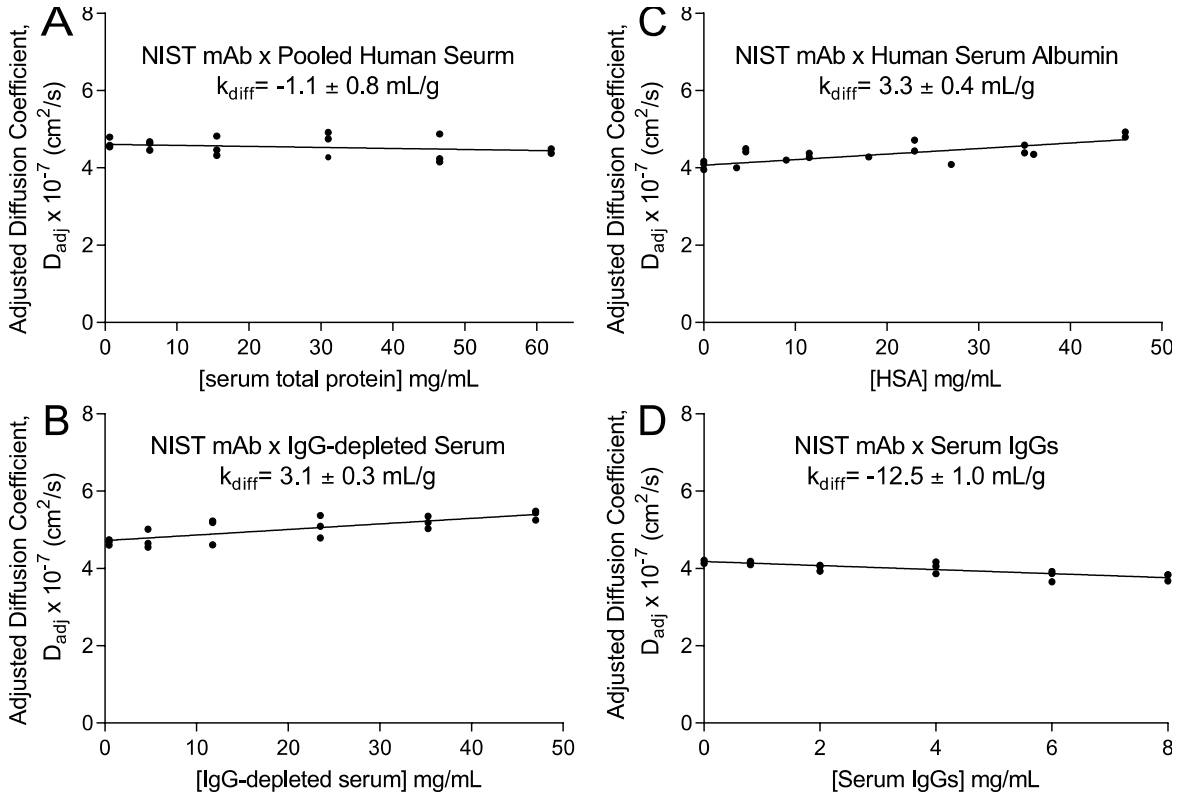

Figure 3.3: $B_{2,app}$ measurements of NIST mAb in various media, with k_{diff} values reported as mean ± S.D. of at least three independent experiments.

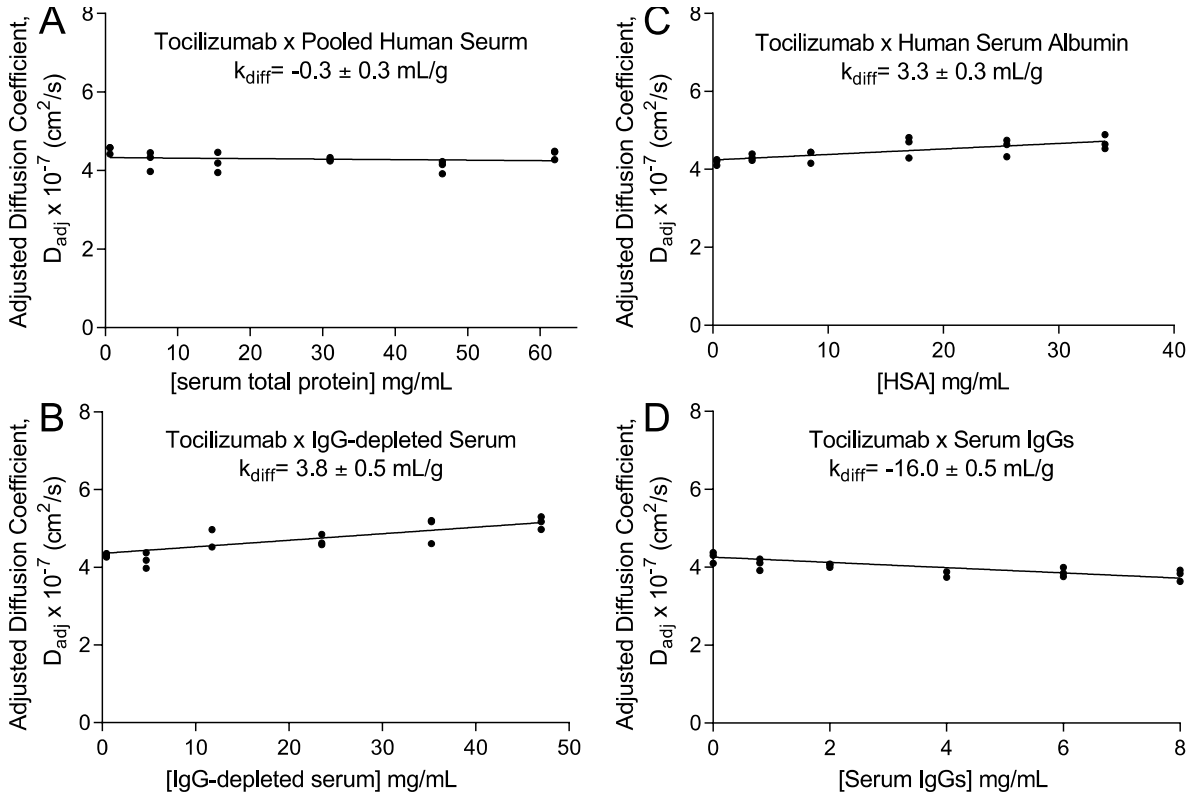

Figure 3.4: $B_{2,app}$ measurements of tocilizumab in various media, with k_{diff} values reported as mean ± S.D. of at least three independent experiments.

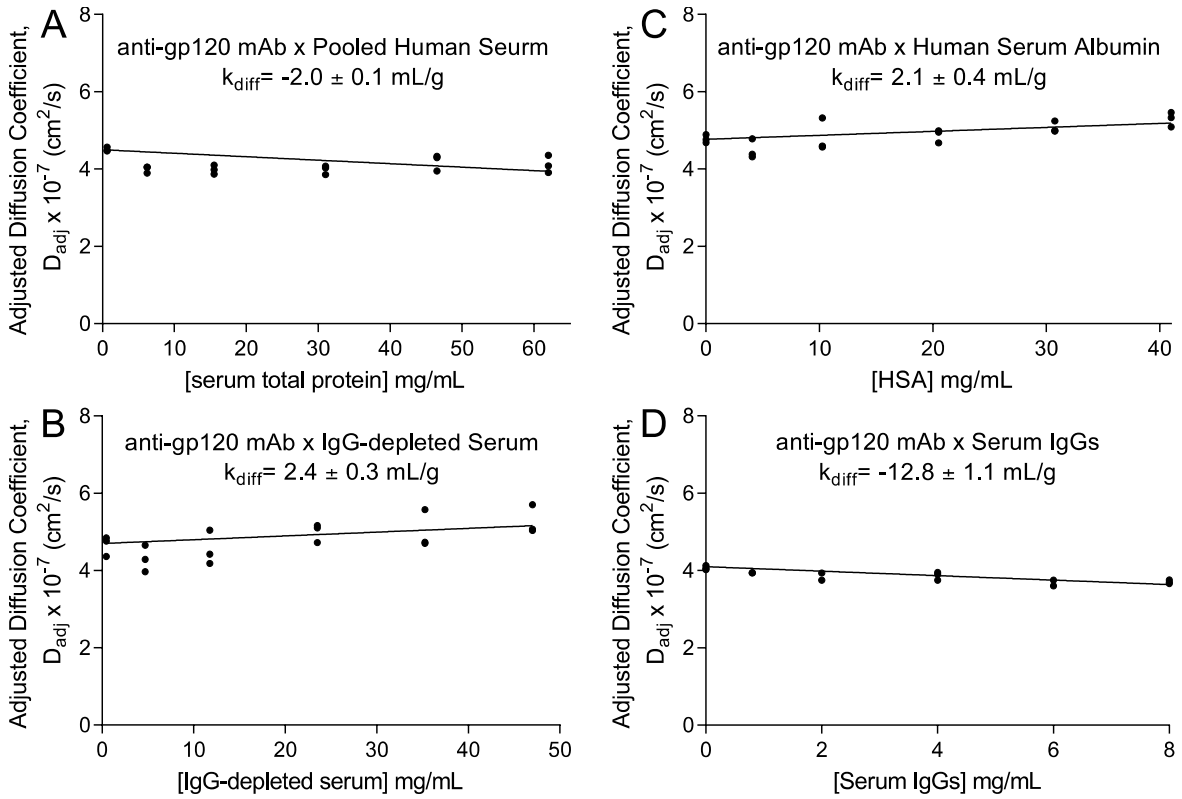

Figure 3.5: $B_{2,app}$ measurements of anti-gp120 mAb in various media, with k_{diff} values reported as mean ± S.D. of at least three independent experiments.

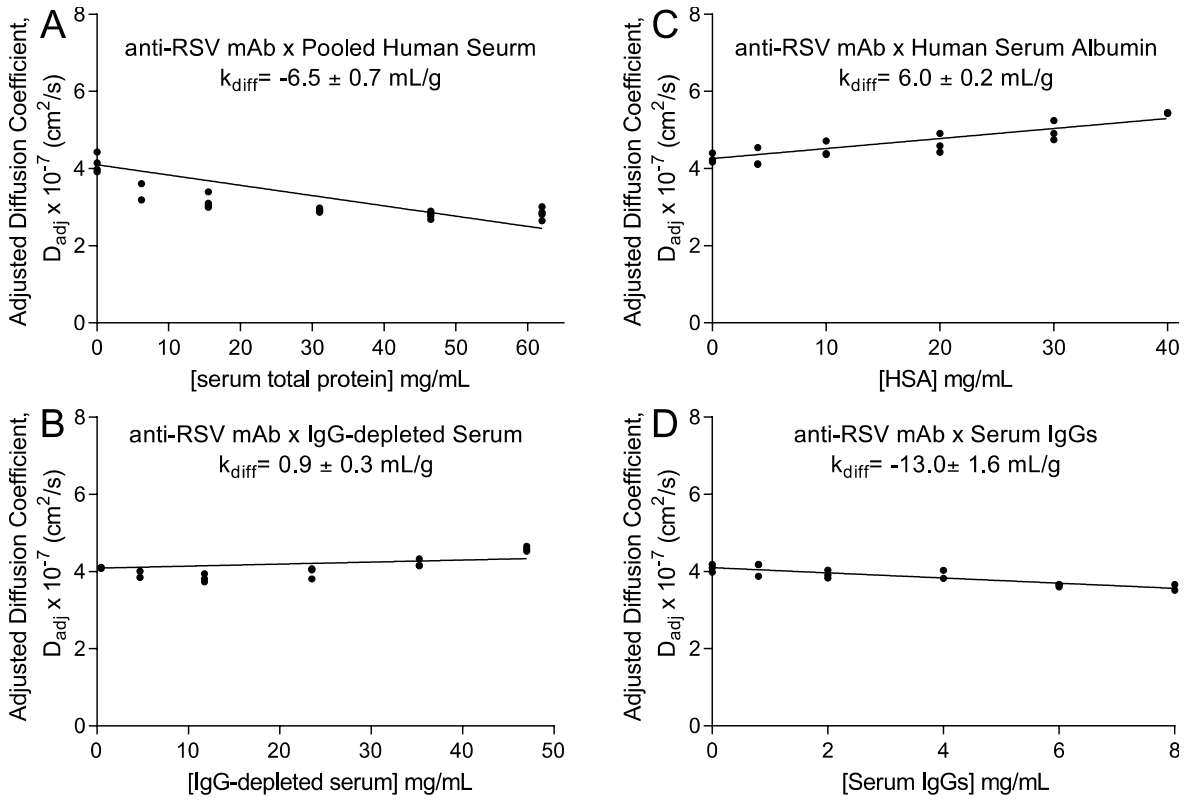

Figure 3.6: $B_{2,app}$ measurements of anti-RSV mAb in various media, with k_{diff} values reported as mean ± S.D. of at least three independent experiments.

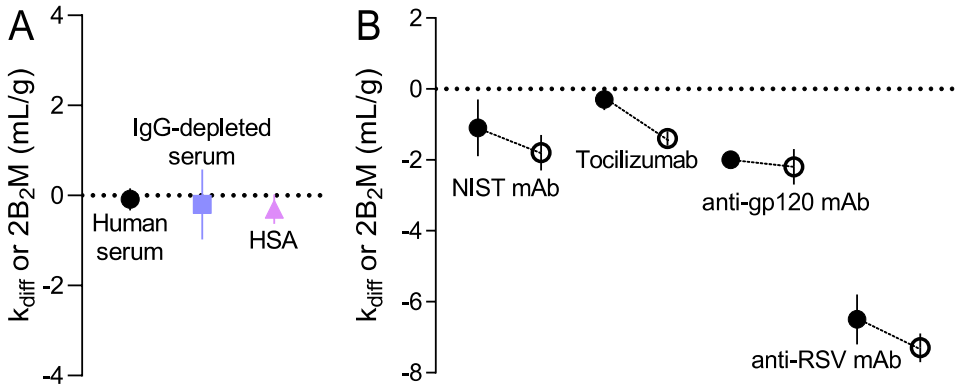

Figure 3.7: Cross term interaction for IgG1 Fc fragment (A) with serum (black circle), IgG-depleted serum (blue square), and HSA (purple triangle). Comparison of cross-term interactions in human serum for glycosylated (closed symbols) and deglycosylated (open symbols) NIST mAb, tocilizumab, anti-gp120 mAb, and anti-RSV mAb (B). D vs. c plots (Supplemental Figures S5, S7) were fit to the linear equation $D = D^0(1 + k_{diff}c)$ to obtain k_{diff} values with results presented as mean ± S.D. from three replicates with independent sample preparations.

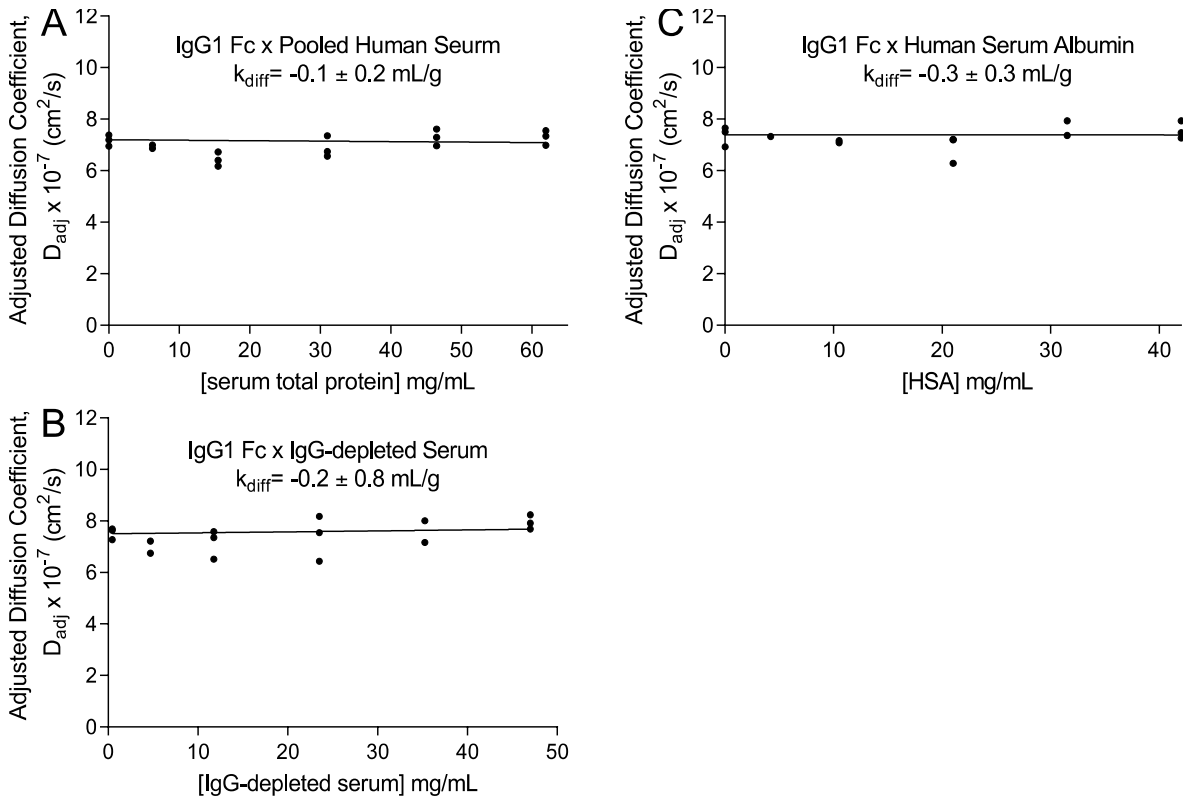

Figure 3.8: $B_{2,app}$ measurements of IgG1 Fc fragment in various media, with k_{diff} values reported as mean ± S.D. of at least three independent experiments.

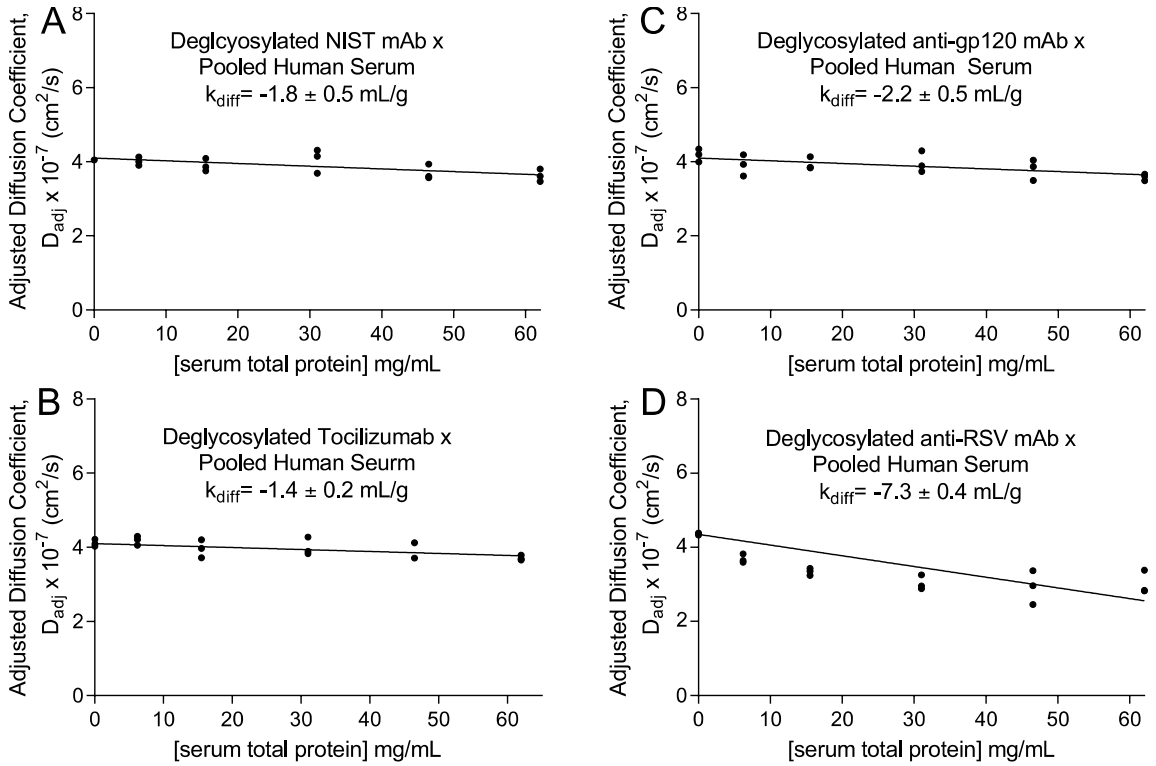

Figure 3.9: $B_{2,app}$ measurements of deglycosylated mAbs in serum, with k_{diff} values reported as mean ± S.D. of at least three independent experiments.

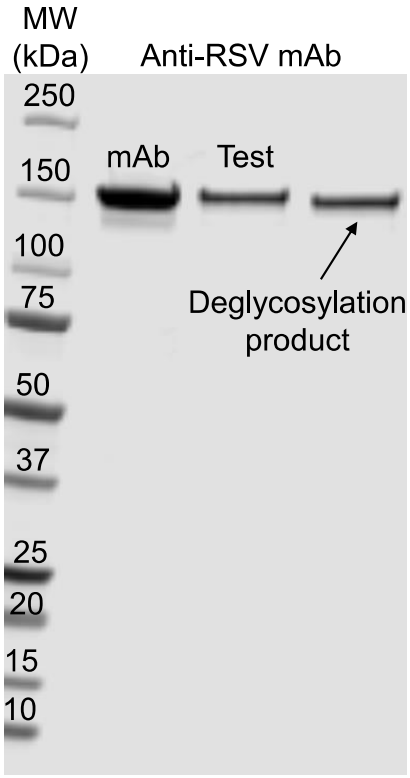

Figure 3.10: Representative non-reducing SDS-PAGE gel confirming deglycosylation of mAbs by PNGaseF.

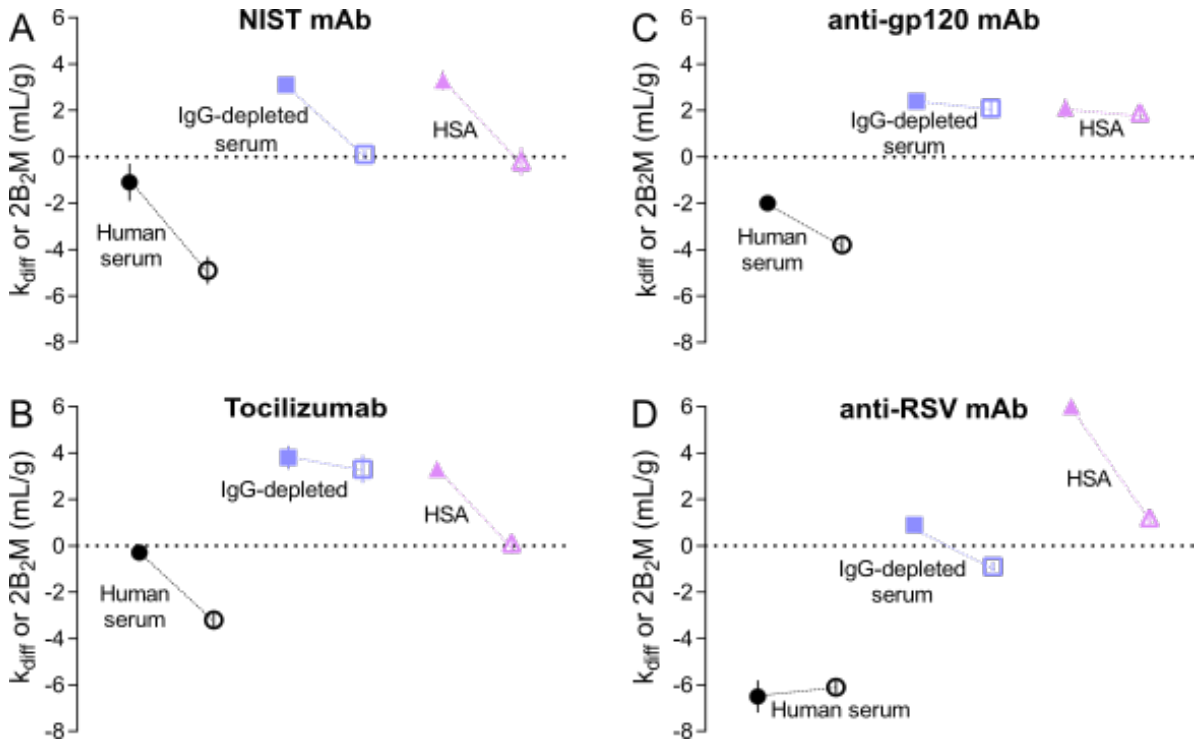

Figure 3.11: Comparison of cross-term interactions in human serum (black circles), IgG-depleted serum (blue squares), and albumin (purple triangles), for full-length antibodies (closed symbols) and Fab fragments (open symbols). NIST mAb (A), Tocilizumab (B), anti-gp120 mAb (C), and anti-RSV mAb (D) D_{adj} vs. c plots (Supplemental Figures S8–11) were fit to the linear equation $D = D^0(1 + k_{diff}c)$ to obtain k_{diff} values, with results presented as mean ± S.D. from three replicates with independent sample preparations.

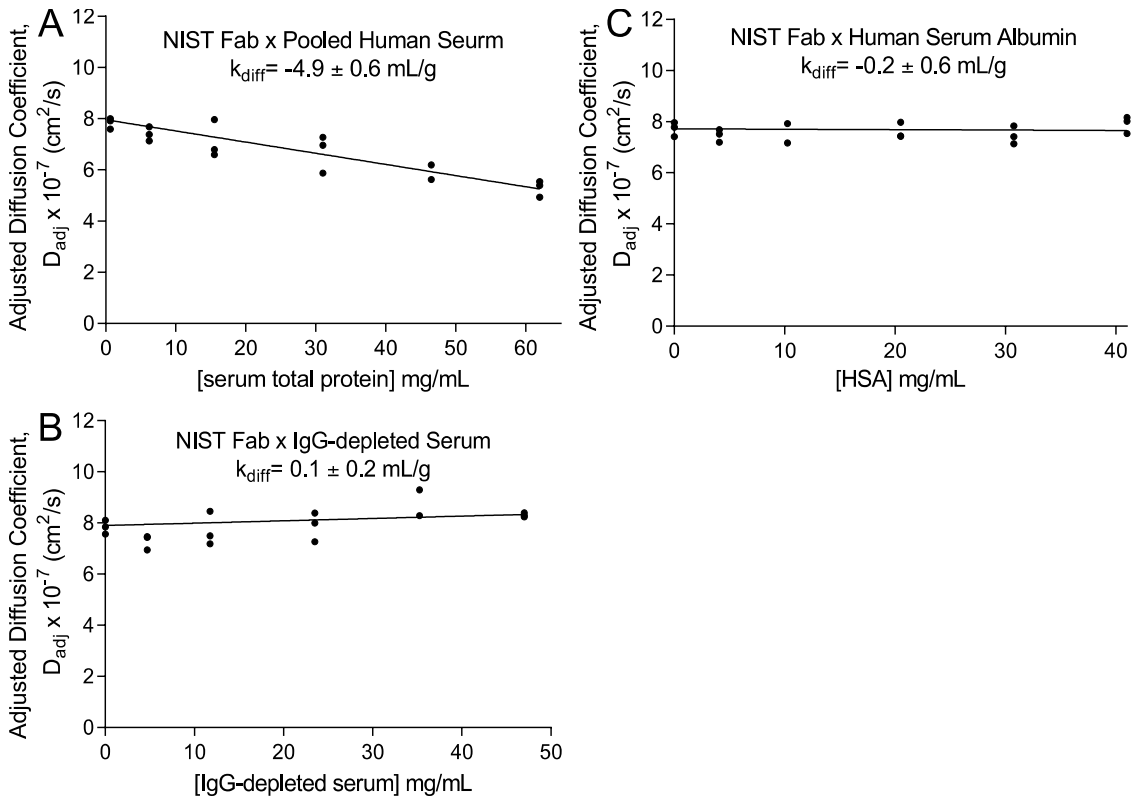

Figure 3.12: $B_{2,app}$ measurements of NIST Fab fragment in various media, with k_{diff} values reported as mean ± S.D. of at least three independent experiments.

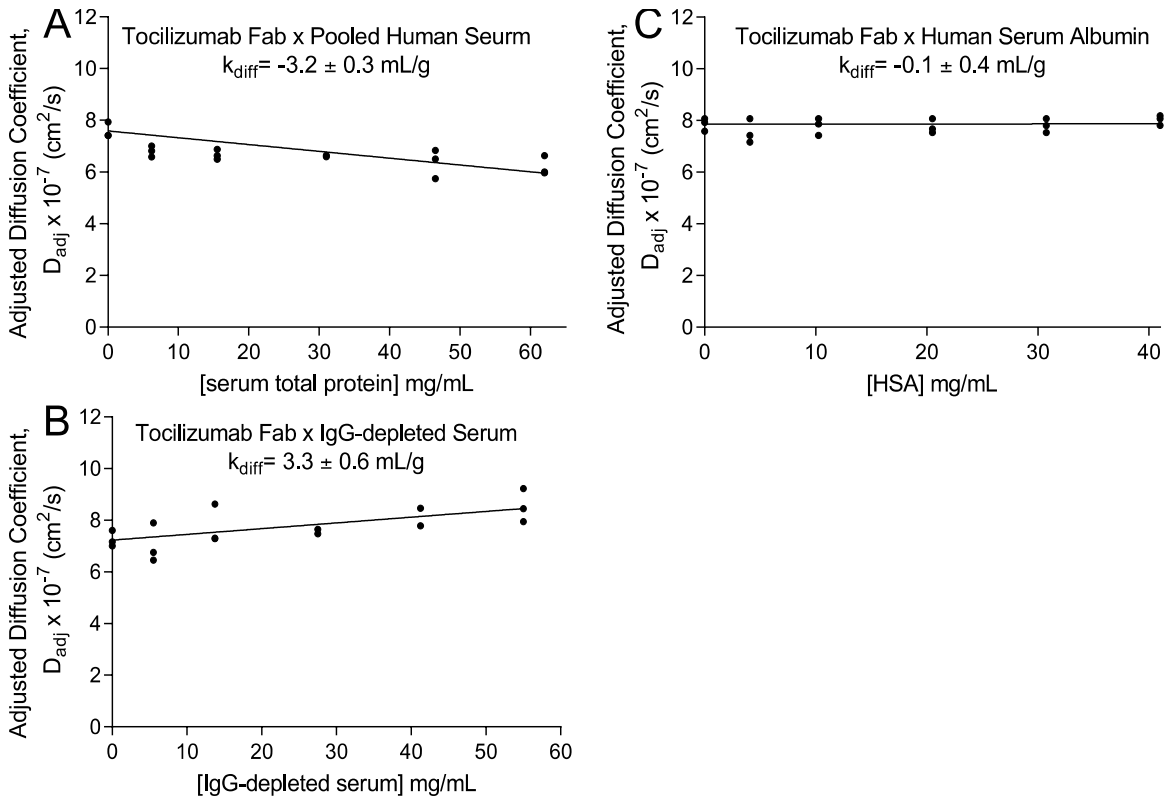

Figure 3.13: $B_{2,app}$ measurements of tocilizumab Fab fragment in various media, with k_{diff} values reported as mean ± S.D. of at least three independent experiments.

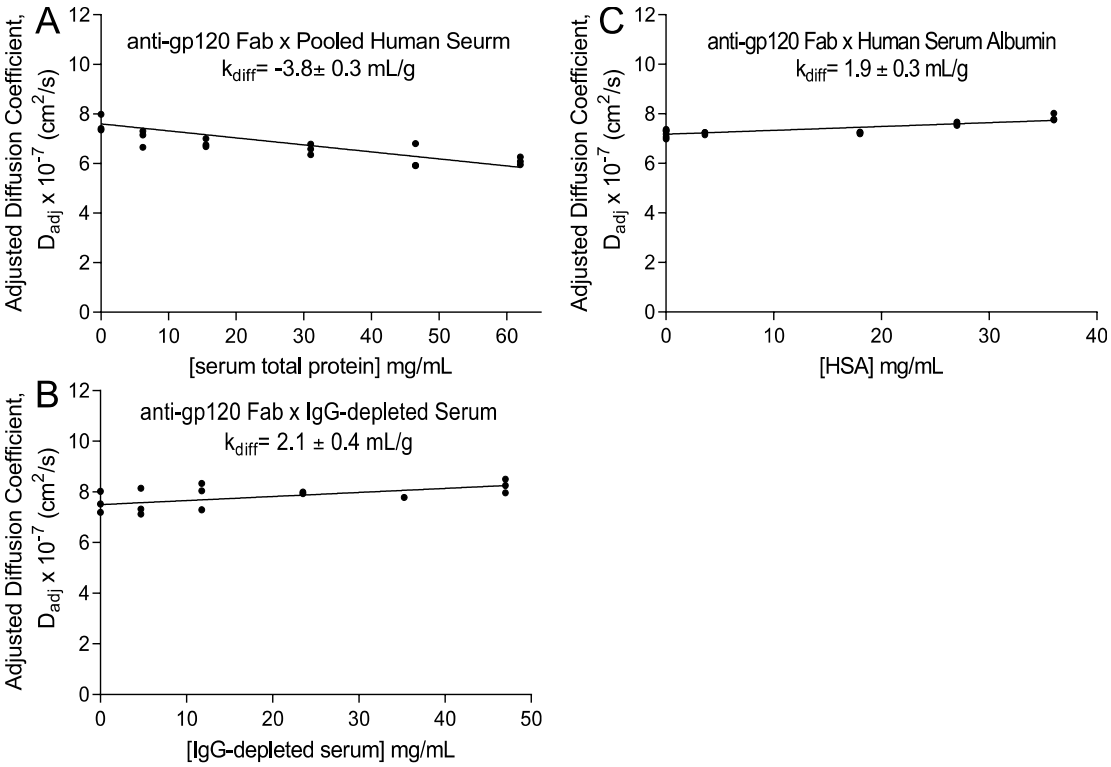

Figure 3.14: $B_{2,app}$ measurements of anti-gp120 Fab fragment in various media, with k_{diff} values reported as mean ± S.D. of at least three independent experiments.

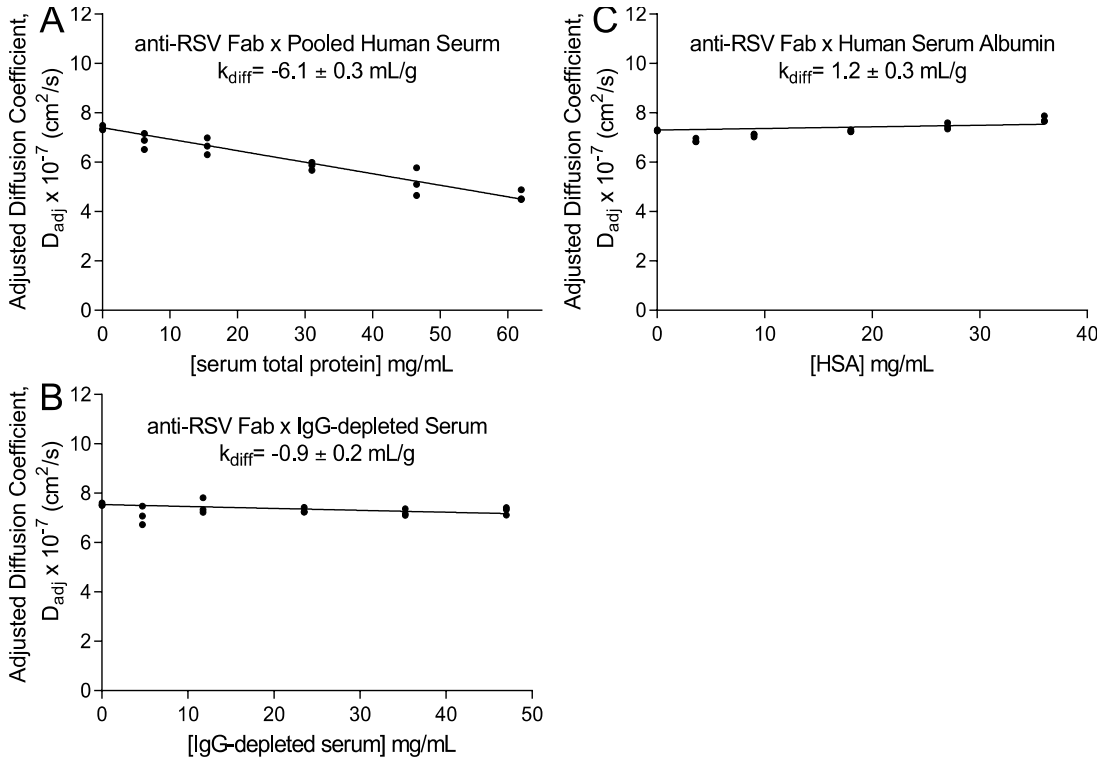

Figure 3.15: $B_{2,app}$ measurements of anti-RSV Fab fragment in various media, with k_{diff} values reported as mean ± S.D. of at least three independent experiments.

TABLES

Table 3.1: Summary of second virial coefficient results. Values presented are mean ± S.D. from at least three independent replicates. *n.d.*: not determined.

Sample		k_{diff} or $2B_2M$ (mL/g)			
		Pooled human serum	IgG-depleted serum	Serum IgG antibodies	HSA
NIST mAb	mAb	–1.1 ± 0.8	3.1 ± 0.3	–12.5 ± 1.0	3.3 ± 0.4
	Fab	–4.9 ± 0.6	0.1 ± 0.2	*n.d.*	–0.2 ± 0.6
Tocilizumab	mAb	–0.3 ± 0.3	3.8 ± 0.5	–16.0 ± 0.5	3.3 ± 0.3
	Fab	–3.2 ± 0.3	3.3 ± 0.6	*n.d.*	0.1 ± 0.4
anti-RSV	mAb	–6.5 ± 0.7	0.9 ± 0.3	–13.1 ± 1.6	6.0 ± 0.2
	Fab	–8.0 ± 1.0	–0.9 ± 0.2	*n.d.*	1.2 ± 0.3
anti-gp120	mAb	–2.0 ± 0.1	2.4 ± 0.3	–12.8 ± 1.1	2.1 ± 0.4
	Fab	–3.8 ± 0.3	2.3 ± 0.3	*n.d.*	1.9 ± 0.3

3.6 References

Abdollahpour-Alitappeh, M., Lotfinia, M., Gharibi, T., Mardaneh, J., Farhadihosseinabadi, B., Larki, P., Faghfourian, B., Sepehr, K. S., Abbaszadeh-Goudarzi, K., Abbaszadeh-Goudarzi, G., Johari, B., Zali, M. R., & Bagheri, N. (2019). Antibody–drug conjugates (ADCs) for cancer therapy: Strategies, challenges, and successes. *Journal of Cellular Physiology*, *234*(5), 5628–5642. https://doi.org/10.1002/jcp.27419

Anderson, N. L., Polanski, M., Pieper, R., Gatlin, T., Tirumalai, R. S., Conrads, T. P., Veenstra, T. D., Adkins, J. N., Pounds, J. G., Fagan, R., & Lobley, A. (2004). The Human Plasma Proteome. *Molecular & Cellular Proteomics*, *3*(4), 311–326. https://doi.org/10.1074/mcp.M300127-MCP200

Baek, Y., & Zydney, A. L. (2018). Intermolecular interactions in highly concentrated formulations of recombinant therapeutic proteins. *Current Opinion in Biotechnology*, *53*, 59–64. https://doi.org/10.1016/j.copbio.2017.12.016

Bhattacharya, A., Kim, Y. C., & Mittal, J. (2013). Protein–protein interactions in a crowded environment. *Biophysical Reviews*, *5*(2), 99–108. https://doi.org/10.1007/s12551-013-0111-5

Blanco, M. A., Perevozchikova, T., Martorana, V., Manno, M., & Roberts, C. J. (2014). Protein–Protein Interactions in Dilute to Concentrated Solutions: α-Chymotrypsinogen in Acidic Conditions. *The Journal of Physical Chemistry B*, *118*(22), 5817–5831. https://doi.org/10.1021/jp412301h

Blanco, M. A., Sahin, E., Li, Y., & Roberts, C. J. (2011). Reexamining protein–protein and protein–solvent interactions from Kirkwood-Buff analysis of light scattering in multi-component solutions. *The Journal of Chemical Physics*, *134*(22), 225103. https://doi.org/10.1063/1.3596726

Burgess, R. R. (2018). A brief practical review of size exclusion chromatography: Rules of thumb, limitations, and troubleshooting. *Protein Expression and Purification*, *150*, 81–85. https://doi.org/10.1016/j.pep.2018.05.007

Chaturvedi, S. K., Parupudi, A., Juul-Madsen, K., Nguyen, A., Vorup-Jensen, T., Dragulin-Otto, S., Zhao, H., Esfandiary, R., & Schuck, P. (2020). Measuring aggregates, self-association, and weak interactions in concentrated therapeutic antibody solutions. *MAbs*, *12*(1). https://doi.org/10.1080/19420862.2020.1810488

Cobb, B. A. (2020). The history of IgG glycosylation and where we are now. *Glycobiology*, *30*(4), 202–213. https://doi.org/10.1093/GLYCOB/CWZ065

Correia, J. J., Wright, R. T., Hayes, D., Sherwood, P. J., & Stafford, W. F. (2018). AUC Measurements of Diffusion Coefficients of Monoclonal Antibodies in the Presence of Human Serum Proteins. *Biophysical Journal*, *114*(3), 62a. https://doi.org/10.1016/j.bpj.2017.11.387

Demeule, B., Shire, S. J., & Liu, J. (2009). A therapeutic antibody and its antigen form different complexes in serum than in phosphate-buffered saline: A study by analytical ultracentrifugation. *Analytical Biochemistry*, *388*(2), 279–287. https://doi.org/10.1016/j.ab.2009.03.012

Dostalek, M., Prueksaritanont, T., & Kelley, R. F. (2017). Pharmacokinetic de-risking tools for selection of monoclonal antibody lead candidates. *MAbs*, *9*(5), 756–766. https://doi.org/10.1080/19420862.2017.1323160

Godar, M., de Haard, H., Blanchetot, C., & Rasser, J. (2018). Therapeutic bispecific antibody

formats: a patent applications review (1994-2017). *Expert Opinion on Therapeutic Patents*, *28*(3), 251–276. https://doi.org/10.1080/13543776.2018.1428307

Gonzalez-Quintela, A., Alende, R., Gude, F., Campos, J., Rey, J., Meijide, L. M., Fernandez-Merino, C., & Vidal, C. (2008). Serum levels of immunoglobulins (IgG, IgA, IgM) in a general adult population and their relationship with alcohol consumption, smoking and common metabolic abnormalities. *Clinical & Experimental Immunology*, *151*(1), 42–50. https://doi.org/10.1111/j.1365-2249.2007.03545.x

Hafeez, U., Gan, H. K., & Scott, A. M. (2018). Monoclonal antibodies as immunomodulatory therapy against cancer and autoimmune diseases. *Current Opinion in Pharmacology*, *41*, 114–121. https://doi.org/10.1016/j.coph.2018.05.010

Haustein, E., & Schwille, P. (2007). Fluorescence Correlation Spectroscopy: Novel Variations of an Established Technique. *Annual Review of Biophysics and Biomolecular Structure*, *36*(1), 151–169. https://doi.org/10.1146/annurev.biophys.36.040306.132612

Hötzel, I., Theil, F.-P., Bernstein, L. J., Prabhu, S., Deng, R., Quintana, L., Lutman, J., Sibia, R., Chan, P., Bumbaca, D., Fielder, P., Carter, P. J., & Kelley, R. F. (2012). A strategy for risk mitigation of antibodies with fast clearance. *MAbs*, *4*(6), 753–760. https://doi.org/10.4161/mabs.22189

Igawa, T., Tsunoda, H., Tachibana, T., Maeda, A., Mimoto, F., Moriyama, C., Nanami, M., Sekimori, Y., Nabuchi, Y., Aso, Y., & Hattori, K. (2010). Reduced elimination of IgG antibodies by engineering the variable region. *Protein Engineering Design and Selection*, *23*(5), 385–392. https://doi.org/10.1093/protein/gzq009

Kamerzell, T. J., Esfandiary, R., Joshi, S. B., Middaugh, C. R., & Volkin, D. B. (2011). Protein–excipient interactions: Mechanisms and biophysical characterization applied to protein formulation development. *Advanced Drug Delivery Reviews*, *63*(13), 1118–1159. https://doi.org/10.1016/j.addr.2011.07.006

Kaplon, H., Chenoweth, A., Crescioli, S., & Reichert, J. M. (2022). Antibodies to watch in 2022. *MAbs*, *14*(1). https://doi.org/10.1080/19420862.2021.2014296

Kim, D. M., Yao, X., Vanam, R. P., & Marlow, M. S. (2019). Measuring the effects of macromolecular crowding on antibody function with biolayer interferometry. *MAbs*, *11*(7), 1319–1330. https://doi.org/10.1080/19420862.2019.1647744

Kimiz-Gebologlu, I., Gulce-Iz, S., & Biray-Avci, C. (2018). Monoclonal antibodies in cancer immunotherapy. *Molecular Biology Reports*, *45*(6), 2935–2940. https://doi.org/10.1007/s11033-018-4427-x

Kuznetsova, I., Zaslavsky, B., Breydo, L., Turoverov, K., & Uversky, V. (2015). Beyond the Excluded Volume Effects: Mechanistic Complexity of the Crowded Milieu. *Molecules*, *20*(1), 1377–1409. https://doi.org/10.3390/molecules20011377

Larsen, H. A., Atkins, W. M., & Nath, A. (2021). Probing interactions of therapeutic antibodies with serum via second virial coefficient measurements. *Biophysical Journal*, *120*(18), 4067–4078. https://doi.org/10.1016/j.bpj.2021.08.007

Le Basle, Y., Chennell, P., Tokhadze, N., Astier, A., & Sautou, V. (2020). Physicochemical Stability of Monoclonal Antibodies: A Review. *Journal of Pharmaceutical Sciences*, *109*(1), 169–190. https://doi.org/10.1016/j.xphs.2019.08.009

Le Brun, V., Friess, W., Bassarab, S., Mühlau, S., & Garidel, P. (2010). A critical evaluation of self-interaction chromatography as a predictive tool for the assessment of protein–protein interactions in protein formulation development: A case study of a therapeutic monoclonal antibody. *European Journal of Pharmaceutics and Biopharmaceutics*, *75*(1), 16–25.

https://doi.org/10.1016/j.ejpb.2010.01.009
Leeman, M., Choi, J., Hansson, S., Storm, M. U., & Nilsson, L. (2018). Proteins and antibodies in serum, plasma, and whole blood—size characterization using asymmetrical flow field-flow fractionation (AF4). *Analytical and Bioanalytical Chemistry*, *410*(20), 4867–4873. https://doi.org/10.1007/s00216-018-1127-2
Liu, L. (2018). Pharmacokinetics of monoclonal antibodies and Fc-fusion proteins. *Protein & Cell*, *9*(1), 15–32. https://doi.org/10.1007/s13238-017-0408-4
Lu, R.-M., Hwang, Y.-C., Liu, I.-J., Lee, C.-C., Tsai, H.-Z., Li, H.-J., & Wu, H.-C. (2020). Development of therapeutic antibodies for the treatment of diseases. *Journal of Biomedical Science*, *27*(1), 1. https://doi.org/10.1186/s12929-019-0592-z
Ma, Y., Acosta, D. M., Whitney, J. R., Podgornik, R., Steinmetz, N. F., French, R. H., & Parsegian, V. A. (2015). Determination of the second virial coefficient of bovine serum albumin under varying pH and ionic strength by composition-gradient multi-angle static light scattering. *Journal of Biological Physics*, *41*(1), 85–97. https://doi.org/10.1007/s10867-014-9367-7
Macháň, R., & Wohland, T. (2014). Recent applications of fluorescence correlation spectroscopy in live systems. *FEBS Letters*, *588*(19), 3571–3584. https://doi.org/10.1016/j.febslet.2014.03.056
Majety, M., Runza, V., Lehmann, C., Hoves, S., & Ries, C. H. (2018). A drug development perspective on targeting tumor-associated myeloid cells. *The FEBS Journal*, *285*(4), 763–776. https://doi.org/10.1111/febs.14277
Minton, A. P. (1998). Molecular crowding: Analysis of effects of high concentrations of inert cosolutes on biochemical equilibria and rates in terms of volume exclusion. *Methods in Enzymology*, *295*, 127–149. https://doi.org/10.1016/S0076-6879(98)95038-8
Moreira, L. A., Boström, M., Ninham, B. W., Biscaia, E. C., & Tavares, F. W. (2007). Effect of the ion-protein dispersion interactions on the protein-surface and protein-protein interactions. *Journal of the Brazilian Chemical Society*, *18*(1), 223–230. https://doi.org/10.1590/S0103-50532007000100026
Mullard, A. (2021). FDA approves 100th monoclonal antibody product. *Nature Reviews Drug Discovery*, *20*(7), 491–495. https://doi.org/10.1038/d41573-021-00079-7
Obrezanova, O., Arnell, A., de la Cuesta, R. G., Berthelot, M. E., Gallagher, T. R. A., Zurdo, J., & Stallwood, Y. (2015). Aggregation risk prediction for antibodies and its application to biotherapeutic development. *MAbs*, *7*(2), 352–363. https://doi.org/10.1080/19420862.2015.1007828
Pham, N. B., & Meng, W. S. (2020). Protein aggregation and immunogenicity of biotherapeutics. *International Journal of Pharmaceutics*, *585*, 119523. https://doi.org/10.1016/j.ijpharm.2020.119523
Quigley, A., & Williams, D. R. (2015). The second virial coefficient as a predictor of protein aggregation propensity: A self-interaction chromatography study. *European Journal of Pharmaceutics and Biopharmaceutics*, *96*, 282–290. https://doi.org/10.1016/j.ejpb.2015.07.025
Rivas, G., & Minton, A. P. (2022). Influence of nonspecific interactions on protein associations: Implications for biochemistry in vivo. *Annual Review of Biochemistry*, *91*, 321–351. https://doi.org/10.1146/ANNUREV-BIOCHEM-040320-104151
Roberts, D., Keeling, R., Tracka, M., van der Walle, C. F., Uddin, S., Warwicker, J., & Curtis, R. (2014). The Role of Electrostatics in Protein–Protein Interactions of a Monoclonal

Antibody. *Molecular Pharmaceutics*, *11*(7), 2475–2489. https://doi.org/10.1021/mp5002334

Röthlisberger, D., Honegger, A., & Plückthun, A. (2005). Domain Interactions in the Fab Fragment: A Comparative Evaluation of the Single-chain Fv and Fab Format Engineered with Variable Domains of Different Stability. *Journal of Molecular Biology*, *347*(4), 773–789. https://doi.org/10.1016/j.jmb.2005.01.053

Saluja, A., Fesinmeyer, R. M., Hogan, S., Brems, D. N., & Gokarn, Y. R. (2010). Diffusion and Sedimentation Interaction Parameters for Measuring the Second Virial Coefficient and Their Utility as Predictors of Protein Aggregation. *Biophysical Journal*, *99*(8), 2657–2665. https://doi.org/10.1016/j.bpj.2010.08.020

Sarkar, M., Li, C., & Pielak, G. J. (2013). Soft interactions and crowding. *Biophysical Reviews*, *5*(2), 187–194. https://doi.org/10.1007/s12551-013-0104-4

Schmitt, S., Huppertsberg, A., Klefenz, A., Kaps, L., Mailänder, V., Schuppan, D., Butt, H.-J., Nuhn, L., & Koynov, K. (2022). Fluorescence Correlation Spectroscopy Monitors the Fate of Degradable Nanocarriers in the Blood Stream. *Biomacromolecules*, *23*(3), 1065–1074. https://doi.org/10.1021/acs.biomac.1c01407

Sharma, V. K., Patapoff, T. W., Kabakoff, B., Pai, S., Hilario, E., Zhang, B., Li, C., Borisov, O., Kelley, R. F., Chorny, I., Zhou, J. Z., Dill, K. A., & Swartz, T. E. (2014). In silico selection of therapeutic antibodies for development: Viscosity, clearance, and chemical stability. *Proceedings of the National Academy of Sciences*, *111*(52), 18601–18606. https://doi.org/10.1073/pnas.1421779112

Shi, S. (2014). Biologics: an update and challenge of their pharmacokinetics. *Current Drug Metabolism*, *15*(3), 271–290.

Velev, O. D., Kaler, E. W., & Lenhoff, A. M. (1998). Protein Interactions in Solution Characterized by Light and Neutron Scattering: Comparison of Lysozyme and Chymotrypsinogen. *Biophysical Journal*, *75*(6), 2682–2697. https://doi.org/10.1016/S0006-3495(98)77713-6

Wills, P. R., Georgalis, Y., Dijk, J., & Winzor, D. J. (1995). Measurement of thermodynamic nonideality arising from volume-exclusion interactions between proteins and polymers. *Biophysical Chemistry*, *57*(1), 37–46. https://doi.org/10.1016/0301-4622(95)00043-W

Wright, R. T., Hayes, D. B., Stafford, W. F., Sherwood, P. J., & Correia, J. J. (2018). Characterization of therapeutic antibodies in the presence of human serum proteins by AU-FDS analytical ultracentrifugation. *Analytical Biochemistry*, *550*, 72–83. https://doi.org/10.1016/j.ab.2018.04.002

Wright, R. T., Hayes, D., Sherwood, P. J., Stafford, W. F., & Correia, J. J. (2018). AUC measurements of diffusion coefficients of monoclonal antibodies in the presence of human serum proteins. *European Biophysics Journal*, *47*(7), 709–722. https://doi.org/10.1007/s00249-018-1319-x

Wu, H., Pfarr, D. S., Johnson, S., Brewah, Y. A., Woods, R. M., Patel, N. K., White, W. I., Young, J. F., & Kiener, P. A. (2007). Development of Motavizumab, an Ultra-potent Antibody for the Prevention of Respiratory Syncytial Virus Infection in the Upper and Lower Respiratory Tract. *Journal of Molecular Biology*, *368*(3), 652–665. https://doi.org/10.1016/j.jmb.2007.02.024

Yadav, S., Scherer, T. M., Shire, S. J., & Kalonia, D. S. (2011). Use of dynamic light scattering to determine second virial coefficient in a semidilute concentration regime. *Analytical Biochemistry*, *411*(2), 292–296. https://doi.org/10.1016/j.ab.2010.12.014

Yang, D., Correia, J. J., Stafford, W. F., Roberts, C. J., Singh, S., Hayes, D., Kroe-Barrett, R., Nixon, A., & Laue, T. M. (2018). Weak IgG self- and hetero-association characterized by fluorescence analytical ultracentrifugation. *Protein Science*. https://doi.org/10.1002/pro.3422

Yu, L., Lei, Y., Ma, Y., Liu, M., Zheng, J., Dan, D., & Gao, P. (2021). A Comprehensive Review of Fluorescence Correlation Spectroscopy. *Frontiers in Physics*, *9*. https://doi.org/10.3389/fphy.2021.644450

Yu, M., Brown, D., Reed, C., Chung, S., Lutman, J., Stefanich, E., Wong, A., Stephan, J.-P., & Bayer, R. (2012). Production, characterization and pharmacokinetic properties of antibodies with N-linked Mannose-5 glycans. *MAbs*, *4*(4), 475–487. https://doi.org/10.4161/mabs.20737

Zhou, H.-X., Rivas, G., & Minton, A. P. (2008). Macromolecular Crowding and Confinement: Biochemical, Biophysical, and Potential Physiological Consequences. *Annual Review of Biophysics*, *37*(1), 375–397. https://doi.org/10.1146/annurev.biophys.37.032807.125817

``

CHAPTER 4

Characterizing Antibody-target Binding in Serum via Fluorescence Correlation Spectroscopy

4.1 Introduction

Marketed therapeutic antibodies, predominantly monoclonal (mAbs), target a variety of soluble and cell-surface antigens distributed in various tissues (i.e., tumors, lymph nodes, lung, etc.) (Tabrizi et al., 2010). Depending on the mode of action, antigen binding (mediated by the antigen binding fragment, Fab), can serve to merely neutralize targets by interfering with activity and interactions with binding partners. As in the case with cancer, antibodies can also elicit an immune response via Fc-mediated effector functions to eliminate target cells (Vidarsson et al., 2014). These effector functions include complement-dependent cytotoxicity (CDC), antibody-dependent cell-mediated cytotoxicity (ADCC), and antibody-dependent cellular phagocytosis (ADCP). These pathways require mAb binding via the crystallizable fragment (Fc) to complement protein C1q (CDC) or Fcγ receptors (FcγRs) on natural killer (NK) cells and phagocytes (ADCC and ADCP, respectively). Furthermore, mAbs bind to neonatal Fc receptor (FcRn) in endosomes to avoid lysosomal degradation and achieve long serum half-lives (Saxena & Wu, 2016). These interactions take place in diverse, complex physiological environments (i.e., serum, tumor microenvironment, endosomal lumen etc.) that can perturb antibody function in ways that are not fully understood. Given that many antibodies target soluble antigens and experience long circulating half-lives, serum is a relevant system to investigate. Furthermore, commercial serum is highly accessible and less complex than other biological fluids. In previous chapters, we demonstrated that antibodies differentially experience nonideality in serum. In this chapter, we expand the approach to determine whether serum-induced nonideality impacts function.

``

As discussed in previous chapters, methods capable of characterizing antibody properties in serum are limited. However, fluorescence correlation spectroscopy (FCS) is capable of measuring diffusion in complex media such as serum. We previously used FCS to probe global nonideality effects in serum for a panel of mAbs (Chapter 2; Larsen et al., 2021). In this approach, we measured the diffusion coefficient of labeled mAbs at varying concentrations of serum to determine the second osmotic virial coefficient ($B_{2,app}$). These measurements served to probe weak, nonspecific interactions between therapeutic antibodies and serum proteins. Here, we use an alternative in-serum FCS approach to determine antibody-target affinity in the Fab and Fc domains of model IgG antibodies through determination of equilibrium dissociation constant (K_D) values. Comparing affinity between buffer and serum conditions could reveal the potential impact of physiological environments on target binding.

Surface plasmon resonance (SPR) is the most common technique used for measuring binding affinity (Wang et al., 2020). Despite agreement between SPR affinity measurements and other solution-based methods (Day et al., 2002), the use of a surface can lead to artifacts in the data. This further complicates methods directly in biological fluids due to nonspecific binding of proteins in the media. Biolayer interferometry (BLI) is an emerging high throughput alternative to SPR that follows similar methodology but suffers from similar limitations. However, BLI utilizes capture tips and follows a "dip-and-read" format that is potentially better for measurements directly in biological fluids (Dzimianski et al., 2020). Perhaps a more established alternative to SPR and BLI capable of measurements directly in undilute biological fluids is the kinetic exclusion assay, KinExA (Bee et al., 2012, 2013; Drake et al., 2010; Rathanaswami et al., 2011). The major drawback of KinExa is that it requires a stationary phase that can lead to artifacts associated with nonspecific bead binding (Hunter & Cochran, 2016). The major advantage of FCS is the ability to

complete measurements directly in complex media in the absence of a stationary phase or immobilization surface.

One major goal of this research is to investigate whether nonideality impacts antibody-target binding *in vivo*. In Chapter 2, we observed trends of attractive interactions with serum IgG antibodies for a panel of mAbs and further isolated those interactions to Fab domains. To further investigate whether these attractive interactions impact antigen binding, we determine if $B_{2,app}$ values correlate with changes in serum affinity. As a preliminary assessment, we use our previously established FCS approach to determine $B_{2,app}$ values for the model IgG antibodies used for antigen binding experiments in this study. These comparisons serve as an initial assessment into the significance of the magnitude of our $B_{2,app}$ values and provide insight into the functional consequences of serum-induced nonideality for therapeutic antibodies.

4.2 Experimental Procedures

4.2.1 Protein samples and other materials

Recombinant protein A (~1mg/mL) was provided by Dr. John Sumida. Tocilizumab (35 mg/mL) IgG1 antibody was provided by the Genentech Outgoing Materials Transfer Agreement program. The VRC26 lineage IgG Abs (1 mg/mL) were kindly provided by the Dr. Kelly Lee's lab which acquired them from VRC (Vaccine Research Center at the NIH). The Lee Lab also provided the BG505 SOSIP trimer (5.6 mg/mL) which was expressed and purified in house as described by Verkerke et al., (2016). Pooled human serum (34019) was purchased from Pel-Freeze Biologics. The antibodies and protein A were stored at 4°C in PBS pH 7.4. The serum was thawed at 4°C before each experiment and used no more than 24h after thawing.

``

4.2.2 Protein labeling

Following the Thermo Scientific labeling protocol, the VRC26 lineage IgG antibodies and protein A were labeled with Alexa-Fluor 488 carboxylic acid, succinimidyl ester (Thermo Scientific A20000; A488) in 1x PBS, pH 7.4 with 10% sodium bicarbonate, pH 8.3. Free Alexa Fluor 488 was removed with Zeba Spin Desalting Columns from Thermo Scientific (89882), following the Thermo Scientific protocol. Labeling ratio was determined through UV-Vis spectroscopy (absorbance measurements at 280 nm and 494 nm) on a Nanodrop One Microvolume UV-Vis spectrometer (Thermo Scientific, ND-ONE-W). Typically, 1-2 A488 molecules covalently attached to VRC26 IgGs or proteins A. Additionally, diffusion time was used to verify the absence of free dye in solution by comparing observed changes to expected changes in diffusion from free dye to protein-bound dye. These calculations are described in Chapter 2. A488-antibodies and protein A were stored in 1x PBS pH 7.4 at 4°C.

4.2.3 FCS K_D and $B_{2,app}$ determination

All experiments were carried out at room temperature on a home-built instrument based on a Zeiss Axio Observer D1 microscope equipped with HydraHarp 400 detection electronics, Tau-SPAD photon counting detector, and pulsed 485 nm laser line driven by a PicoQuant PDL 828 Sepia II driver (PicoQuant GmbH, Berlin, Germany). Sample aliquots of 50 µL were placed on a 22x22 cover glass (VWR 48366-067). Five 30 s measurements of 10 nM A488 were used to calibrate the instrument at the start of each experiment while five 60 s measurements were completed for each sample.

4.2.3.1 K_D determination

To determine binding affinity, A488-labeled VRC26 IgGs or A488-labeled protein A were diluted to ~15-25 nM in varying concentrations of unlabeled binding partners (BG505 SOSIP and

IgG1, respectively) in either 1X PBS, pH 7.4 or serum. Earlier binding experiments with protein A were carried out in 25% fetal bovine serum (FBS) (~10 mg/mL serum protein), whereas later experiments with the VRC26 IgGs were carried out in 50% pooled human serum (~31 mg/mL serum protein). The concentration range of BG505 SOSIP was determined for each VRC26 IgG antibody based on previously determined BLI results (**Table 4.1**). The BG505 SOSIP concentration spanned at least 6x above and below reported BLI K_D values, apart from VRC26.08 due to having limited BG505 SOSIP at the time of experiment. The viscosity of PBS was matched to 50% serum by FCS using a dye standard in most cases. The concentration range of IgG1 (0-500 nM) for protein A experiments was based on low nM affinity reported in the literature (Choe et al., 2016). Protein A experiments were repeated after 24 hours at room temperature to determine time-dependent changes in affinity to IgG1 Fc. Note that IgG1 and protein A were kept in separate tubes until the time of analysis.

FCS intensity time traces were imported into PRISM Graphpad software and fit to a single component FCS equation to yield diffusion time, τ_D, using the following equation (Haustein Schwille, 2007):

$$G_{FCS}(\tau) = \frac{1}{N}\left(\frac{1}{1+{}^{\tau}/_{\tau_D}}\right)\sqrt{\frac{1}{1+{}^{s^2\tau}/_{\tau_D}}} \quad \text{.....(1)}$$

where N is the mean number of molecules in observation volume, τ_D is the correlation decay time due to translational diffusion, and *s* is the axial ratio of the detection volume (0.2 for our instrument). Translational diffusion time (τ_D) of the labeled protein was plotted against unlabeled protein concentration (P_T) and fit to the following quadratic binding equation to yield the equilibrium dissociation constant, K_D:

$$\tau_D = (\tau_{max} - \tau_{min})\frac{(E_{TOT}+P_T+K_D)-\sqrt{(E_{TOT}+P_T+K_D)^2-4E_{TOT}P_T}}{2E_{TOT}} + \tau_{min} \quad \text{.....(2)}$$

where τ_{max} represents τ_D at saturation, τ_{min} the τ_D of the labeled protein at infinite dilution (constrained in the model as τ_D of the labeled protein at 0nM P_T), and E_{TOT} the concentration of labeled protein (constrained in the model as the labeled protein concentration).

4.2.3.2 $B_{2,app}$ determination

A488-labeled VRC26 IgGs were diluted to ~20 nM in varying concentrations pooled human serum, ranging from 0% to 100% (62 mg/mL). FCS intensity vs. time traces were imported into PRISM Graphpad software and fit to **Equation 1** to obtain the translation diffusion time, τ_D. Translational diffusion coefficients (*D)* were determined from diffusion time measurements and used to calculate interaction parameter (k_{diff}) values, that are directly proportional to the second osmotic virial coefficient (B_2). The methodology behind these measurements is outlined in Chapter 2 and our previous publication. (Larsen et al., 2021).

4.3.4 Biolayer interferometry (BLI)

The binding kinetics of BG505 SOSIP to VRC26.25 IgG antibody were studied via BLI on an Octet Red system (FortéBio). Anti-human IgG Fc capture biosensors (FortèBio 18-506) were presoaked in binding buffer (PBS pH 7.4, 0.1% BSA, 0.005% Tween 20, and 0.02% NaN3) for 10 minutes. VRC26.25 IgG was loaded at 8μg/mL in binding buffer for 80 seconds, then allowed to baseline in either binding buffer or 10% pooled human serum. Upon baseline stabilization, antibody-immobilized biosensors were moved into wells containing a 2-fold dilution series of BG505 SOSIP (125 nM to 1.25 nM in either binding buffer or 10% pooled human serum) to monitor association for 3 minutes. Biosensors were moved back into wells containing binding buffer or 10% pooled human serum to monitor dissociation for 3 minutes. The above-mentioned steps were repeated in the absence of capturing VRC26.25 IgG to determine a reference signal. The corresponding signal was subtracted from the binding responses (double referenced) to

account for nonspecific binding to biosensor in the absence of VRC26.25. Regeneration was carried out between experiments by moving the biosensor between PBS and binding buffer 6 times to remove VRC26.25 and BG505 SOSIP. Kinetic data were analyzed using FortéBio Data Analysis 11.0 software and processed by Savitzky-Golay filtering prior to fitting with a 1:1 binding model. Reported values are data from a single experiment.

4.3 Results

4.3.1. Antibody-antigen affinity in buffer and serum

Broadly neutralizing antibodies (bnAbs) have become a major focus in human immuno-deficiency virus (HIV) research and vaccine development due to their ability to bind and neutralize multiple strains of the virus (Pancera et al., 2017). VRC26 bnAbs bind BG505 envelope glycoprotein trimers to block entry into host cells (Yin et al., 2021). Affinity maturation of the VRC26 lineage results in IgGs with varying affinities to BG505, providing a good model system for antibody-antigen binding experiments in serum. Here, we investigate the impact of serum on antigen binding four VRC26 lineage IgGs: VRC26.01, VR26.03, VRC26.08, and VRC26.25 via FCS. FCS diffusion time measurements were used to determine K_D values in buffer and pooled human serum as described in the above **Experimental Procedures** section. Note that the VRC26 IgGs (~150 kDa) were labeled due to their lower molecular weights compared to BG505 SOSIP trimer (~360 kDa). It is standard to label the smaller binding partner in FCS binding experiments, as it results in larger shifts in diffusion time, leading to less uncertainty in the fit, and therefore more accurate estimates of K_D.

Affinity maturation of VRC26.01 to VRC26.25 resulted in increased affinity from ~496 nM to 9 nM based on BLI results in buffer (**Table 4.1**). VRC26.03 and VRC26.08 IgGs served as intermediates with BLI affinities of 149 nM and 114 nM, respectively. The range of FCS K_D values

is comparable to BLI (~20 nM to ~500 nM), where VRC26.25 exhibited the tightest affinity (**Figure 4.1**) and VRC26.01 the lowest affinity (**Figure 4.4**) to BG505 SOSIP. VRC26.08 exhibited a slightly tighter affinity in serum (~1.6x)(**Figure 4.3a,b**), whereas the other three IgGs exhibited no significant differences in K_D between buffer and serum conditions. The significance in the decrease in affinity for VRC26.08 could be attributed to viscosity since the buffer was not viscosity-matched to serum for VRC26.08 as it was for the other three IgGs. It should be noted that only a single binding experiment was carried out for VRC26.01 due to limited materials, while experiments for the other three IgGs were carried out in triplicate. Therefore, for VRC26.01, the uncertainty in K_D was calculated from standard error of the mean (SEM) for n=5 measurements at each BG505 concentration, whereas the standard deviation in $K_D$was calculated from the averaged results over three independent experiments for the other three IgGs. This can explain the higher uncertainty observed in K_D values for VRC26.01.

Binding comparisons in buffer and serum were also carried out by BLI for VRC26.25 (**Figure 4.5**) to compare to FCS results and obtain additional kinetic information. Tight and comparable affinity (~5nM) was observed in buffer compared to previous BLI (~9nM) and FCS (~20nM) results (**Figure 4.5A**). However, in-serum measurements were unsuccessful, largely due to an inability to measure the dissociation rate constant (**Figure 4.5B)**. This is likely a result of nonspecific binding of serum IgGs to the Fc capture biosensor. Therefore, further investigation into other capture methods is necessary.

4.3.2. VRC26 IgG interactions with serum proteins

Using our previously established FCS approach (Larsen et al., 2021), apparent second virial coefficients ($B_{2,app}$) were also determined for the panel of VRC26 IgGs in pooled human serum to investigate correlations between nonideality and changes in serum affinity. Values of k_{diff}

for VRC26.01 (0.6 ± 0.2 mL/g), VRC26.03 (-1.4 ± 0.3 mL/g), VRC26.08 (0.2 ± 0.2 mL/g), and VRC26.25 (-2.3 ± 0.4 mL/g) IgGs, suggests that VRC26.01 and VRC26.08 do not exhibit deviations from ideal behavior in serum, while VRC26.03 and VRC26.25 exhibit slight attraction to serum proteins (**Figure 4.6**). Interestingly, VRC26 IgGs exhibit a trend of increasing attraction to serum proteins with increasing affinity to BG505 as well as increasing fold change in K_D (**Figure 4.7a,b**). However, the changes in affinity between buffer and serum were determined to be insignificant as mentioned above. The slightly attractive interactions in the higher affinity antibodies could be a result of mutations, either due to the properties of the amino acid mutation themselves or via conformational changes associated with mutation that render certain residues more susceptible to interactions. For example, mutations with charged amino acids in the CDR or can increase the overall strength of the interaction with the antigen but could also render the antibody more susceptible to long-range attractive interactions with charged residues on serum proteins, such as IgGs. In the same vein, incorporating additional hydrophobic residues may increase attraction to serum proteins (such as IgGs), given that hydrophobic patches can be hot spots for antibody aggregation (Li et al., 2016). In addition, incorporating point mutations outside of the binding interface may cause conformational changes that increase affinity but also lead to greater exposure of existing charged residues, thereby indirectly increasing propensity for attractive interactions with charged serum proteins. However, these effects need further investigation. Nonetheless, the attractive interactions observed with VRC26.03 and VRC26.25 were not significant enough to impact antigen binding, as evident by comparable affinities observed in buffer and serum. A summary of $B_{2,app}$ and K_D results can be found in **Table 4.1**.

``

4.3.3 Protein A binding IgG1 Fc in buffer and serum

Protein A is a surface protein originally found in the cell wall of *Staphylococcus aureus* that binds to the Fcγ domain of IgGs to prevent clearance (Becker et al., 2014). Protein A is also commonly used in purification of most IgG antibodies due to high affinity to human IgG1, IgG2, and IgG4 (Rispens & Vidarsson, 2014). Therefore, protein A binding IgG1 served as a good model system to compare Fc binding in buffer and serum. Here, A488-labeled protein A (~42 kDa) was diluted into varying concentrations of IgG1 mAb, ranging from 0 nM to 500 nM, in either 1x PBS, pH 7.4 or 25% fetal bovine serum (FBS). There were no significant differences observed in affinity, as evident by comparable K_D values in buffer and serum (**Figure 4.8 and Figure 4.9**). Higher K_D values were observed after 24 hours at room temperature (1.8x in buffer and 4.8 serum), potentially suggesting time-dependent decreases in affinity. However, the changes were determined to not be statistically significant (**Figure 4.9**). Note that results are reported from a single time course experiment and should be verified through additional replicates.

4.4 Discussion

Characterization of antibody-target interactions is an essential part of therapeutic development. *In vitro* affinity estimates are particularly critical in early stages of discovery and development as they guide lead candidate selection, PK/PD modeling, dose regimes, and efficacy (Wang, et al., 2020). Discrepancies between *in vitro* and *in vivo* affinity have been reported as causes of failure in the clinic (Majety et al., 2018). Therefore, there is continued pressure to improve existing or develop new *in vitro* assays.

Many traditional analytical techniques attempt to infer in *vivo* binding properties from buffer systems that are vastly different from relevant physiological environments. Such environments are highly complex and difficult to predict, given that they are not fully understood

(Feig et al., 2017). Furthermore, completing measurements in complex media is out of the scope of many analytical approaches. At present, FCS is not common in the therapeutic antibody industry, but the ability to measure binding affinity directly in serum and other complex biological fluids may make it an appealing alternative to some of the most well-established techniques.

Surface plasmon resonance (SPR) is considered the gold standard for measuring binding affinity in therapeutic antibody development (Wang et al., 2020). BLI is an emerging high throughput alternative to SPR that follows similar methodology (Kamat & Rafique, 2017). The advantage of SPR and BLI is the ability to characterize binding kinetics and affinity under label-free conditions in real-time (Murali et al., 2022). However, surface heterogeneity and mass transport limitation are major drawbacks that can affect the kinetic analysis, resulting in inaccurate affinity estimates (Schuck & Zhao, 2010). These effects complicate in-serum measurements due to the presence of serum proteins that can nonspecifically bind the surface or immobilized protein. Therefore, BLI and SPR methods in biological fluids are not well-established. Failure to determine binding affinity in serum for VR26.25 in our BLI experiment (**Figure 4.5**) highlights the limitations of the technique. KinExa is an established alternative to SPR and BLI capable of completing measurements directly in serum (Bee et al., 2013; Rathanaswami et al., 2011). However, the use of a stationary phase can also lead to nonspecific binding of serum proteins that can impact affinity measurements (Hunter & Cochran, 2016). FCS serves as an orthogonal method for determining binding affinity directly in undilute serum. One major advantage of FCS is that determination of K_D does not depend on measurements of individual rate constant as it does for BLI and SPR. Furthermore, FCS affinity measurements are relatively easy, do not require large quantities of protein, and avoid the challenges associated with immobilization. One drawback of

FCS is that labeling is required. However, low labeling ratios were used in our experiments (~1-2 per protein) to mitigate the potential impact of label on target binding.

Although serum had no apparent effect on binding affinity in the two model systems used for this study, the results should not be overinterpreted or generalized to all antibody systems. The physiological impact on target binding is likely antibody dependent, given the diversity in both antibody design and mechanism of action. Specific differences in subclass, isotype, and engineering of monoclonal antibodies and other antibody-based platforms (i.e. antibody-drug conjugates, bispecific antibodies, etc.) can impact both the primary and tertiary structure in variable and constant domains that can influence target binding (Goulet & Atkins, 2020). Furthermore, antibody-based therapeutics target a wide range of antigens both soluble and cell-surface within specific and diverse tissue environments (Dunlap & Cao, 2022). These factors combined can have variable impacts on antigen and Fc-mediated interactions. Perhaps serum is a more relevant model for investigating interactions with soluble antigens compared to therapeutics that target cell-surface receptors. In any case, probing the effects of crowding and nonideality is relevant to all antibody systems.

The diffusion of a therapeutic antibody in buffer can be dramatically different than biological fluids that contain high concentrations of macromolecules. Therefore, diffusion coefficient measurements in buffer inadequately model the antibodies ability to traverse the crowded physiological environments necessary for target binding (Davies et al., 2002; Dunlap & Cao, 2022). One phenomenon that can impact the diffusion is weak, nonspecific interactions with proteins. The ability of FCS to determine both antibody-target binding affinity (K_D) and probe nonideality ($B_{2,app}$) directly in serum, provides the opportunity to assess whether weak, nonspecific interactions with serum proteins impact target binding. Despite weak attraction to

serum for VRC26.03 and VRC26.25 IgGs (**Figure 4.6**), serum had no apparent effect on antigen binding affinity (**Figure 4.3 and Figure 4.1**). This could provide initial insight into the magnitude of our $B_{2,app}$values. Perhaps antibodies with greater attraction, represented by more negative k_{diff} values, will display differences in antigen affinity due to local unfolding events in the Fab domain. Developing a complementary hydrogen deuterium exchange mass spectrometry (HDX-MS) approach that evaluates time-dependent conformational changes in the Fab domains of therapeutic antibodies may investigate this hypothesis. That said, additional antigen binding experiments with antibodies that display a wider range of k_{diff} values are necessary to determine if, and at what point, nonideal interactions with serum proteins influence binding affinities.

In chapter 3, nonideality was not observed in the IgG1 Fc domain (**Figure 3.7a**). This is unspringing given that the Fc has likely evolved to avoid interactions with serum proteins that negatively impact function. However, Fc-focused engineering efforts (Goulet & Atkins, 2020) may render certain therapeutic Fc domains more susceptible to nonideality. That said, correlating nonideality to changes in serum K_D in the Fc is likely not feasible by FCS. Observed changes in K_D could be combination of serum IgG antibodies competitively binding Fc-targeted proteins and nonideality. However, the effect of competitive binding would far outpower nonideality and it would be impossible to extract the contribution of nonideality to the change in K_D. In this study, serum had no effect on Fc binding affinity in our IgG1 model system (**Figure 4.8**), suggesting that serum IgG antibodies did not compete for binding. This is unspringing given protein A affinity to IgG1 is species dependent and has been reported to have low affinity to bovine IgGs (Phillips, 2005). Completing binding experiments in IgG-depleted serum would eliminate the attractive contributions of IgGs and would therefore not be a representative model for determining the impact of nonideality on Fc-mediated binding affinity in serum.

``

A major limitation of our $B_{2,app}$measurements is that there may be dramatic differences between local target environment and serum (i.e., microtumor environment). The local environment may contain different protein concentration and composition compared to serum. Therefore, nonideality in serum may not be representative of the nonideality effects in the local target environment. However, probing nonideality in serum may reflect the propensity to experience nonideality in more complex environments that are challenging to model.

An alternative hypothesis for the utility and significance of our $B_{2,app}$ measurements is that they probe the propensity of therapeutic antibodies to aggregate with serum proteins, in a similar way that B_{22} measurements predict aggregation propensity in highly concentrated antibody formulations. Such aggregation may lead to changes in biodistribution, clearance, and off-target toxicity, all of which can impact therapeutic effect. Further investigation into these effects is needed but could uncover the utility of this approach in therapeutic antibody development. While aggregation characterization in formulation buffer is a major part of the development process, approaches that characterize aggregation of the therapeutic product following administration are not well-established.

FIGURES

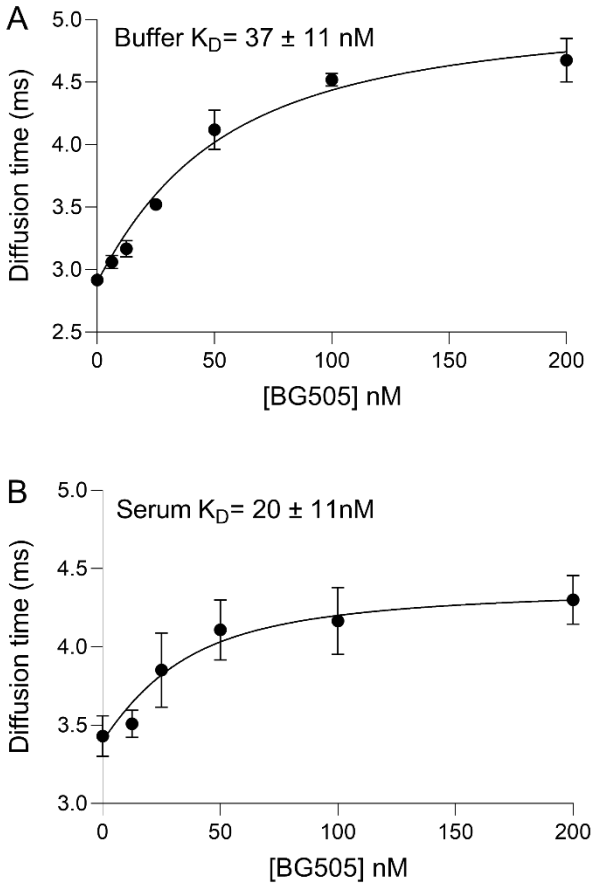

Figure 4.1: Comparison of VRC26.25 IgG binding BG505 SOSIP in 1x PBS pH, 7.4 glycerol buffer (A) and human serum (B). Diffusion times, obtained from fitting FCS traces to a single component FCS equation, were plotted against antigen (BG505) concentration and fit to a quadratic binding equation to yield K_D values, with values reported as mean ± S.D. of at least three independent experiments.

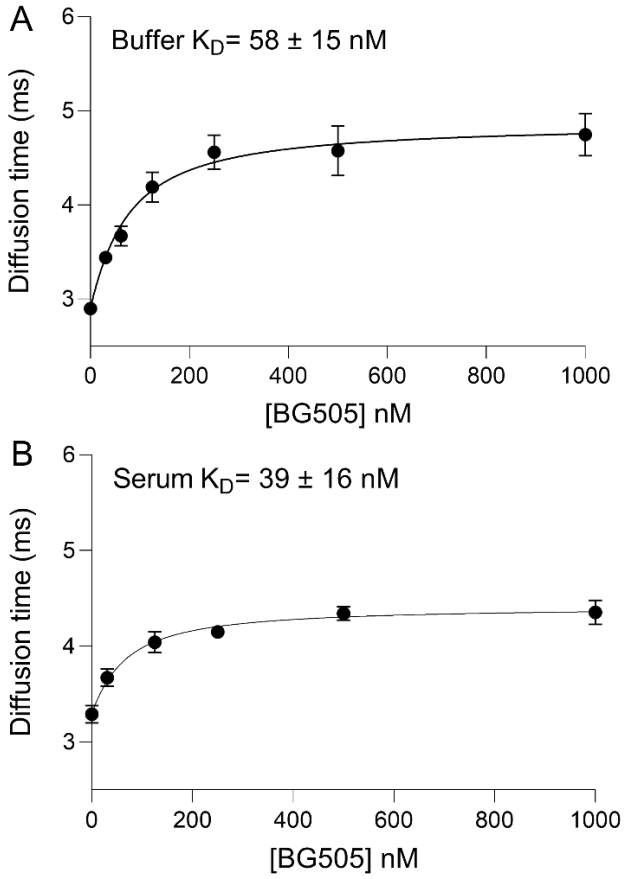

Figure 4.2: Comparison of VRC26.03 IgG binding BG505 SOSIP in 1x PBS, pH 7.4 buffer (A) and human serum (B).Diffusion times, obtained from fitting FCS traces to a single component FCS equation, were plotted against antigen (BG505) concentration and fit to a quadratic binding equation to yield a K_D values, with values reported as mean ± S.D. of at least three independent experiments.

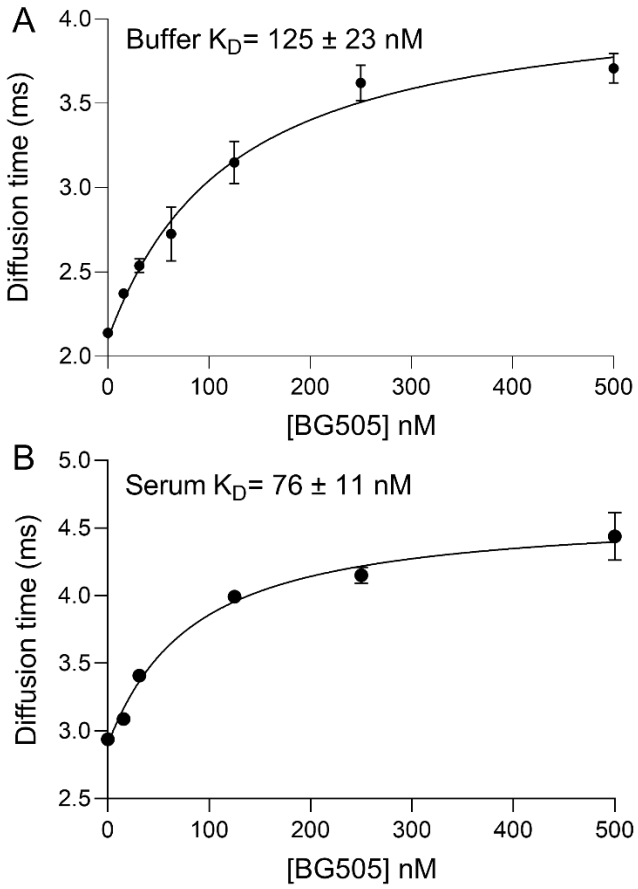

Figure 4.3: Comparison on VRC26.08 IgG binding BG505 SOSIP in 1x PBS, pH 7.4 buffer (A) and human serum (B). Diffusion times, obtained from fitting FCS traces to a single component FCS equation, were plotted against antigen (BG505) concentration and fit to a quadratic binding equation to yield K_D values, with values reported as mean ± S.D. of at least three independent experiments.

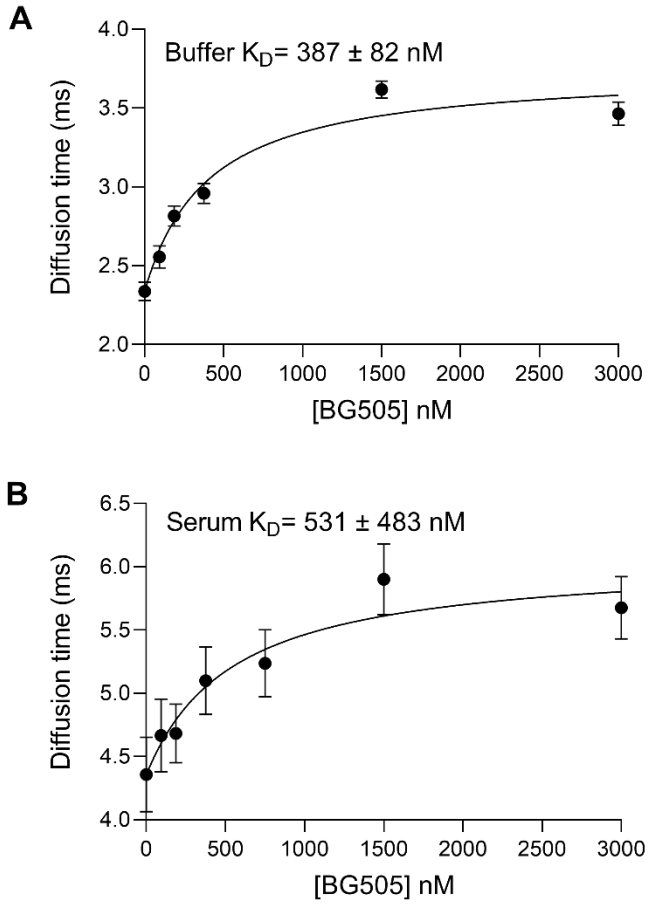

Figure 4.4: VRC26.01 IgG binding BG505 SOSIP in 1x PBS, pH 7.4 glycerol buffer (A) and human serum (B). Diffusion times, obtained from fitting FCS traces to a single component FCS equation, were plotted against unlabeled antigen (BG505) concentration and fit to a quadratic binding equation to yield K_D values. Values ± SD are reported from a single experiment, where the error is based on the SEM in diffusion time measurements (n=5) at each BG505 concentration.

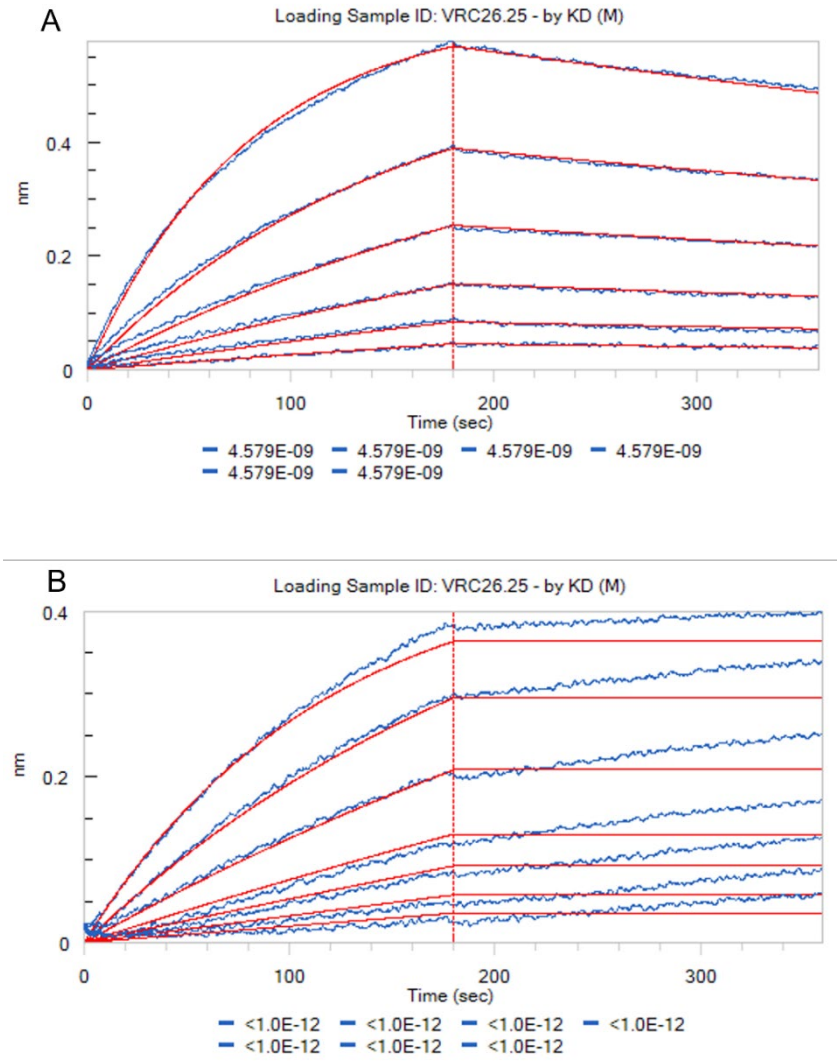

Figure 4.5: BLI results for BG505 binding VRC26.25 IgG Ab in buffer (A) and serum (B). The observed K_D value in buffer (~4.6 nM) is comparable to previous BLI and FCS results. A reliable K_D value was not achieved in serum, likely attributed to serum proteins interacting with binding sites and skewing the kinetic analysis, mainly in the off rate. Results are from a single experiment.

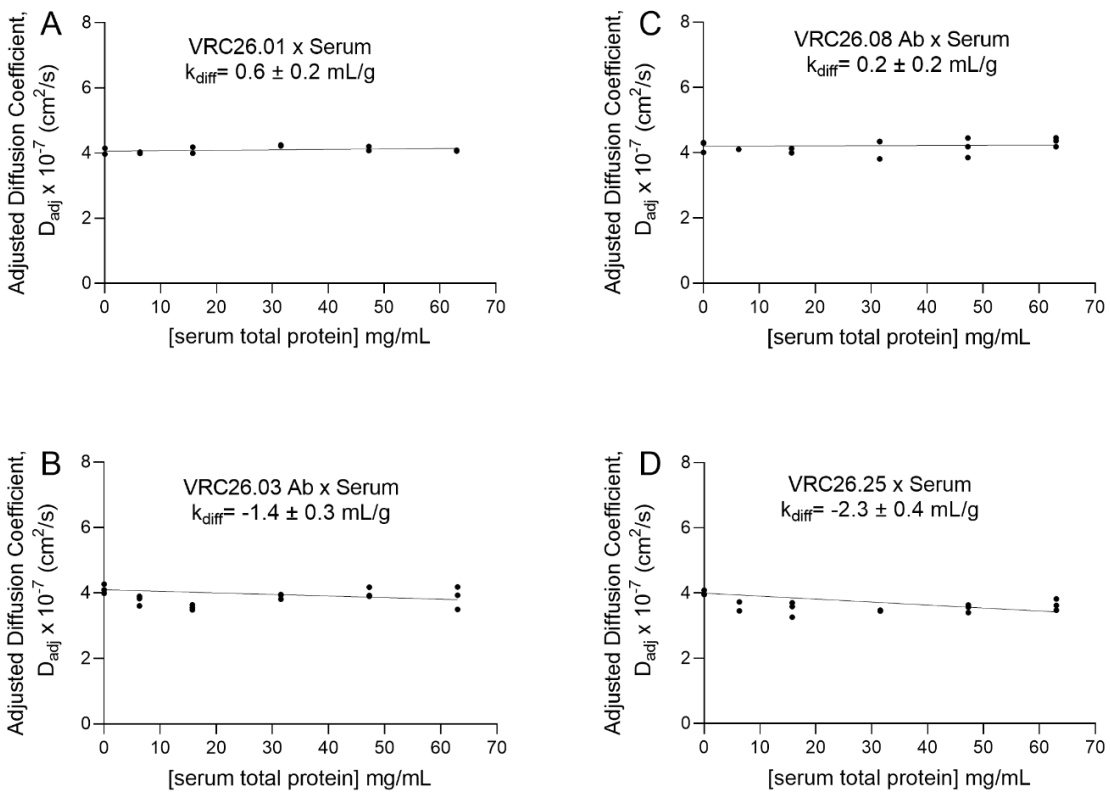

Figure 4.6: Apparent second virial coefficients for anti-BG505 lineage IgG antibodies: D_{adj} vs. [human serum] for VRC26.01 (A), VRC26.03 (B), VRC26.08 (C), and VRC26.25 (C). VRC26.01 and VRC26.08 Abs show negligible deviations from ideal behavior, while VRC26.03 and VRC26.25 Abs show a decrease in diffusion coefficient indicative of slight attractive interactions with one or more components of serum. Points indicate data from three replicates with k_{diff} (or $2B_2M$) values reported as mean ± S.D. of at least two independent experiments (n=3 in most cases).

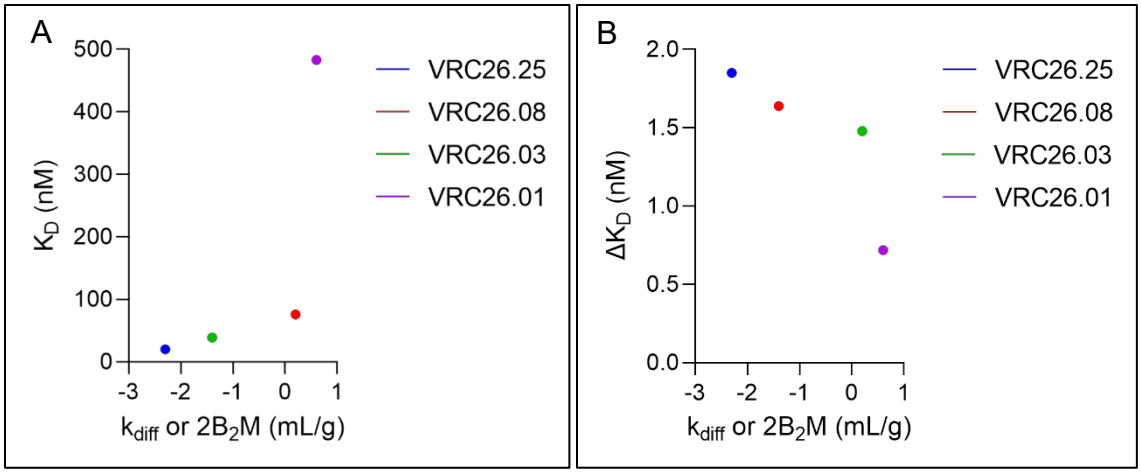

Figure 4.7: K_D vs k_{diff} (A) and fold ΔK_D vs k_{diff} for VRC26 lineage IgG antibodies in human serum. VRC26.01 and VRC26.03 exhibit negligible deviations from ideal behavior, as evident by k_{diff} values not significantly different than 0 mL/g, whereas slightly negative values observed for VRC26.08 and VRC26.25 are indicative of slight attraction to serum components. There is a trend of decreasing k_{diff} with decreasing K_D values, indicating Abs with higher affinity to BG505 (VRC26.08 and VRC26.25) exhibit greater propensity for attractive interactions with serum components. There was also a trend of decreasing k_{diff} with increasing fold change in K_D. However, this is unsurprising based on higher levels of uncertainty in lower K_D values. However, the fold change in all cases was determined insignificant, suggesting serum had no effect on antigen binding.

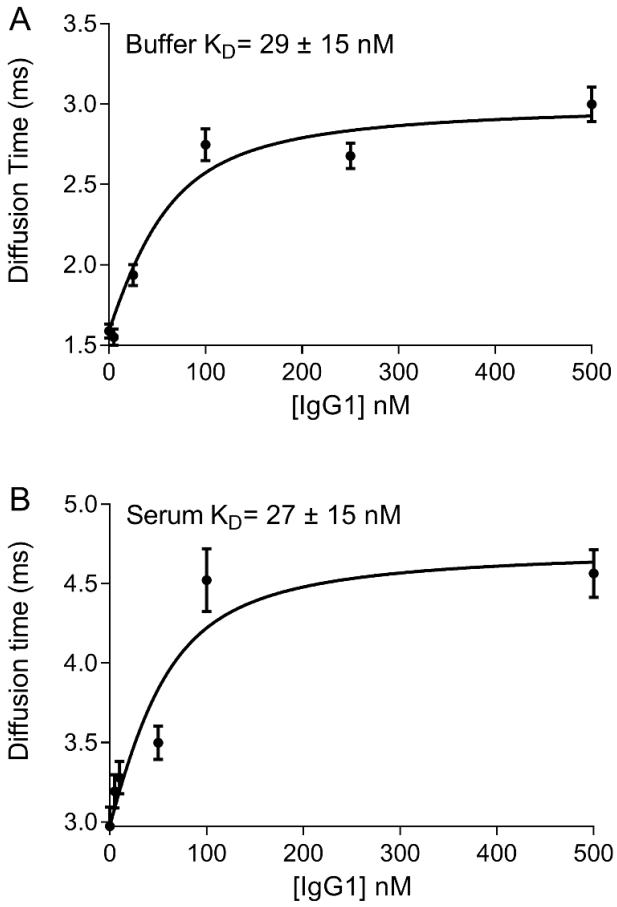

Figure 4.8: Binding interactions in the Fc domain of IgG1: Protein A binding a model IgG1 antibody in buffer (A) and serum (B). The diffusion times obtained from fitting FCS traces to a single component FCS equation, were plotted against unlabeled IgG1 concentration and fit to a quadratic binding equation to yield a K_D values, with values reported from single experiments. No significant difference in K_D was observed between buffer and serum conditions.

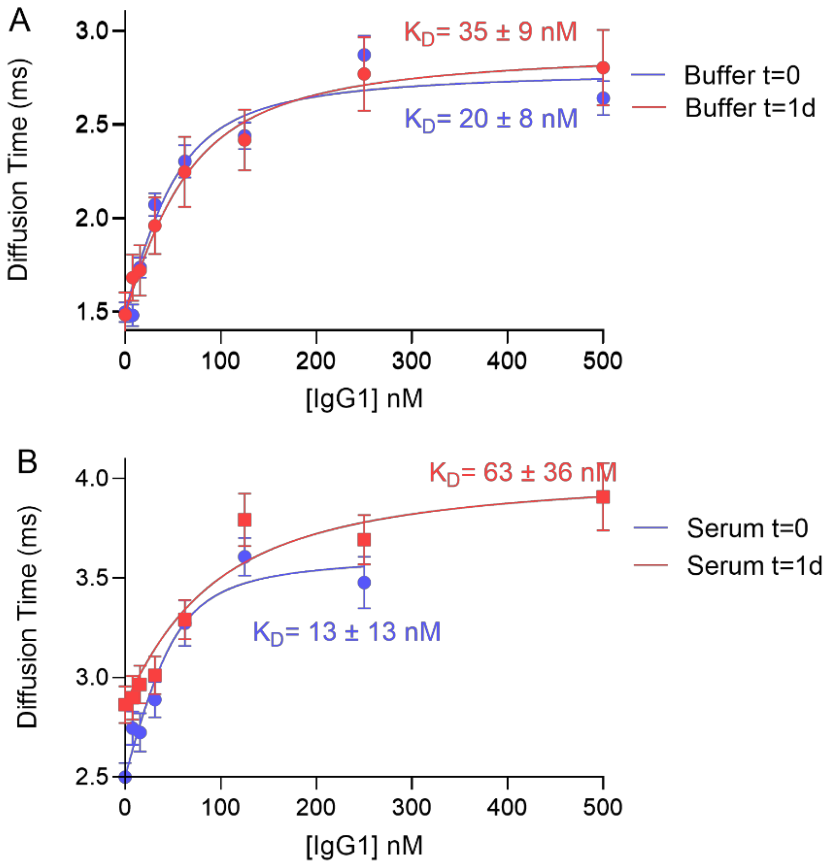

Figure 4.9: FCS comparisons of protein A binding IgG1 in buffer (A) and serum (B) at t=0 and after 24 hours at room temperature. Diffusion times, obtained from fitting FCS traces to a single component FCS equation, were plotted against unlabeled IgG1 concentration and fit to a quadratic binding equation to yield a K_D values, with values reported from single experiments.

``

TABLES

Table 4.1: *Summary of* K_D *values* $B_{2,app}$ *values*

Sample	k_{diff} or $2B_2$M (mL/g)	Buffer K_D (nM)	Serum K_D (nM)
VRC26.01	0.6 ± 0.2	387 ± 32[a] 495[b]	531 ± 483[a] ND
VRC26.03	-1.4 ± 0.3	125 ± 23[a] 149[b]	76 ± 11[a] ND
VRC26.08	0.2 ± 0.2	58 ± 15[a] 115[b]	39 ± 16[a] ND
VRC26.25	-2.3 ± 0.4	37 ± 11[a] 9[b]	20 ± 11[a] ND

[a]FCS; [b]BLI (measured by Edgar Hodge); not determined (ND)

``

4.5 References

Becker, S., Frankel, M. B., Schneewind, O., & Missiakas, D. (2014). Release of protein A from the cell wall of Staphylococcus aureus. *Proceedings of the National Academy of Sciences*, *111*(4), 1574–1579. https://doi.org/10.1073/pnas.1317181111

Bee, C., Abdiche, Y. N., Pons, J., & Rajpal, A. (2013). Determining the Binding Affinity of Therapeutic Monoclonal Antibodies towards Their Native Unpurified Antigens in Human Serum. *PLoS ONE*, *8*(11), e80501. https://doi.org/10.1371/journal.pone.0080501

Bee, C., Abdiche, Y. N., Stone, D. M., Collier, S., Lindquist, K. C., Pinkerton, A. C., Pons, J., & Rajpal, A. (2012). Exploring the dynamic range of the kinetic exclusion assay in characterizing antigen-antibody interactions. *PLoS ONE*. https://doi.org/10.1371/journal.pone.0036261

Choe, W., Durgannavar, T., & Chung, S. (2016). Fc-Binding Ligands of Immunoglobulin G: An Overview of High Affinity Proteins and Peptides. *Materials*, *9*(12), 994. https://doi.org/10.3390/ma9120994

Davies, C. de L., Berk, D. A., Pluen, A., & Jain, R. K. (2002). Comparison of IgG diffusion and extracellular matrix composition in rhabdomyosarcomas grown in mice versus in vitro as spheroids reveals the role of host stromal cells. *British Journal of Cancer*, *86*(10), 1639–1644. https://doi.org/10.1038/sj.bjc.6600270

Day, Y. S. N., Baird, C. L., Rich, R. L., & Myszka, D. G. (2002). Direct comparison of binding equilibrium, thermodynamic, and rate constants determined by surface- and solution-based biophysical methods. *Protein Science*, *11*(5), 1017–1025. https://doi.org/10.1110/ps.4330102

Drake, A. W., Myszka, D. G., & Klakamp, S. L. (2010). Characterizing High Affinity Antigen/Antibody Complexes by Kinetic and Equilibrium Based Methods. In *Current Trends in Monoclonal Antibody Development and Manufacturing* (pp. 179–192). Springer New York. https://doi.org/10.1007/978-0-387-76643-0_11

Dunlap, T., & Cao, Y. (2022). Physiological Considerations for Modeling in vivo Antibody-Target Interactions. *Frontiers in Pharmacology*, *13*. https://doi.org/10.3389/fphar.2022.856961

Dzimianski, J. V., Lorig-Roach, N., O'Rourke, S. M., Alexander, D. L., Kimmey, J. M., & DuBois, R. M. (2020). Rapid and sensitive detection of SARS-CoV-2 antibodies by biolayer interferometry. *Scientific Reports*, *10*(1), 21738. https://doi.org/10.1038/s41598-020-78895-x

Feig, M., Yu, I., Wang, P., Nawrocki, G., & Sugita, Y. (2017). Crowding in Cellular Environments at an Atomistic Level from Computer Simulations. *The Journal of Physical Chemistry B*, *121*(34), 8009–8025. https://doi.org/10.1021/acs.jpcb.7b03570

Goulet, D. R., & Atkins, W. M. (2020). Considerations for the Design of Antibody-Based Therapeutics. *Journal of Pharmaceutical Sciences*, *109*(1), 74–103. https://doi.org/10.1016/j.xphs.2019.05.031

Haustein, E., & Schwille, P. (2007). Fluorescence Correlation Spectroscopy: Novel Variations of an Established Technique. *Annual Review of Biophysics and Biomolecular Structure*, *36*(1), 151–169. https://doi.org/10.1146/annurev.biophys.36.040306.132612

Hunter, S. A., & Cochran, J. R. (2016). Cell-Binding Assays for Determining the Affinity of Protein–Protein Interactions. In *Methods in Enzymology* (pp. 21–44). https://doi.org/10.1016/bs.mie.2016.05.002

Kamat, V., & Rafique, A. (2017). Designing binding kinetic assay on the bio-layer interferometry (BLI) biosensor to characterize antibody-antigen interactions. *Analytical Biochemistry*, *536*, 16–31. https://doi.org/10.1016/j.ab.2017.08.002

Larsen, H. A., Atkins, W. M., & Nath, A. (2021). Probing interactions of therapeutic antibodies with serum via second virial coefficient measurements. *Biophysical Journal*, *120*(18), 4067–4078. https://doi.org/10.1016/j.bpj.2021.08.007

Li, W., Prabakaran, P., Chen, W., Zhu, Z., Feng, Y., & Dimitrov, D. (2016). Antibody Aggregation: Insights from Sequence and Structure. *Antibodies*, *5*(3), 19. https://doi.org/10.3390/antib5030019

Majety, M., Runza, V., Lehmann, C., Hoves, S., & Ries, C. H. (2018). A drug development perspective on targeting tumor-associated myeloid cells. *The FEBS Journal*, *285*(4), 763–776. https://doi.org/10.1111/febs.14277

Pancera, M., Changela, A., & Kwong, P. D. (2017). How HIV-1 entry mechanism and broadly neutralizing antibodies guide structure-based vaccine design. *Current Opinion in HIV and AIDS*, *12*(3), 229–240. https://doi.org/10.1097/COH.0000000000000360

Phillips, T. M. (2005). *Handbook of Affinity Chromatography: Affinity Chromatography in Antibody and Antigen Purification* (D. S. Hage (ed.); 2nd ed.). Taylor & Francis Group.

Rathanaswami, P., Richmond, K., Manchulenko, K., & Foltz, I. N. (2011). Kinetic analysis of unpurified native antigens available in very low quantities and concentrations. *Analytical Biochemistry*, *414*(1), 7–13. https://doi.org/10.1016/j.ab.2011.02.034

Rispens, T., & Vidarsson, G. (2014). Human IgG Subclasses. In *Antibody Fc* (pp. 159–177). Elsevier. https://doi.org/10.1016/B978-0-12-394802-1.00009-1

Saxena, A., & Wu, D. (2016). Advances in Therapeutic Fc Engineering – Modulation of IgG-Associated Effector Functions and Serum Half-life. *Frontiers in Immunology*, *7*. https://doi.org/10.3389/fimmu.2016.00580

Schuck, P., & Zhao, H. (2010). The Role of Mass Transport Limitation and Surface Heterogeneity in the Biophysical Characterization of Macromolecular Binding Processes by SPR Biosensing. In *Methods in molecular biology (Clifton, N.J.)* (pp. 15–54). https://doi.org/10.1007/978-1-60761-670-2_2

Tabrizi, M., Bornstein, G. G., & Suria, H. (2010). Biodistribution Mechanisms of Therapeutic Monoclonal Antibodies in Health and Disease. *The AAPS Journal*, *12*(1), 33–43. https://doi.org/10.1208/s12248-009-9157-5

Verkerke, H. P., Williams, J. A., Guttman, M., Simonich, C. A., Liang, Y., Filipavicius, M., Hu, S.-L., Overbaugh, J., & Lee, K. K. (2016). Epitope-Independent Purification of Native-Like Envelope Trimers from Diverse HIV-1 Isolates. *Journal of Virology*. https://doi.org/10.1128/jvi.01351-16

Vidarsson, G., Dekkers, G., & Rispens, T. (2014). IgG Subclasses and Allotypes: From Structure to Effector Functions. *Frontiers in Immunology*, *5*. https://doi.org/10.3389/fimmu.2014.00520

Wang, X., Phan, M. M., Li, J., Gill, H., Williams, S., Gupta, N., Quarmby, V., & Yang, J. (2020). Molecular Interaction Characterization Strategies for the Development of New Biotherapeutic Antibody Modalities. *Antibodies*, *9*(2), 7. https://doi.org/10.3390/antib9020007

Yin, Y., Quinlan, B. D., Ou, T., Guo, Y., He, W., & Farzan, M. (2021). In vitro affinity maturation of broader and more-potent variants of the HIV-1–neutralizing antibody CAP256-VRC26.25. *Proceedings of the National Academy of Sciences*, *118*(29).

``

https://doi.org/10.1073/pnas.2106203118

CHAPTER 5

Final Discussion

5.1 Summary and future directions

Therapeutic antibodies are a promising drug class due to several advantageous properties such as high antigen specificity, specialized effector functions, and long circulating half-lives. However, major gaps remain in our understanding of antibody PK/PD compared to small molecule drugs. This arises from many properties unique to proteins and differences in biological mechanisms (e.g., clearance, biodistribution, target engagement, etc.) that are challenging to predict and model. Although *in vitro* characterization is critical during development, many traditional analytical techniques are confined to buffer systems that inadequately model physiological environments. Implementing techniques capable of completing measurements in *ex vivo* biological samples may advance our understanding of antibody PK/PD and further optimize the development process. The research presented in this dissertation addresses this issue directly by characterizing antibody-target binding and serum-induced nonideality effects directly in serum using fluorescence correlation spectroscopy (FCS).

The progressive shift in macromolecular crowding theory to include contributions from enthalpically-driven weak protein-protein interactions has prompted interest in studying the effects of nonideality on protein thermodynamics (Bhattacharya et al., 2013; Gesper et al., 2020; Hatters et al., 2002; Phillip et al., 2012; Sukenik et al., 2013; Zhou et al., 2006). These effects can perturb stability and molecular recognition in ways that are difficult to predict, especially in buffer systems. Nonideality has only recently been applied to therapeutic antibodies, specifically in the context of serum, due to their long circulating half-lives. There is growing interest in exploring

how serum impacts antigen-target binding and how therapeutic antibodies interact with serum proteins (Chaturvedi et al., 2020; Kim et al., 2019; Larsen et al., 2021; Wright et al., 2018). The in-serum FCS approach in our first publication (Larsen et al., 2021; Chapter 2) is the first documented method capable of probing nonideality directly in biological fluids via determination of apparent second virial coefficients ($B_{2,app}$). $B_{2,app}$ measurements effectively capture nonideality between serum proteins in addition to their bulk effects on therapeutic antibodies. This provides a more representative model of global nonideality effects *in vivo* than commonly used buffer systems. Interestingly, the BsAb in Chapter 2 (**Figure 2d,e,f**) and Fab fragments in Chapter 3 (**Figure 3.11**) exhibited more attraction to serum, as evident by more negative c_{liff} values, compared to parental abs which could render them more susceptible to nonideality-driven perturbations. It would be interesting to explore this further with a larger panel of mob's and antibody-based platforms (i.e., ADCs, Fc-fusion proteins, etc.). $B_{2,app}$ results for the panel of IgG1 antibodies in Chapter 2 (**Figure 2.7**), suggests that serum-induced nonideality effects are antibody dependent. One disadvantage of $B_{2,app}$ measurements in whole serum is the inability to determine which specific serum proteins contribute to nonideality. However, this was addressed via the component assessment presented in Chapter 3.

In Chapter 3, we use FCS-derived $B_{2,app}$ measurements to identify the components of human serum responsible for non-ideal interactions with mAbs and Fab fragments. Most mAbs exhibit neutral or slightly attractive interactions with intact serum (**Figures 3.2-3.6**). Generally, mAbs display repulsive interactions with albumin and mildly attractive interactions with IgGs in the context of whole serum. Crucially, however, these attractive interactions are much stronger with pooled IgGs isolated from other serum components, indicating that the effects of serum nonideality can only be understood by studying the intact medium (rather than isolated

components). This complicates approaches that measure cross-term virial coefficients with isolated serum proteins to probe serum-induced nonideality effects and highlights the advantage of our in-serum FCS approach. Attractive interactions with serum IgGs were isolated to Fab domains (**Figure 3.11**), which could have functional consequences to antigen binding if near the CDR. Therefore, future studies should explore which regions of the Fab are involved in nonideal interactions (CDR vs. framework regions). It would also be interesting to explore differences in other properties, such as hydrophobicity and isoelectric point to further investigate the contributions of hydrophobic and electrostatic interactions.

To further investigate functional consequences of nonideality on antigen binding, Chapter 4 focused on comparing antigen binding affinity between buffer and serum conditions with a VRC26 HIV lineage model system via FCS. Despite no differences in binding affinity to BG505 in serum, k_{diff} values ranged from 0.6 mL/g to –2.3 mL/g (**Table 4.1**), indicating a balance to slight attraction to serum proteins. This suggests that slight attraction on the order of –2.3 mL/g does not negatively impact antigen binding. Although this provides initial insight into the magnitude of our $B_{2,app}$ values, additional experiments with other antibody systems, especially those that exhibit greater attraction to serum (more negative k_{diff} values) should be further investigated. Implementing in-serum affinity measurements in early stages of lead candidate selection may facilitate better estimates of *in vivo* K_D. Furthermore, $B_{2,app}$ measurements may also facilitate lead candidate selections as well as assist characterization of antibody leads as they go through various process changes and optimization steps. There is still work ahead to determine the significance of our $B_{2,app}$ values but the research presented here has laid the foundation for future experiments and provided novel insight into serum-induced nonideality effects.

5.2 References

Bhattacharya, A., Kim, Y. C., & Mittal, J. (2013). Protein–protein interactions in a crowded environment. *Biophysical Reviews*, *5*(2), 99–108. https://doi.org/10.1007/s12551-013-0111-5

Chaturvedi, S. K., Parupudi, A., Juul-Madsen, K., Nguyen, A., Vorup-Jensen, T., Dragulin-Otto, S., Zhao, H., Esfandiary, R., & Schuck, P. (2020). Measuring aggregates, self-association, and weak interactions in concentrated therapeutic antibody solutions. *MAbs*, *12*(1). https://doi.org/10.1080/19420862.2020.1810488

Gesper, A., Wennmalm, S., Hagemann, P., Eriksson, S.-G., Happel, P., & Parmryd, I. (2020). Variations in Plasma Membrane Topography Can Explain Heterogenous Diffusion Coefficients Obtained by Fluorescence Correlation Spectroscopy. *Frontiers in Cell and Developmental Biology*, *8*. https://doi.org/10.3389/fcell.2020.00767

Hatters, D. M., Minton, A. P., & Howlett, G. J. (2002). Macromolecular Crowding Accelerates Amyloid Formation by Human Apolipoprotein C-II. *Journal of Biological Chemistry*, *277*(10), 7824–7830. https://doi.org/10.1074/jbc.M110429200

Kim, D. M., Yao, X., Vanam, R. P., & Marlow, M. S. (2019). Measuring the effects of macromolecular crowding on antibody function with biolayer interferometry. *MAbs*, *11*(7), 1319–1330. https://doi.org/10.1080/19420862.2019.1647744

Larsen, H. A., Atkins, W. M., & Nath, A. (2021). Probing interactions of therapeutic antibodies with serum via second virial coefficient measurements. *Biophysical Journal*, *120*(18), 4067–4078. https://doi.org/10.1016/j.bpj.2021.08.007

Phillip, Y., Kiss, V., & Schreiber, G. (2012). Protein-binding dynamics imaged in a living cell. *Proceedings of the National Academy of Sciences*, *109*(5), 1461–1466. https://doi.org/10.1073/pnas.1112171109

Sukenik, S., Sapir, L., Gilman-Politi, R., & Harries, D. (2013). Diversity in the mechanisms of cosolute action on biomolecular processes. *Faraday Discussions*. https://doi.org/10.1039/c2fd20101a

Wright, R. T., Hayes, D., Sherwood, P. J., Stafford, W. F., & Correia, J. J. (2018). AUC measurements of diffusion coefficients of monoclonal antibodies in the presence of human serum proteins. *European Biophysics Journal*, *47*(7), 709–722. https://doi.org/10.1007/s00249-018-1319-x

Zhou, Y.-L., Liao, J.-M., Chen, J., & Liang, Y. (2006). Macromolecular crowding enhances the binding of superoxide dismutase to xanthine oxidase: Implications for protein–protein interactions in intracellular environments. *The International Journal of Biochemistry & Cell Biology*, *38*(11), 1986–1994. https://doi.org/10.1016/j.biocel.2006.05.012